

**Radicals, Radical ion, Diradical and Diradicaloid Based on Silicon**

Journal:	<i>Chemical Society Reviews</i>
Manuscript ID	CS-REV-09-2015-000739
Article Type:	Review Article
Date Submitted by the Author:	27-Sep-2015
Complete List of Authors:	Roesky, Herbert; Universitat Gottingen, Institut fur Anorganische Chemie Roy, Sudipta; Universitat Göttingen, Instute für Anorganische Chemie Mondal, Kartik; Institut fur Anorganische Chemie, ; Universitat Göttingen, Instute für Anorganische Chemie



Silicon Based Radical, Radical ion, Diradical and Diradicaloid

Kartik Chandra Mondal, Sudipta Roy and Herbert W. Roesky*

Received 00th January 20xx,
Accepted 00th January 20xx

DOI: 10.1039/x0xx00000x

www.rsc.org/

Radicals are an important class of species which act as intermediates in numerous chemical and biological processes. Most of the radicals have short lifetimes. However, radicals with longer lifetimes can be isolated and stored in a pure form. They are called stable radicals. Over the last five decades, the syntheses of several stable radicals have been reported. Recently, highly unstable radicals have been successfully stabilized via strong σ -donation of singlet carbenes. Cyclic alkyl(amino) carbene (cAAC) is regarded as a stronger σ -donor and a better π -acceptor when compared with that of an N-heterocyclic carbene (NHC). In this article we review preferentially the results of our group to generate stable radical centers on the carbene carbon atoms by employing the so far hidden and unique ability of the cAACs. We focus on the development of new synthetic routes to stable and isolable radicals containing silicon atoms. All the compounds have been well characterized by single crystal X-ray analysis; the mono-radicals have been distinguished by EPR spectroscopy and the ground state of the diradicals have been studied by magnetic susceptibility measurements and theoretical calculations. Many of these compounds are studied by cyclic voltammetry and are often converted to their corresponding radical cations or radical anions via electron abstraction or addition processes. Some of them are stable, having long lifetimes and hence are isolated and characterized thoroughly. Not much information has been obtained on the short lived persistent radical species. Herein, we discuss some of the examples of such a type of species and focus on what kind of chemical reactions are initiated by these short-lived radical species in solution. We also briefly mention the syntheses and characterization of the so far reported stable silicon centered radicals.

1. Introduction

Radicals are captivating chemical species which have attracted the interest of experimental as well as theoretical chemists and physicists for over a century.¹ The first organic radical (trityl radical; $\text{Ph}_3\text{C}^\bullet$) was synthesized in 1897 by the Russian scientist Moses Gomberg and was reported in 1900.^{1a} Trityl radical is the first organic radical which was produced within a glass container in a laboratory. It was accidentally obtained in an attempt to synthesize sterically crowded $\text{Ph}_3\text{C-CPh}_3$ by reduction of $\text{Ph}_3\text{C-Cl}$ with Zn or Ag metal. Trityl radical ($\text{Ph}_3\text{C}^\bullet$) mostly exists in the dimeric form and a small percentage of the monomeric radical form is in equilibrium with its dimer. Seven decades later the molecular structure of $\text{Ph}_3\text{C}^\bullet$ analogues were studied and confirmed by X-ray single crystal diffraction. The chemists then tried to understand and unlock the hidden mystery behind the unusual stability of such open shell species. Finally, it has been concluded that substitution with six chlorine atoms (at 2,6-position of each phenyl ring) is enough to make this class of radical to be stable in air. Radicals are mostly stabilized by the steric effect preventing them from

taking part in further chemical processes such as dimerization, proton abstraction etc. A large number of chemical²⁻³ and biological⁴ procedures are functioning via radical pathways.²⁻⁴ Radicals play crucial roles of our daily biological systems to laboratory chemical processes. A large number of radical species have been even found in the interstellar atmosphere such as methylidyne ($^\bullet\text{CH}$), ethynyl radical ($^\bullet\text{C}_2\text{H}$), methylene diradical ($^\bullet\text{CH}_2^\bullet$), amino radical ($^\bullet\text{NH}_2$), formyl radical (HCO^\bullet), hydroxyl radical ($^\bullet\text{OH}$), cyanogen radical ($^\bullet\text{CN}$) etc. They could not combine with each other due to the very low density of the interstellar medium.

In general the most of the radicals are short-lived species.^{1h,5} The lifetimes of some radicals are extremely short and thus they cannot be even characterized by electron paramagnetic resonance (EPR) measurements. Radicals having relatively longer lifetimes can be studied by EPR spectroscopy at low temperatures. The instability of the unstable radicals arises mainly from their high reactivity due to thermodynamic and kinetic reasons. Highly reactive radicals are prone to undergo dimerization, polymerization, bond activation, fragmentation or atom abstraction from solvents etc. The radicals are mainly divided into two categories, viz. persistent radicals⁵ and stable radicals. The former have sufficiently long lifetimes and can be characterized in solution by EPR. The persistent radicals cannot be isolated in a pure form, while the stable radicals are isolable and storable even at room temperature (rt).^{1h,5} Stable radicals

Institut für Anorganische Chemie, Georg-August-Universität, 37077 Göttingen, Germany. Phone: +49 551 39 33001, Fax: +49 551 39 33373, E-mail: hroesky@gwdg.de

can be structurally characterized by X-ray single crystal diffraction.⁶ They are utilized in many areas of chemistry for different means. They can catalyse polymerization reactions and hence are of huge interest in polymer chemistry.⁷ They have been combined with metal salts for oxidation of alcohols to the corresponding aldehydes.⁸ Stable radicals have often been used for trapping unstable radical intermediates in organic and inorganic chemical transformations.⁹ When radicals are combined with anisotropic metals ions on the molecular level, the composite can act as single molecule magnets (SMMs)¹⁰ or single chain magnets (SCMs),¹¹ which are promising candidates for the construction of molecule based electronics.¹² Moreover, radicals have the ability to act as antioxidants.¹³

MONORADICAL, BIRADICAL, DIRADICAL AND DIRADICALOID

Monoradical: Atom or functional group or molecule containing an unpaired electron is called monoradical. A free electron has a spin quantum number $S = 1/2$ and further possesses an electric charge. An electron has a magnetic momentum with magnetic components $m_s = +1/2$ and $m_s = -1/2$ which are energetically degenerate in the absence of a magnetic field. However, the degeneracy is lifted when an external magnetic field (H) is applied in a certain direction. The magnetic moment of an electron can align itself either parallel ($m_s = -1/2$, β spin) or antiparallel ($m_s = +1/2$, α spin) to the direction of the applied magnetic field (Figure 1, a).

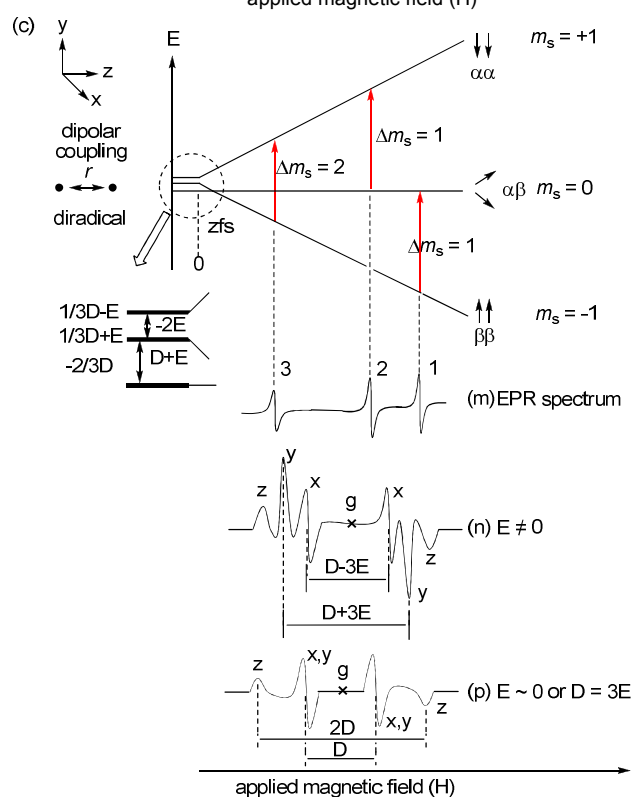
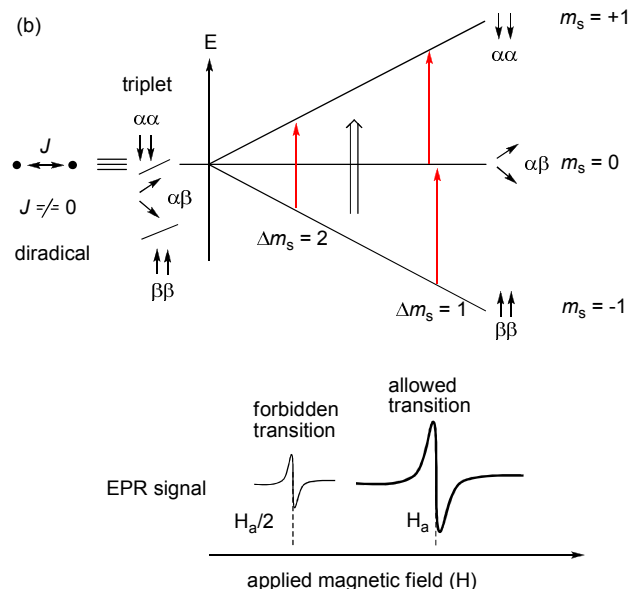
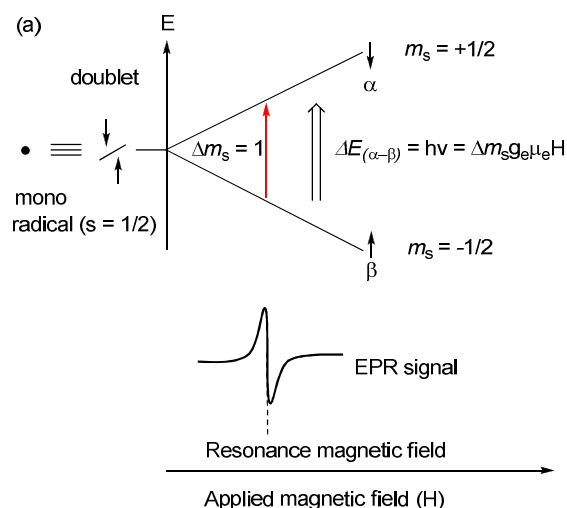


Figure 1. (a) Zeeman effect on unpaired electrons and EPR spectrum ($\Delta m_s = \pm 1$ transition) for a free electron, (b) electron-electron interaction in a diradical and EPR resonances ($\Delta m_s = \pm 1$ and ± 2 transitions) and (c) effect of zfs on $S = 1$ ground state.

The spin multiplicity ($2S + 1$) of monoradicals is two and hence they are also called doublet species. Two fine energy states (β and α) of a monoradical are split into well resolved energy states (by Zeeman effect) and their separation is proportional to the strength of the applied magnetic field (H). These

energies (E_α and E_β) are calculated by the equation of $E = m_e g_e \mu_e H$, where g_e is the so-called g factor ($g_e = 2.0023$ for a free electron), μ_e is the Bohr magneton (9.274078×10^{-24} J T^{-1}). The only possible electronic transition is from $\beta \rightarrow \alpha$ or $\beta \leftarrow \alpha$ ($\Delta m_s = \pm 1$) for a monoradical. The separation ($\Delta E = E_\alpha - E_\beta$) between two Zeeman energy states (β and α) is given by $\Delta E = g_e \mu_e H$. Electron paramagnetic resonance (EPR) occurs when the frequency (ν) matches the energy $\Delta E = E_\alpha - E_\beta = g_e \mu_e H = h\nu$. In principle a free electron will produce one EPR signal due to $\Delta m_s = \pm 1$ transition. An unpaired electron of an atom or a functional group or a molecule further interacts with the magnetic moment of the spin-active nucleus (if any) to produce additional hyperfine lines energy states. The satellites will be observed due to the interaction of the nuclear spin with the electron spin. When a radical electron resides on an atom having spin-active nucleus then a number of hyperfine lines can be given by $(2nI+1)$ [n = number of nucleus and I = spin of that nucleus]. The radical electron can further interact with neighboring nuclei via bond or space. In that case, the number of hyperfine lines can be calculated by $(2n_1I_1+1)(2n_2I_2+1)\dots$ and so on. A radical electron in general couples with its own nucleus (on which it is localized) more strongly than to its neighboring nuclei and thus might have a higher hyperfine coupling constant for its own nucleus than those of neighboring nuclei. It might not be always the case. However, the magnitude of the hyperfine coupling constants is expected to decrease with decreasing spin density due to radical electron (if all these nuclei are identical). It also depends upon the spin density at that atom as well as the particular element (isotope). EPR coupling constants of some nuclei are frequently large due to the high nuclear magnetic moment, not necessarily reflecting very large spin densities. Often it happens that the magnitudes of hyperfine coupling constants of different atomic nuclei are close to each other and the hyperfine lines appear in similar regions leading less number of hyperfine lines than one can expect from the above mentioned formula.

Biradical and diradical: When two unpaired electrons (radicals) of a molecule interact with each other, the molecule is termed as biradical^{14a} or diradical (open-shell molecule).^{14b,1d,1h} In general the shorter the distance between two radical centers, the stronger is the interaction. For biradicals the electron exchange interaction (J) between the two unpaired electrons is negligible or nearly negligible ($J \approx 0$) due to the long distance (r) between them.^{1a} Biradicals are like two doublets within the same molecule. The stronger electron dipole-dipole interactions lead to two classical situations; (1) both spins align in the same direction ($\uparrow\uparrow$; $S = 1$, $2S+1 = 3$; triplet) in a triplet diradical or (2) two spins are directed opposite to each other ($\uparrow\downarrow$; $S = 0$, $2S+1 = 1$; singlet) in a singlet diradical (Figure 1b). Two electrons occupy two separate orbitals in both ground state triplet diradical and singlet diradical. For example, molecular oxygen (O_2) has a triplet ground state since two electrons occupy a double degenerated π^* -orbital ($\uparrow\uparrow$). The strength of the exchange interaction is evaluated in terms of J which is positive for a

triplet diradical and negative for a single diradical. The exchange interaction between two electrons in a (non radical) closed-shell singlet molecule is negative and extremely high in magnitude. Both the electrons occupy the same orbital with opposite spin in a closed-shell singlet molecule. For example, the exchange interactions between two π -electrons of an ethylene ($H_2C=CH_2$) molecule is extremely negative and hence they eventually form a π -bond between two p_z -orbitals of each CH_2 group. Both the CH_2 groups of ethylene are in the same plane and thus it does not have radical character. Ethylene has a singlet ground state (with $S = 0$). The radical character can be induced in an ethylene molecule if the CH_2 groups are twisted around each other making the overlap between two p_z orbitals weaker. When the twisting angle reaches 90° , the orbital overlap between two p_z -orbitals becomes negligible and the molecule attains a diradical ground state. Such an electronic state is not the ground state of an ethylene molecule rather an excited state.

The through-space exchange interaction (J) between the two radical spins, can be experimentally studied by the electron paramagnetic resonance (EPR) spectroscopic analysis using stable radicals (Figure 1b). For example, when the two carbon centered radicals [$R_2N-C^*(R_2)$] in a molecule are isolated or separated from each other at a large distance, three hyperfine line signals ($2nI+1 = 2 \times 1 \times 1 + 1 = 3$) will be typically observed from the coupling of the electron with nitrogen nucleus (^{14}N ; $I = 1$), appear in the EPR spectrum (for biradical). Additionally satellites with low intensity are observed due to coupling of the radical electron with the ^{13}C nucleus ($I = 1/2$). Thus, interaction between the two spins is negligible. When the J is large enough ($J \gg \alpha(^{14}N)$) due to the short distance (r), five hyperfine line signals ($2 \times 2I + 1 = 5$) will be observed with additional satellites in the EPR spectrum (for a diradical).

Diradicals can be divided into two categories; localized and delocalized diradicals. Delocalized diradicals have been even divided into Kekulé and non-Kekulé molecules. Antiaromatic molecules can be regarded as delocalized diradicals.

The singlet diradicals ($\uparrow\downarrow$; $S = 0$, $2S+1 = 1$; singlet) does not have a net magnetic moment and hence they are diamagnetic and are EPR silent. If a molecule with a singlet diradical character has a low lying triplet (excited state) state which can be fractionally populated, then such molecule can show EPR signals. The temperature dependent intensity of the EPR signal can be used to predict the nature of the ground state. The intensity of the signal will decrease with decreasing temperature due to depopulation of the low lying excited state (magnetic) and population of the diamagnetic ground state. This is typically the case when J is negative (antiferromagnetic exchange interaction or dipole-dipole interaction) for a diradical. When J is positive, the triplet ($S = 1$) is the ground state and hence the intensity of EPR signal will increase with decreasing temperature due to the population of $S = 1$ spin state. If the singlet and triplet states of a diradical are thermally activated, the similar effect can be studied by measuring the temperature dependent magnetic susceptibility. The product (χT) of magnetic susceptibility (χ) and T will decrease when J is negative and will increase for

positive J value. The value of J and $\Delta E_{\text{singlet-triplet}}$ by fitting the χT vs T plot by two interacting $S = \frac{1}{2}$ spins model. The effect will not be clearly reflected on χT vs T plot if the population-depopulation effect is negligible. The EPR is more informative than magnetic susceptibility measurements when the electronic interactions at the fine levels are concerned.

For a monoradical one set of EPR resonance [due to allowed ($\Delta m_s = \pm 1$) transition only (Figure 1a)] is obtained while two sets of EPR signals are a triplet diradical [due to both allowed ($\Delta m_s = \pm 1$; $m_s = -1 \rightarrow 0$ and $0 \rightarrow +1$) and forbidden ($\Delta m_s = \pm 2$; $m_s = +1 \rightarrow -1$ and $m_s = -1 \rightarrow +1$) transitions] (Figure 1b). When three energy levels are degenerate under zero applied magnetic field, two resonances (Figure 1b) are observed for a triplet diradical.

The dipolar coupling between two electronic spins in triplet diradicals produces an internal magnetic field which split the energy level into three levels under zero applied magnetic fields. Three resonance absorptions are obtained for triplet states in a rigid solid state (Figure 1c; m). Two resonances (signal-1 and signal-2; Figure 1c) are observed due to $\Delta m_s = \pm 1$ transition while third resonance (signal-3; Figure 1c) is originated due to $\Delta m_s = \pm 2$ transition (half-field signal). This suggests that the three energy levels (as shown in Figure 1c) are not energetically degenerate even when the external magnetic field is switched off.

The features of the EPR signal are changed if zero-field splitting (zfs) parameters D and E are introduced in the system. The two zero-field splitting parameters are determined from triplet EPR signals (Figure 1c; n,p). Two allowed transitions are expected to originate as six lines for a genuine triplet species because of the three magnetic axes of x , y , and z (Figure 1c; n).

The zero-field splitting is derived from the dipole-dipole interaction and D is related to the distance r between the two unpaired electrons. The value of D can be used to calculate the average distance r between the two unpaired electrons by the point-dipole approximation;^{14c-d} $D = 1.39 \times 10^4 (G/r^3)$. D is given in Gauss (G), and r is in angstroms (\AA). The distance ($< 10 \text{\AA}$) between two spins can be determined from the above mentioned relation and can be correlated with the experimental distance. When the distance between the two spin centers is greater than 10\AA , the signal intensity corresponding to the forbidden transition ($\Delta m_s = \pm 2$) becomes extremely weak or vanishes. The resonance signal of $\Delta m_s = \pm 2$ might be absent when the D value is small ($D < 25 \text{ G}$). Thus, detection of the EPR signal due to forbidden transition ($\Delta m_s = \pm 2$) can confirm the genuine triplet state of a diradical species. The zfs parameter E is significantly related to the symmetry of two electrons in a triplet species. Two triplet sublevels of E_x and E_y are degenerate for a molecular structure with 3-fold or higher symmetry. Consequently, the EPR signal of the allowed transitions (signal-1 and signal-2) will look like as shown in Figure 1c,p and the numerical value of D can be evaluated.

It also has been established that, at short distances or in delocalized systems, the validity of the point-dipole approximation is not good enough for correlating the D value to the inter spin-spin distance (r).^{14e-f} When the two electronic spins have a large separation with a small D value, the half-

field signal ($\Delta m_s = \pm 2$) might not be observed. Thus, it is not easy to unambiguously distinguish between triplet and doublet signals using continuous-wave (cw) EPR spectroscopy. In that case measurement of the two-dimensional electron spin transient nutation (2D-ESTN) utilizing a pulsed EPR spectrometer is a powerful tool for the determination of the spin multiplicity of high-spin molecules. The nutation frequency (ω_{NT}) depends on the spin-quantum number S by the equation $\omega_{\text{NT}} = [S(S+1) - m_s(m_s)]^{1/2} \omega_1$, where ω_1 is the strength of the magnetic field of the microwave irradiation field.^{14g}

Other than EPR, negative-ion photoelectron spectroscopy (NIPES) is a useful method for studying the physical properties of highly reactive intermediates. A beam of mass-selected negative ions (R^-) is intersected with an intense laser beam in gas-phase experiments. When a photodetachment of an electron occurs, a neutral reactive intermediate is generated. The plot of the number of photodetached electrons as a function of electron binding energy gives the electron affinity and energies of the electronic states of the neutral intermediate. Additional quantum chemical calculations and combined with experimental results produce important information on the structure and electronic configuration of the intermediate species. The photoelectron spectrum of the negative anion of an open-shell molecule provides valuable information on the $E_{\text{singlet-triplet}}$ energy gap. A radical anion yields both singlet and triplet states of the neutral open-shell molecules in the photoelectron spectrum and hence the $E_{\text{singlet-triplet}}$ energy gap can be experimentally obtained.^{14h}

Diradicaloid: When the electronic interactions between two radical centers within a molecule are very strong they are called diradicals. Singlet diradicals generally exhibit a relatively small energy gap between their lowest energy singlet and triplet states. The stability of diradicals is increased with the increasing HOMO-LUMO energy gap which leads to a larger singlet-triplet separation. When the value of occupation of the LUMO of the molecule reaches zero, they are rationalized as closed-shell molecules. Thus they are not referred as diradical or diradicaloid. However, the occupation of the LUMO is not negligible for diradicaloids¹⁴ⁱ due to the small HOMO-LUMO energy gap. Diradicaloids are comparatively more reactive than closed-shell molecules.^{14j}

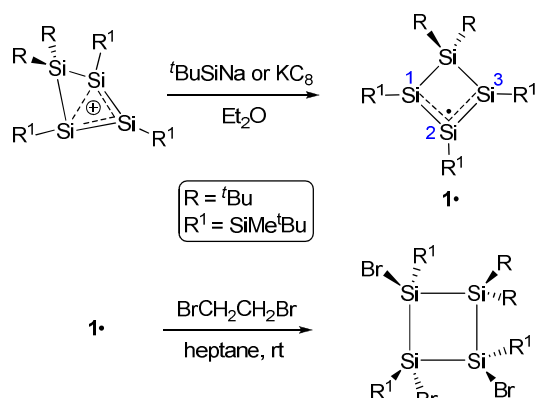
There are several theoretical methods¹⁵ for computationally study of the radicals, diradicals and diradicaloids. The $E_{\text{singlet-triplet}}$ can be also theoretically calculated. There are some limitations of different level of theories. However, they are extremely helpful to study bond and spin density distribution of these species.

In this review, we will first discuss the effect of bulky organic ligands on the stabilization of several silicon centered stable radicals and radical ions and then we will focus on how π -accepting cyclic alkyl(amino) carbenes (CAACs) can be utilized as neutral mono-dentate ligands for the stabilization of radical, radical ions, diradical, and diradicaloid species. We will also highlight some of the radical and radical ions which have been stabilized by σ -donating N-heterocyclic carbenes (NHCs). The

stability and bonding of those compounds will also be discussed.

RESULT AND DISCUSSION

Silicon being the sister element of carbon has attracted huge research interest for the past four decades. The syntheses and characterizations of several silicon containing compounds have been reported so far.¹⁵⁻³⁰ However, radicals containing silicon functional group are limited in number.³⁰ Silicon centered radicals known as silyl radicals are the open shell species bearing an unpaired electron on the silicon atom. They act as reactive intermediates in numerous organometallic transformations and their existence have long been speculated through spectroscopic characterizations.³¹ Although, persistent silyl radicals stabilized by bulky groups³² have been reported almost three and a half decades ago, it was only in 2001 when stable and isolable silyl radicals were successfully synthesized for the first time by Sekiguchi et al.³³ (Scheme 1, top). In their report, initially the precursor cyclotetrasilenylium cation ($\mathbf{1}^+$) was synthesized by reacting tetrakis[di-*tert*-butyl(methyl)silyl]cyclotrisilene with $[\text{Et}_3\text{Si}(\text{benzene})]^+\text{TPFPB}^-$ (TPFPB⁻ = tetrakis(pentafluorophenyl) borate).³⁴ The successive one electron reduction of $\mathbf{1}^+$ at room temperature (rt) with a bulky trialkylsilylsodium reagent ${}^t\text{Bu}_3\text{SiNa}$ in diethyl ether results in the formation of the first stable cyclotetrasilenylium radical ($\mathbf{1}\cdot$) in 67% yield.³³

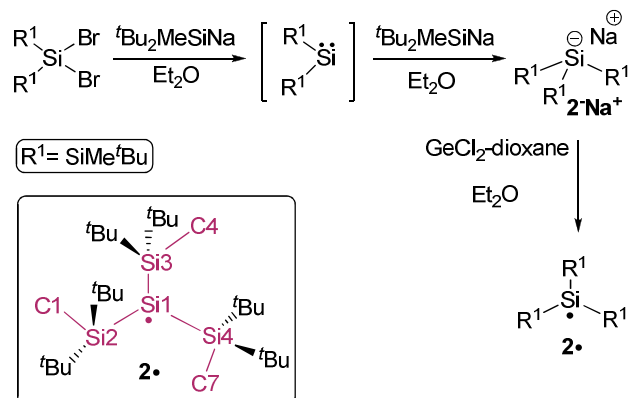


Scheme 1. Synthesis and reactivity of cyclotetrasilenylium radical ($\mathbf{1}\cdot$) (top) and its reaction with $\text{BrCH}_2\text{CH}_2\text{Br}$ (bottom).

The same product is also obtained by using KC_8 as the reducing agent with a much increased yield of 83%. X-ray single crystal analysis on $\mathbf{1}\cdot$ reveals that the four-membered ring in $\mathbf{1}\cdot$ is nearly planar with a very small dihedral angle of 4.7° between the $\text{Si}1\text{-Si}2\text{-Si}3$ and $\text{Si}1\text{-Si}4\text{-Si}3$ planes. This is in marked contrast with the cationic precursor $\mathbf{1}^+$ which has a large corresponding dihedral angle of 46.6° . Although $\mathbf{1}\cdot$ is best represented as an allyl type radical, the $\text{Si}1$, $\text{Si}2$, and $\text{Si}3$ atoms in it are not exactly symmetrical. While $\text{Si}1$ and $\text{Si}2$ have a planar geometry, the $\text{Si}3$ atom has slightly pyramidal geometry. A similar trend is also observed in case of the bond lengths. The $\text{Si}1\text{-Si}2$ [$2.226(1)$ Å] is found to be slightly shorter

than $\text{Si}2\text{-Si}3$ [$2.263(1)$ Å] and are in-between the $\text{Si}=\text{Si}$ double bond [$2.174(4)$ Å] and the Si-Si single bond [$2.349(4)\text{-}2.450(4)$ Å] found in the previously reported four-membered ring of hexakis-(*tert*-butyldimethylsilyl)cyclotetrasilene.³⁵ The interatomic distance between $\text{Si}1$ and $\text{Si}3$ is found to be [$3.225(2)$ Å] indicating the absence of any 1,3-orbital interaction. The radical character of $\mathbf{1}\cdot$ is confirmed by the EPR resonances observed both in the solid state and in a dilute *n*-heptane solution of $\mathbf{1}\cdot$. The crystalline sample of $\mathbf{1}\cdot$ exhibits an intense EPR signal with a comparable *g* value of 2.0058 found in case of the typical tris(trialkylsilyl)silyl radicals (2.0053-2.0063).³¹⁻³² The typical allylic nature of the cyclotetrasilenylium radical is concluded by assigning the larger hyperfine coupling constants (at 40.7 and 37.4 G) to the coupling of the radical electron with the terminal ${}^{29}\text{Si}1$ and ${}^{29}\text{Si}3$ nuclei and the relatively smaller hyperfine coupling constant (at 15.5 G) to the coupling with the central ${}^{29}\text{Si}2$ nucleus. This in turn supports the typical delocalization of the unpaired electron in the allylic radical $\mathbf{1}\cdot$ over the two terminal silicon atoms. The reactivity of this unprecedented silyl radical is also studied by treating $\mathbf{1}\cdot$ with 1,2-dibromoethane. The tribrominated product of $\mathbf{1}\cdot$ is obtained in 79% yield (Scheme 1, bottom).

Soon after the synthesis report of the first silyl radical stabilized by delocalization, the first air stable silyl radical without any π -conjugation is prepared by the same research group.³⁶ It is the first example of an air stable silyl radical. The straightforward synthesis of this air stable silyl radical follows three consecutive steps. In the first step bis[di-*tert*-butyl(methyl)silyl]dibromosilane is reacted with di-*tert*-butyl(methyl)silylsodium in di-ethyl ether at room temperature to *in situ* generate the corresponding intermediate carbene species [$(\text{R}^1)_2\text{Si}:$]. This upon treatment with another equiv of the reducing agent produces the corresponding sodium salt of tris[di-*tert*-butyl(methyl)silyl]silyl anion $\mathbf{2}^-\text{Na}^+$. The one electron oxidation of the *in situ* generated anion $\mathbf{2}^-$ with germanium(II)dichloride-dioxane complex at room temperature results in the formation of the stable tris[di-*tert*-butyl(methyl)silyl]silyl radical $\mathbf{2}\cdot$ (Scheme 2) in 44% yield.³⁶



Scheme 2. Synthesis of tris[di-*tert*-butyl(methyl)silyl]silyl radical ($\mathbf{2}\cdot$).

The single crystal X-ray analysis of **2** \cdot reveals that Si1 adopts planar geometry and is surrounded by three bulky electropositive per-silyl substituents (Scheme 2, bottom). The presence of the bulky and electropositive substituents leads to the lowering of the inversion barrier at Si1 radical center resulting in a planar geometry. All the methyl groups present at Si1-Si4 are found to be arranged in a “gear”-type fashion where the C_{Me} atoms are located in the same plane of Si1-Si2-Si-3-Si4 (Scheme 2 and Figure 2) which could effectively minimize the steric strain of the molecule. This special arrangement without any doubt contributed extra stability by the delocalization of the radical electron over the σ^* orbitals of the planar Si-C bonds. The EPR spectroscopy reveals that this specific planar arrangement of the radical **2** \cdot is also present in solution.³⁶ The EPR spectrum of an *n*-hexane solution of **2** \cdot at rt exhibits a strong signal with the *g* value of 2.0056 which is comparable to that of a typical persilyl-substituted Si-centered radical (2.0050-2.0063).³² The two pairs of satellites observed in the EPR spectrum can be attributed to the coupling of the radical electron with the two different sets of ²⁹Si nuclei (*I* = 1/2). The satellites with larger value of the hyperfine coupling constant [$\alpha(^{29}\text{Si}) = 58.0$ G] could be assigned to the coupling of the radical electron with the central Si1 nucleus, and the satellites with much smaller hyperfine coupling constant [$\alpha(^{29}\text{Si}) = 7.9$ G] could be assigned to that with the Si atoms of the three substituents (Si2, Si3, and Si4). The small value of the hyperfine coupling constants observed for **2** \cdot signifies that the radical electron resides in an orbital with a higher degree of p-character, predominantly indicating a planar sp² hybridized Si-centered π -radical. The highly reactive tris[di-*tert*-butyl(methyl)silyl]silyl radical (**2** \cdot) produces the corresponding halogenated products in almost quantitative yields upon treatment with carbon tetrachloride, 1,2-dibromoethane, and benzyl bromide.³⁶

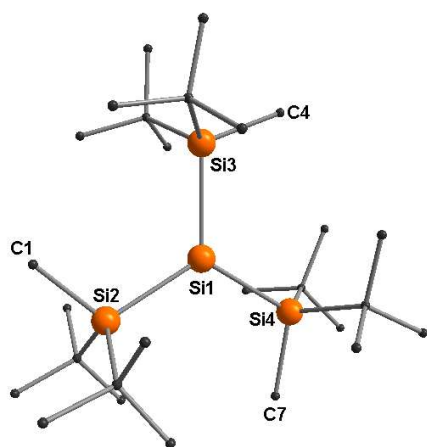
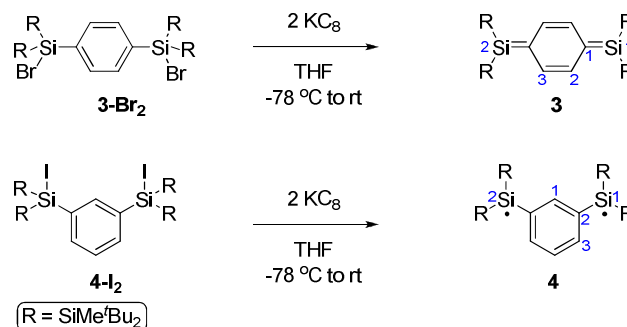


Figure 2. Molecular structure of tris[di-*tert*-butyl(methyl)silyl]silyl radical (**2** \cdot).

The *para*- and *meta*-quinodimethane derivatives are well known in the literature as the carbon centered radicals, where the *para*- isomer possesses a singlet ground state with a closed-shell quinoid form³⁷ and the *meta*-isomer possesses a

triplet ground state.³⁸ The synthesis of the higher analogues of these group 14 compounds with two or more radical centers has been elusive until Sekiguchi et al. reported the syntheses and characterization of the isomeric *para*- and *meta*-disilaquinodimethanes in 2011 (Scheme 3).³⁹



Scheme 3. Synthesis route of disilaquinodimethane (**3**) and bis(silyl radical) (**4**).

When the 1,4-bis(bromosilyl)benzene derivative (**3-Br**₂) is treated with two equiv of KC₈ in THF at -78 °C a dark purple solution of 3,6-bis[bis(di-*tert*-butylmethylsilyl)silylidene]cyclohexa-1,4-diene (**3**) is produced (Scheme 3) in 23% yield.

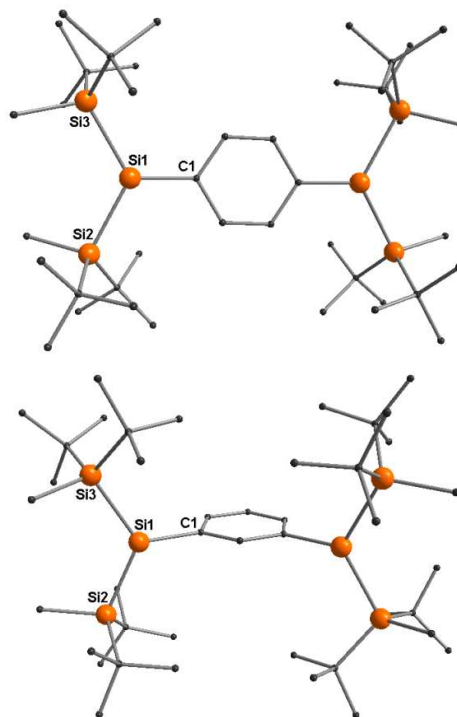


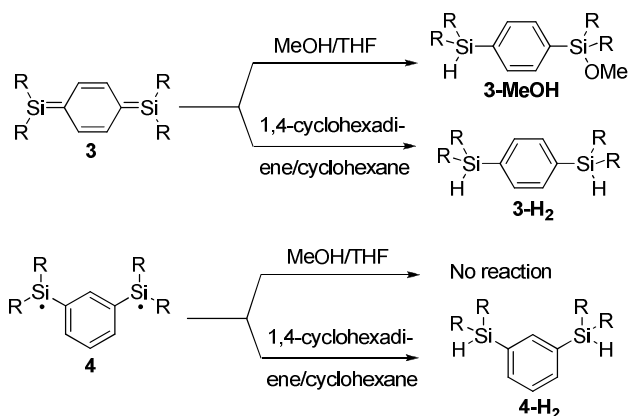
Figure 3. Molecular structures of diradicaloid (**3**) (top) and diradical (**4**) (bottom).

The X-ray single crystal diffraction shows that the Si1 center of **3** adopts a trigonal planar geometry (Figure 3, top). The co-

planarity of the 3p orbital of Si and the 2p orbital C atom of the six-membered aromatic ring suggests an effective π -conjugation between these two orbitals ensuring a closed-shell quinoid structure. The Si1-C1 bond [1.8174(14) Å] is found to be shorter than the typical Si-C_{sp2} single bond (1.879 Å), but longer than the Si=C bonds (1.702-1.775 Å). The ²⁹Si NMR spectrum of **3** shows the resonances at 91.1 ppm. The bond parameters suggest that **3** features two silicon-carbon double bonds. Compound **3** has a 1,4-quinoid structure with a smaller contribution of a singlet bis(silyl radical) character. The UV-vis absorption band of **3** observed at 555 nm.

Similarly, when the 1,3-bis(iodosilyl)benzene derivative (**4-I₂**) is treated with two equiv of KC₈ under the comparable reaction condition as employed for the *para*-analogue, light yellow crystals of 1,3-bis[bis(di-*tert*-butylmethylsilyl) silyl]benzene-1',1''-diyl (**4**) are obtained (Scheme 3) in 29% yield. The UV-vis absorption bands are observed at 433 and 413 nm. The single crystal X-ray diffraction of **4** reveals that although the Si1 and Si2 centers attain a near trigonal planar geometry, The Si-3p and C_{aryl}-2p orbitals are orthogonal to each other, hence preventing their overlap. The Si1-C2 and Si2-C2' bond lengths are found to be 1.9108(19) Å, showing a normal Si-C single bond. The C-C bond distances within the six-membered ring also indicate a typical aromatic ring structure. According to these experimentally obtained bond parameters and the theoretically obtained results, it can be easily concluded that **4** is a *m*-phenylene bridged bis(silyl radical) (Figure 3, bottom). Computational studies reveal that the triplet ground state is energetically more favourable than the singlet state by 20 Kcal mol⁻¹ energy. The EPR spectrum of a solution of **4** in 3-methylpentane at 80 K exhibits the characteristic signal with six hyperfine lines at 3352 G ($g = 2.0034$) due to allowed ($\Delta m_s = \pm 1$) transition. The zero field splitting parameters are found to be $D = 6.4 \times 10^{-3} \text{ cm}^{-1}$ (at 138 G) and $E = 0.80 \times 10^{-3} \text{ cm}^{-1}$ (at 17.2 G). Considering the point dipole approximation, the calculated distance between the unpaired electrons in **4** is found to be 5.89 Å, which is close to the value (5.72 Å) obtained from the X-ray crystal structure. These values prove that the two unpaired electrons in **4** reside mainly on the two silicon atoms. Another weak signal which appears exactly at the half field 1674 G confirms the triplet diradical ground state of **4** due to forbidden ($\Delta m_s = \pm 2$) transition.

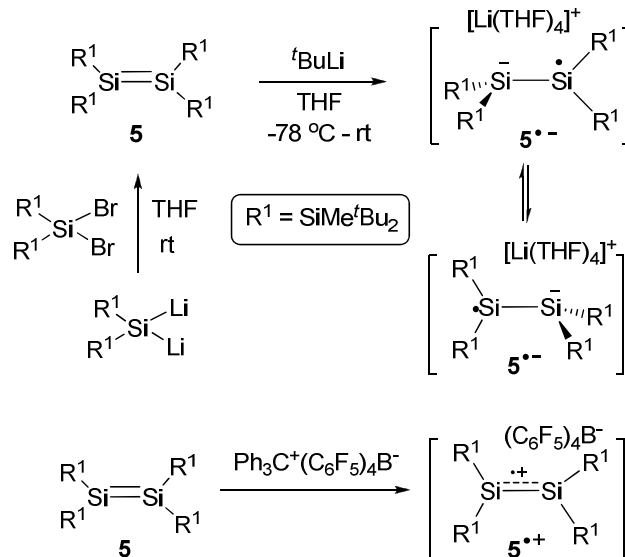
These major structural differences in **3** and **4** are also reflected in their reactivity patterns (Scheme 4). While **3** reacts with both MeOH, and 1,4-cyclohexadiene to produce quantitatively the desired 1,6-adduct **3-MeOH** and the hydrogen-abstraction product **3-H₂**, respectively; **4** fails to react with MeOH which is known as a typical reagent for silene. However, **4** reacts quantitatively with the hydrogen donor 1,4-cyclohexadiene to produce the *m*-bis(hydrosilyl)benzene **4-H₂** indicating its bis(silyl radical) nature.



Scheme 4. Reactivity of *para*- and *meta*-[(^tBu₂MeSi)₂Si]₂C₆H₄ (**3** and **4**) towards MeOH and 1,4-cyclohexadiene.

DISILENE AND DISILYNE RADICAL ANIONS

In 2004, Sekiguchi et al. reported the synthesis and characterization of a red colored disilene radical anion **5^{•-}** in the form of its lithium salt via the one-electron reduction of the dark blue colored tetrakis(di-*tert*-butylmethylsilyl)disilene **5** by ^tBuLi (1.2 equiv) in THF (Scheme 5).^{40a}



Scheme 5. Synthesis strategy of tetrakis(di-*tert*-butylmethylsilyl)disilene radical anion (**5^{•-}**) (top) and cation (**5^{•+}**) (bottom).

The X-ray crystal structure analysis of **5^{•-}** reveals a near orthogonal arrangement along the Si1-Si2 bond. The EPR spectrum of a solution of **5^{•-}** in 2-methyltetrahydrofuran is measured at rt which exhibits a strong signal ($g = 2.0061$). Additionally, the pair of satellites observed is corroborated to the coupling of the unpaired electron with the ²⁹Si nuclei having the hyperfine coupling constant of $\alpha(^{29}\text{Si}) = 24.5 \text{ G}$. This value is half of that observed in the case of tris(di-*tert*-

butylmethylsilyl)silyl radical (58.0 G).³⁶ Based on these observations, it is assumed that a rapid spin exchange occurs between Si1 and Si2 atoms in the solution. The EPR spectrum measured in the solid state at 120 K exhibits a pair of satellites with a coupling constant of 45 G indicating the suppression of the spin exchange at lower temperature.^{40b}

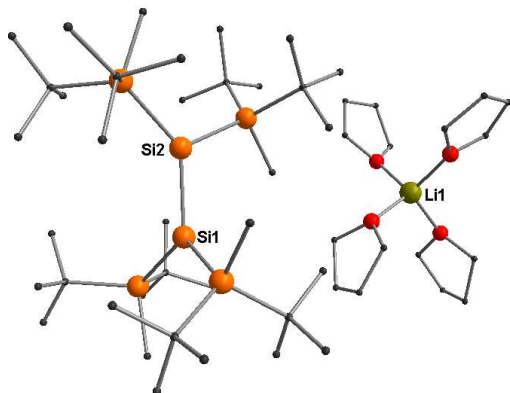


Figure 4. Molecular structure of disilene radical anion $[5^{\bullet-}][Li(OTf)_4]^+$.

The radical cation $5^{\bullet+}$ is obtained via abstraction of one electron from compound **5** by trityl cation (Ph_3C^+) in toluene (Scheme 4, bottom). The disilene cation radical $5^{\bullet+}$ is isolated as air and moisture sensitive borate $[(C_6F_5)_4B^-]$ salt in 65% yield.^{40c} It has been characterized by X-ray single crystal diffraction (Figure 4). The central Si-Si bond length and its twisting angle of neutral **5** are 2.2598(18) Å and 54.5°, respectively while the corresponding values of cation $5^{\bullet+}$ are 2.307(2) Å and 64.9°, respectively. This suggests that Si-Si bond distance increases after the one-electron oxidation. The geometry around the Si1 and Si1' atoms of $5^{\bullet+}$ is nearly planar. This is in significant contrast to the disilene anion radical $5^{\bullet-}$ with twisting angle 88° and the Si-Si bond distance of 2.341(5) Å. The unpaired electron and negative charge in $5^{\bullet-}$ cause the bond rotation around the central Si-Si bond (Scheme 4).

The EPR spectrum of $5^{\bullet+}$ measured^{40c} in the range of 298 to 200 K in fluorobenzene exhibited a resonance at $g = 2.0049$, having a pair of satellite signals (23.0 G) due to coupling of the unpaired electron with the central ^{29}Si nuclei. This coupling constant is less than half that of the similar $(tBu_2MeSi)_3Si\cdot$ (58.0 G), suggesting the radical electron is delocalized over two silicon centers. In contrast the radical electron of $5^{\bullet-}$ ^{40a} shows a rapid spin exchange between the two central Si atoms on the EPR time scale, featuring a sp^3 -silyl anion and a sp^2 -silyl radical.

Following a comparable synthesis strategy to that of $5^{\bullet-}$, the disilyne radical anion $6^{\bullet-}$ with the potassium counter cation^{40d} is prepared and characterized by X-ray crystallography and EPR measurements in 2007 (Scheme 6, Figure 5).

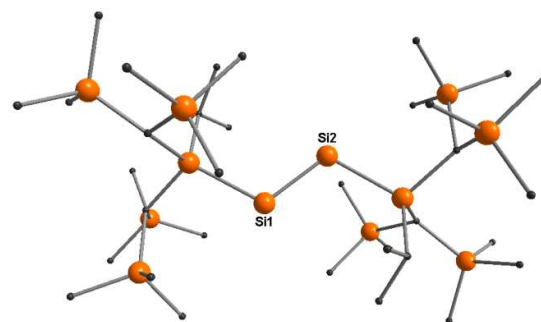
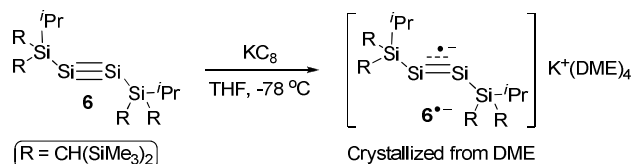


Figure 5. Molecular structure of disilyne radical anion $[6^{\bullet-}][K(DME)_4]^+$. The cation $[K(DME)_4]^+$ is omitted for clarity.



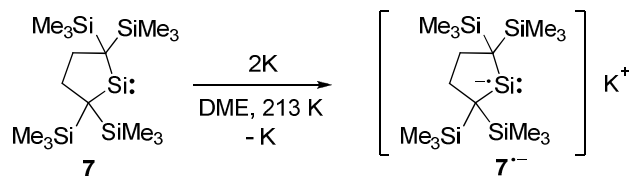
Scheme 6. Synthesis strategy of disilyne radical anion ($6^{\bullet-}$).

The reaction of the disilyne **6**^{30b} containing two bulky substituents, $Si^iPr[CH(SiMe_3)_2]$ groups at the triply bonded silicon atoms with one equiv of KC_8 in THF at $-78^\circ C$ results in the formation of the corresponding disilyne radical anion $6^{\bullet-}$. It is crystallized from pentane and 1,2-dimethoxyethane (DME) as dark brown crystals in 63% yield. The EPR spectrum of $6^{\bullet-}$ exhibits a triplet resonance with two pairs of satellites arising from the coupling with ^{29}Si . The experimentally obtained g value ($g = 1.99962$) is found to be the smallest for any reported silicon centered radicals till now.^{31b}

SILYLENE RADICAL ANIONS AND RADICAL CATIONS

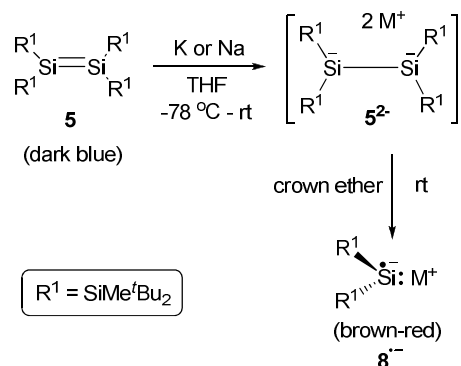
Since early 1970s, the radical ions of carbenes and their analogues have been suggested as the reactive intermediates in redox reactions of diazo compounds both in the liquid and in the gas phases.⁴¹ In recent years, the heavier group 14 analogues of carbenes known as the metallylenes and their corresponding radical ions have attracted huge interest of the scientific community. The isolation and structural characterization of the metallylene radical ions are highly challenging due to their very high reactivity. Although the existence of several group 14 element-centered radical anions $R_2E^{\bullet-}$ ($E = Ge, Sn$) have been long ago synthesized and characterized by EPR spectroscopy.⁴² The characterization of silylene radical anions in solution has not been reported until Kira et al. published the synthesis of persistent dialkylsilylene radical anion **7**^{•-} via the one electron reduction of 1,2-dilithiodisilane **7** using two equiv of KC_8 in THF at 213 K (Scheme 7).⁴³ The EPR spectrum of the *in situ* generated

radical anion is recorded at 213 K which reveals its unique structural characteristics. Radical anion $7^{\bullet-}$ is stable at $-70\text{ }^\circ\text{C}$ in DME but decomposes rapidly at rt with a half-life time of 20 min.⁴³



Scheme 7. Generation of persistent dialkylsilylene radical anion $7^{\bullet-}$.

The first isolable silylene radical anion ($8^{\bullet-}$) is reported in 2007⁴⁴ by reacting the disilene **5** (dark blue) with 2.2 equiv of lithium naphthalenide in THF at $-78\text{ }^\circ\text{C}$ and treating the resultant dark red solution with 4.3 equiv of 12-crown-4 (Scheme 8).

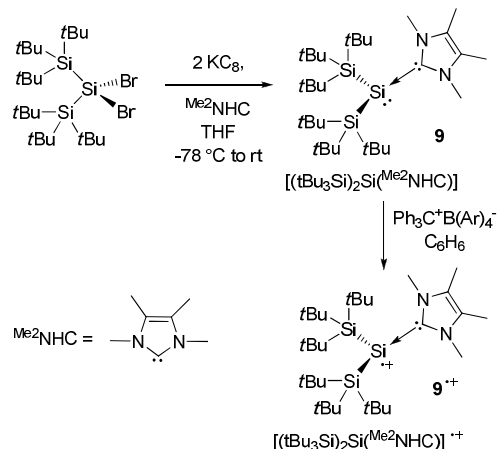


Scheme 8. Generation of persistent dialkylsilylene radical anion ($8^{\bullet-}$).

The air and moisture sensitive red crystals of bis(*di-tert*-butylmethylsilyl) silylene anion radical 5^{2-} are isolated as the corresponding lithium salt in 56% yield (Scheme 8). Mechanistically, the reaction is proposed to proceed via the initial formation of the 1,2-dianionic species $(^t\text{Bu}_2\text{MeSi})_2\text{Si}(\text{Li})\text{Si}(\text{Li})(\text{SiMe}^t\text{Bu}_2)_2$ upon reduction which undergoes dissociation on further treatment with the crown ether to produce the corresponding radical anion $8^{\bullet-}$.⁴⁴ The formation of the 1,2-dianionic species can be also established by NMR spectroscopy. The structure of 5^{2-} in the solid state is characterized by X-ray single crystal diffraction. The EPR spectrum of a dilute solution of 5^{2-} in THF shows signals ($g = 2.0074$) with two sets of satellites due to the coupling with ^{29}Si nuclei. No hyperfine coupling with the lithium atom was observed suggesting the formation of a metal-free silylene radical anion. However, the EPR spectrum of the sodium salt of the radical anion ($5^{2-}2\text{Na}^+$) in toluene at rt exhibits a well resolved quartet ($g = 2.0074$) which could be attributed to the coupling with ^{23}Na nucleus ($I = 3/2$) with hyperfine coupling constant of $\alpha(^{23}\text{Na}) = 1.9\text{ G}$. This indicates the presence of a Si-Na bond in case of $5^{2-}2\text{Na}^+$. The two sets of satellite signals observed are due to coupling with the ^{29}Si nuclei. When the

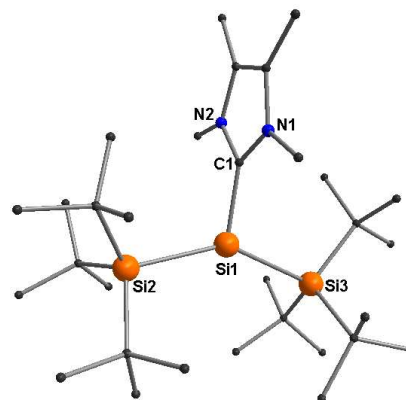
EPR spectrum of $5^{2-}2\text{Na}^+$ is recorded in polar solvents like THF, the quartet signal disappears. This indicates that a shift from the contact ion pair structure to the solvent separated ion-pair structure has occurred due to the polarity of the particular solvent. Detection of a radical cation (diphenylcarbene radical cation) in solution by EPR spectroscopy was first accomplished in 1993.⁴⁵ Both the radical anions $7^{\bullet-}$ and $8^{\bullet-}$ are not characterized by X-ray single crystal diffraction due to short lifetimes of former and poor crystalline nature of the later.

The silylene radical cations are rarely characterized. Silylene radical cation $\text{H}_2\text{Si}^{\bullet+}\cdots\text{H}_2$ can be considered as a hydrogen complex of the parent $\text{H}_2\text{Si}^{\bullet+}$ species.⁴⁶ It is generated under neon matrix deposition at 4 K by the photoionization of SiH_4 .



Scheme 9. Synthesis routes of $[(^t\text{Bu}_3\text{Si})_2\text{Si}(\text{Me}^2\text{NHC})]^{\bullet+}\text{B}(\text{Ar})_4^-$ ($9^{\bullet+}\text{B}(\text{Ar})_4^-$).

In 2012 Sekiguchi et al. reported the synthesis of NHC stabilized silylene radical cation $[(^t\text{Bu}_3\text{Si})_2\text{Si}\leftarrow\text{Me}^2\text{NHC}]^{\bullet+}(\text{Ar}_4\text{B})^-$ ($9^{\bullet+}$)(Ar_4B)⁻ (Scheme 9). The dibromosilane $(^t\text{Bu}_3\text{Si})_2\text{SiBr}_2$ is treated with two equiv of KC_8 in the presence of Me^2NHC in THF. The orange crystals of the silyl substituted silylene-NHC complex $(^t\text{Bu}_3\text{Si})_2\text{Si}:\leftarrow\text{Me}^2\text{NHC}$ (**9**) is obtained in 43% yield. When a mixture of **9** and one equiv of $\text{Ph}_3\text{C}^+\text{Ar}_4\text{B}^-$ ($\text{Ar}_4\text{B}^- = \text{tetrakis}[4-(\text{tert}-\text{butyldimethylsilyl})-2,3,5,6\text{-tetrafluorophenyl}]\text{-borate}$) have been reacted stable radical cation $9^{\bullet+}$ is formed in 83% yield.



ARTICLE

Journal Name

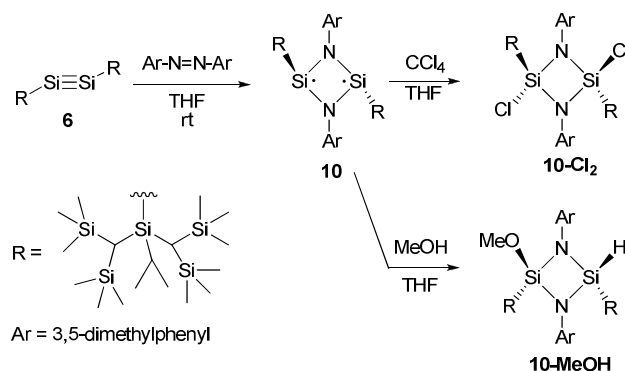
Figure 6. Molecular structure of $[(t\text{-Bu}_3\text{Si})_2\text{Si}(\text{Me}_2\text{NHC})]^{+\bullet}\text{B}(\text{Ar})_4^-$. H-atoms and $\text{B}(\text{Ar})_4^-$ group are omitted for clarity.

Cation $\mathbf{9}^{+\bullet}$ is structurally characterized by the single crystal X-ray analysis (Figure 6). The central silicon atom of $\mathbf{9}^{+\bullet}$ adopts a planar three coordinate geometry. The five-membered NHC ring and the $\text{Si}_2\text{-Si}_1\text{-Si}_3$ plane are found to be nearly perpendicular to each other. The $\text{Si}_1\text{-C}_{\text{NHC}}$ bond length in $\mathbf{9}^{+\bullet}$ is 1.915(3) Å which is slightly shorter than that in the precursor $\mathbf{9}$ [1.933(4) Å]. This indicates an increase in the s character of the $\text{Si}_1\text{-C}_{\text{NHC}}$ bond resulting from the change in hybridization of the central silicon atom. The comparatively larger $\text{Si}_1\text{-Si}_2$ and $\text{Si}_1\text{-Si}_3$ bond lengths in $\mathbf{9}^{+\bullet}$ [2.4664(11) and 2.4659(10) Å, respectively] than those in $\mathbf{9}$ [2.4542(15) and 2.4419(14) Å, respectively] can be explained by the steric repulsion between the two extremely bulky $t\text{-Bu}_3\text{Si}$ groups which suppress any bond shortening. The NBO analysis at the level of (U)B3LYP/6-31G(d) for compounds $\mathbf{9}$ and $\mathbf{9}^{+\bullet}$ suggests that an electron is removed from the lone pair of the silylene $\mathbf{9}$ upon oxidation resulting in a change in geometry from the pyramidal to a planar structure in $\mathbf{9}^{+\bullet}$. This also shows that the spin density in $\mathbf{9}^{+\bullet}$ is mainly located on the tricoordinate silicon atom. The EPR spectrum of a benzene solution of $\mathbf{9}^{+\bullet}$ recorded at rt exhibits a quintet with a g value of 2.00466. The nature of this spectrum can easily be attributed to the coupling of the radical electron with two ^{14}N nuclei ($I = 1$) of the NHC with a hyperfine coupling constant of $\alpha(^{14}\text{N}) = 2.6$ G. The satellite signals with a hyperfine coupling constant of $\alpha(^{29}\text{Si}) = 71.6$ G are observed due to the coupling of the radical electron with the central Si1 nucleus.

DIRADICALOIDS

The organic diradicals are very often too unstable to be isolated.^{48a,c} However, there are some examples of stable organic diradicals.⁴⁸ Although the heavier congeners of the group 14 element centered diradicals are reported by Lappert⁴⁹ and Power⁵⁰ in 2004, the syntheses of the analogous silicon compounds remain challenging until 2011. The dark purple colored singlet diradicaloid species $\text{RSi}(\mu\text{-NAR})_2\text{SiR}$ ($\mathbf{10}$) was first synthesized in 58% yield when the disilylene $\mathbf{6}$ slowly reacts with *trans*-3,3',5,5'-tetramethylazobenzene in THF at room temperature under light-shielded condition. The reaction is faster (complete in 5 min) and the same compound is isolated when $\mathbf{6}$ is reacted with *cis*-3,3',5,5'-tetramethylazobenzene. The chemical shift value of the skeletal silicon has been observed at 19.4 ppm. The UV-vis absorption band at 529 nm in *n*-hexane corresponds to its blue color (HOMO-1 \rightarrow LUMO, HOMO \rightarrow LUMO). Compound $\mathbf{10}$ possesses a perfectly planar centrosymmetric four-membered Si_2N_2 ring with both the silicon atoms having a pyramidal geometry (Figure 7, top). The Si-Si bond length of the Si_2N_2 ring is 2.6380(9) Å which is significantly longer than a normal Si-Si single bond length (2.341 Å). Theoretical calculations show that the compound $\mathbf{10}$ has a singlet diradicaloid spin ground state. The singlet-triplet energy gap is 12.8 Kcal mol⁻¹. The calculated frontier orbitals of $\mathbf{10}$ include the four π -orbitals with six π -electrons in the cyclic Si_2N_2 ring corresponding to

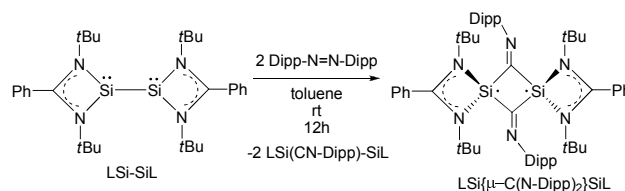
6 π -aromatic character. The HOMO is generated by a nonbonding combination of silicon centered radical electrons. The HOMO-1 and LUMO correspond to the bonding and antibonding π -orbitals, respectively of the four-membered Si_2N_2 ring.



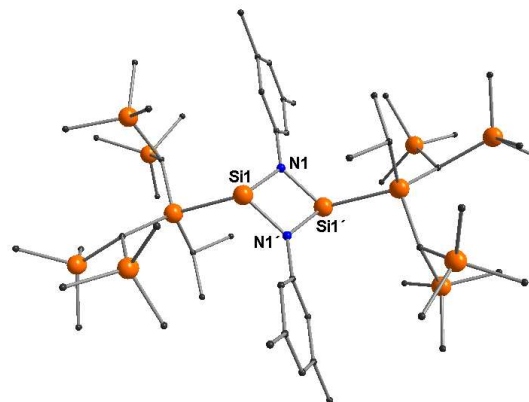
Scheme 10. Synthesis routes of diradicaloid $\mathbf{10}$ and its reaction with CCl_4 and MeOH.

Carbon tetrachloride is well known as a silyl radical scavenger. Compound $\mathbf{10}$ also reacts with CCl_4 to give the colorless dichlorinated *trans*-product $\mathbf{10}\text{-Cl}_2$ in 55% yield. $\mathbf{10}$ also reacts with methanol to produce the corresponding *cis*-product $\mathbf{10}\text{-MeOH}$ in 65% yield (Scheme 10). Both of these reactions confirmed the 1,3-diradical character of $\mathbf{10}$.⁵¹

The bis-silylene LSi-SiL [$\text{L} = \text{PhC}(\text{N}^t\text{Bu})_2$] reacts with Dipp-N=N-Dipp [$\text{Dipp} = 2,6\text{-diisopropylphenyl}$] to produce the yellow-brown crystals of diradical $\text{LSi}(\mu\text{-C}(\text{N-Dipp})_2)_2\text{SiL}$ ($\mathbf{11}$) in 25.7% yield (Scheme 11; Figure 7, top).



Scheme 11. Synthesis route of $\text{LSi}(\mu\text{-C}(\text{N-Dipp})_2)_2\text{SiL}$ ($\mathbf{11}$) from LSi-SiL .



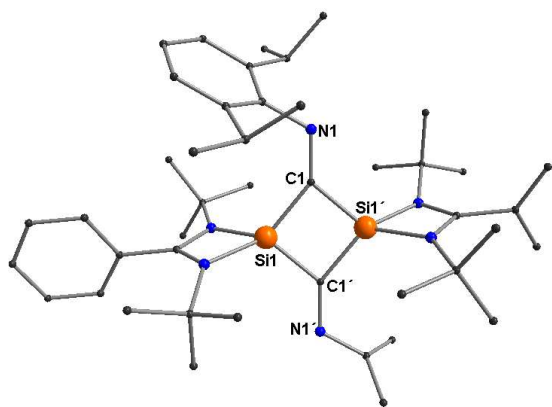


Figure 7. Molecular structures of diradicaloid **10** (top) and LSi{μ-C(N-Dipp)}₂SiL (**11**) (bottom).

The resonance of ²⁹Si NMR is observed as a singlet at -39.9 ppm. Theoretical calculations show that the singlet is the ground state of LSi{μ-C(N-Dipp)}₂SiL (**11**) while the triplet state is 30.1 Kcal mol⁻¹ higher in energy. The radical electrons are delocalized in the four-membered Si₂C₂ ring (Figure 7, bottom) and additionally conjugated with two central exo-cyclic C=N double bonds. The Si-Si bond length is 2.553(2) Å which is significantly larger than that of the precursor LSi-SiL (2.413(2) Å).⁵²

cAAC-SILICON COMPOUNDS

Stable singlet N-heterocyclic carbene (NHC)²⁶ has been synthesized and isolated as storable crystalline solid in 1991. The strong σ-donor ability of NHCs as ligands was slowly realized by the chemists. The low coordinate (Si)₂Cl₂ and Si₂ species have been successfully trapped by two ⁱP NHCs [ⁱP NHC = :C(N(2,6-*i*Pr₂C₆H₃)(CH))₂].²⁷ ⁱP NHC can also stabilize dichlorosilylene (SiCl₂) in the form of (ⁱP NHC)SiCl₂.²⁸ NHCs are employed as ligands for the stabilization of several unusual main group species in different oxidation states. Over the last two decades NHCs are utilized as efficient ligands in different areas of chemistry.²⁹

Bertrand et al. has isolated cyclic alkyl(amino) carbenes (cAACs) in 2005.⁵³ The carbene carbon atom of NHC is bound to two σ-withdrawing and two π-donating N-atoms while one N-atom is replaced by one σ-donating quaternary C-atom in a cAAC. The HOMO of cAAC is little higher in energy and LUMO of cAACs is slightly lower in energy than those of NHCs. The HOMO-LUMO energy gap is smaller in cAAC when compared with that of NHC (Figure 8).⁵⁴ As a result cAACs are stronger σ-donor and better π-acceptor than those of NHCs. This has been experimentally established by ³¹P NMR chemical shifts⁵⁵ of carbene-phosphinidene adducts. cAACs are different in certain respects and thus can activate very strong bonds (e.g., H-H, H-NH₂, etc.) which are not achievable when NHCs are employed instead of cAACs.⁵⁶ The cAAC has been utilized for the stabilization of several radical species of main group elements.¹⁸

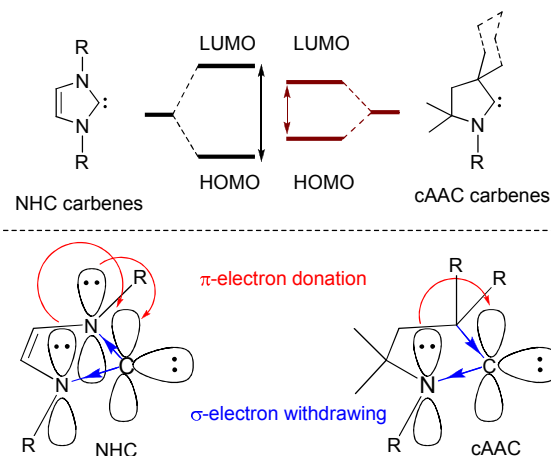
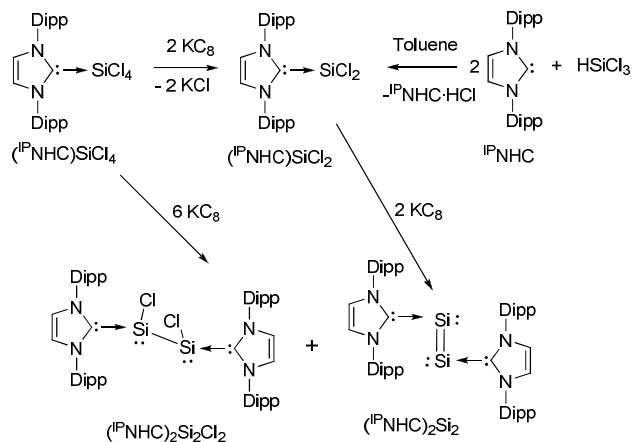


Figure 8. Comparison between NHC (left) and cAAC (right) carbenes.

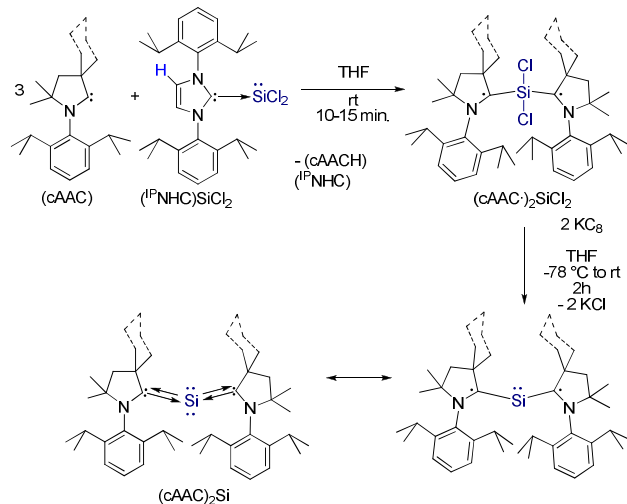
The unstable species dichlorosilylene (SiCl₂)^{16a} is usually generated under the elimination of HCl from trichlorosilane (HSiCl₃) in the presence of a strong base (such as R₃N). It is stable in the monomeric form at low temperatures (< -50 °C). However, SiCl₂ cannot be isolated and stored at room temperature in its monomeric form, since it undergoes polymerization to produce polychlorosilane on raising the temperature of the solution. ⁱP NHC [ⁱP NHC = :C(N(2,6-*i*Pr₂C₆H₃)(CH))₂] behaves as a strong σ-donor ligand and a base as well. ⁱP NHC reacts with HSiCl₃ in 1:1 molar ratio to generate SiCl₂ species under the elimination of ⁱP NHC-HCl. The light yellow crystalline powder of ⁱP NHC anchored (ⁱP NHC)SiCl₂²⁸ (Scheme 12) is isolated as air and moisture sensitive compound in 75% yield if the reaction of ⁱP NHC and HSiCl₃ is carried out in 2:1 molar ratio in toluene. (ⁱP NHC)SiCl₂ is completely soluble in toluene but partially soluble in *n*-hexane and tetrahydrofuran (THF).



Scheme 12. Synthesis routes of (ⁱP NHC)SiCl₂, (ⁱP NHC)₂Si₂Cl₂ and (ⁱP NHC)₂Si₂.

The cyclic alkyl amino carbene (cAAC) is expected to substitute ⁱP NHC from (ⁱP NHC)SiCl₂ since cAAC is a slightly stronger σ-

donor and considerably better π -acceptor. A dark blue solution is obtained on addition of THF to the 1:1 molar mixture of cAAC and ($^{\text{IP}}\text{NHC}$)SiCl₂ at rt. The X-ray single crystal diffraction on the dark blue blocks, reveals the composition of the compound as (cAAC)₂SiCl₂ (Scheme 13).⁵⁷ The yield of (cAAC)₂SiCl₂ is increased from 35% to 78% and 91% when the molar ratio of cAAC and ($^{\text{IP}}\text{NHC}$)SiCl₂ is increased to 2:1 and 3:1, respectively. The third equivalent of cAAC is required to form (cAACH)($^{\text{IP}}\text{NHC}$) carbene as a side product under C-H functionalization of the five-membered ring of $^{\text{IP}}\text{NHC}$.



Scheme 13. Synthesis routes of (cAAC)₂SiCl₂ and (cAAC)₂Si. [cAAC = Me₂-cAAC and Cy-cAAC].

(Me₂-cAAC)₂SiCl₂ exists in two polymorphs (-I and -II). The polymorph-II is experimentally found to be the major conformer.⁵⁷

Both the polymorphs are characterized by X-ray structural analysis and showed only small differences (Figure 9, bottom). The central silicon atom of (Me₂-cAAC)₂SiCl₂ is bound to two chlorine atoms and two carbene carbon atoms to adopt a near tetrahedral coordination geometry (Figure 9).⁵⁷ In contrast, the silicon atom of ($^{\text{IP}}\text{NHC}$)SiCl₂ features trigonal pyramidal geometry at the three-fold coordinate silicon atom.²⁸ The silicon atom of ($^{\text{IP}}\text{NHC}$)SiCl₂ possesses a lone pair of electrons which is available for the coordination to acceptors.^{16a} The C_{cAAC}-Si bond lengths (~1.8455(16)-1.8482(17) Å) in (Me₂-cAAC)₂SiCl₂ are shorter by 0.14 Å when compared to that of ($^{\text{IP}}\text{NHC}$)SiCl₂ (1.985(4) Å).²⁸ The Si-C bonds in (Me₂-cAAC)₂SiCl₂ are even shorter than Si-C_{aryl} single bonds (1.879 Å)²⁵ but slightly longer than Si-C bonds (1.8174(14) Å) of 3,6-bis[bis(*tert*-butylmethylsilyl)silylidene]cyclohexa-1,4-diene and much longer than Si=C double bonds (1.702-1.775 Å).²⁵ The C_{cAAC}-N bond distances are 1.3994(19) and 1.395(2) Å, respectively and larger than those found in the similar free carbenes (~1.315 Å).⁵³ Combined valence bond electron count and coordination geometry of the central silicon atom of (cAAC)₂SiCl₂ leads to an initial impression that it might be a diradical with one unpaired electron on each carbene carbon atom of cAAC.

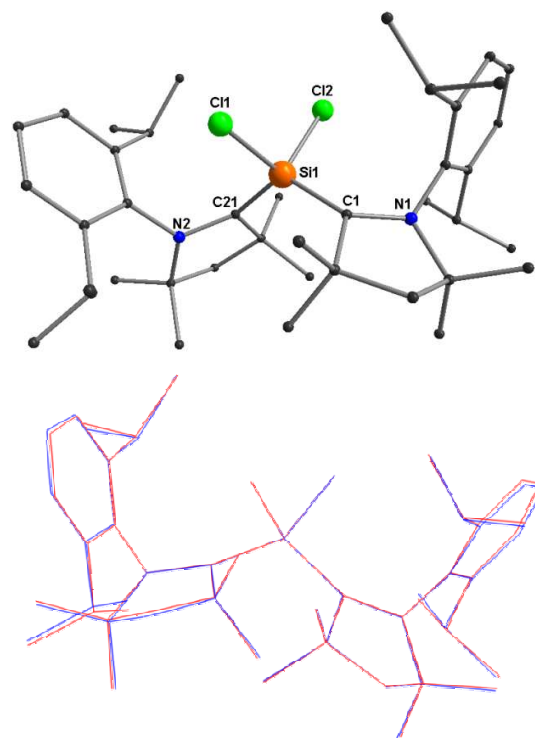
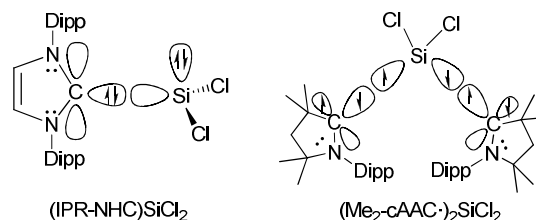


Figure 9. Molecular structure of polymorph-I of (Me₂-cAAC)₂SiCl₂ (top). An overlap picture (bottom) of polymorph-I and polymorph-II. Reproduced from ref. 57 with permission of John Wiley and Sons. Color version courtesy of Prof. G. Frenking.

Theoretical calculations show that the distributions of spin density of the unpaired electrons are mainly located at the C_{cAAC} of Me₂-cAAC ligands and to a minor extent at the nitrogen atoms and to a negligible extent at the central silicon atom. The bonding situations in (Me₂-cAAC)₂SiCl₂⁵⁷ and ($^{\text{IP}}\text{NHC}$)SiCl₂²⁸ are quite different. The C→Si bond in the NHC complex ($^{\text{IP}}\text{NHC}$)SiCl₂ comes from the donation of the carbene lone-pair orbital into the vacant acceptor orbital of SiCl₂ (Scheme 14). In contrast, the C-Si bonds in (Me₂-cAAC)₂SiCl₂ are electron-sharing bonds between the triplet states of SiCl₂ and the ligands Me₂-cAAC where the unpaired electrons in the singly occupied σ orbitals of the carbene carbon atoms couple with the unpaired electrons of SiCl₂ (Scheme 14).⁵⁷ There remains one unpaired electron at each of the carbene carbon atoms of the ligand Me₂-cAAC, which couples with the nitrogen lone pair orbital. This explains why there is some spin density at nitrogen as well.⁵⁷



Scheme 14. Schematic representation of donor-acceptor bonding in precursor (^{19}NHC) SiCl_2 (left) and electron-sharing bonding in product $(\text{Me}_2\text{-cAAC}\cdot)_2\text{SiCl}_2$ (right).

The singlet-triplet energy difference in $(\text{Me}_2\text{-cAAC}\cdot)_2\text{SiCl}_2$ has been computed to be different in magnitude and is dependent on the level of theory employed. It is approximately 2.5 to 4.5 Kcal mol^{-1} . Singlet diradical ground state of $(\text{Me}_2\text{-cAAC}\cdot)_2\text{SiCl}_2$ is more stable than the triplet diradical state. The optimized geometry of $(\text{Me}_2\text{-cAAC}\cdot)_2\text{SiCl}_2$ in the singlet state at the CASSCF(2,2)/SVP level and the wave function shows that the compound is an open-shell singlet species (Figure 10). The coefficients for the three singlet components are 0.80 (2/0), -0.60 (1/1), 0.0 (0.2). The preference for singlet diradical ground state suggests that the interactions between the two radical electrons of $(\text{Me}_2\text{-cAAC}\cdot)_2\text{SiCl}_2$ through bond/space is slightly dominant over each other (through-bond and through-space communication).⁵⁷

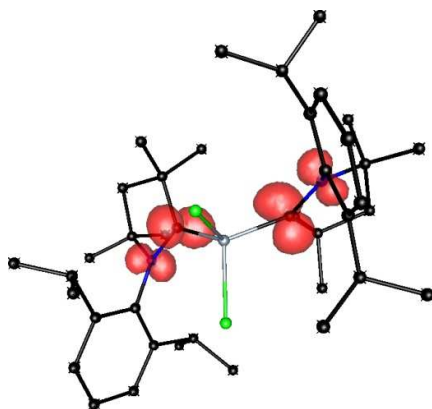


Figure 10. Calculated (M05-2x/SVP) spin density of $(\text{Me}_2\text{-cAAC}\cdot)_2\text{SiCl}_2$. Reproduced from ref. 57 with permission of John Wiley and Sons. Color version courtesy of Prof. G. Frenking.

The magnetic susceptibility measurements on a polymorph-I rich solid sample of $(\text{Me}_2\text{-cAAC}\cdot)_2\text{SiCl}_2$ shows ~16% of paramagnetic contribution and remaining 84% is diamagnetic polymorph-II.⁵⁷

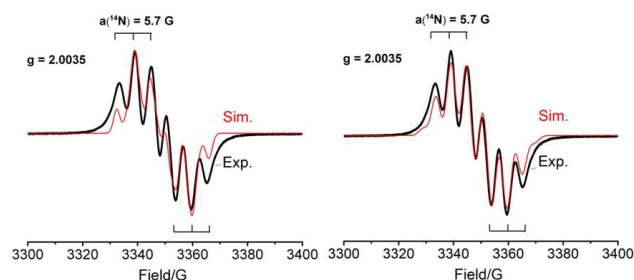


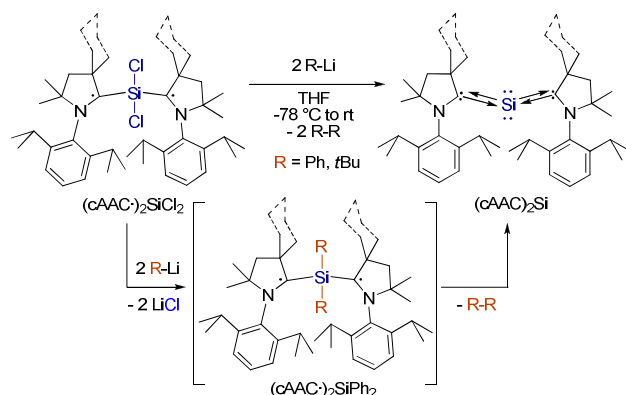
Figure 11. Experimental EPR spectra (black lines) of C_6D_6 solution of polymorph-I of $(\text{Me}_2\text{-cAAC}\cdot)_2\text{SiCl}_2$. Simulated spectra (red lines); models with two $S_{\text{eff}} = 1/2$; (left) and $S_{\text{eff}} = 1$ (right). Reproduced from ref. 57 with permission of John Wiley and Sons.

The origin of EPR signal of polymorph-II of $(\text{Me}_2\text{-cAAC}\cdot)_2\text{SiCl}_2$ is expected from small a percentage of polymorph-I as a minor component, since diamagnetic polymorph-II must be EPR silent. However, a diluted C_6D_6 solution of $(\text{Me}_2\text{-cAAC}\cdot)_2\text{SiCl}_2$ shows six hyperfine lines at room temperature.⁵⁷ This pattern suggests that the splitting is due to the coupling with two ^{14}N nuclei ($l = 1$) via a dipole-dipole interaction of two coupled radicals and their hyperfine interaction with the closest ^{14}N neighbour nuclei, respectively. The data of the EPR spectrum of polymorph I of $(\text{Me}_2\text{-cAAC}\cdot)_2\text{SiCl}_2$ given in Figure 11 is fitted with the use of the Easy Spin simulation package considering two different models. Firstly, EPR spectrum could be simulated as two weakly coupled electrons (two $S_{\text{eff}} = 1/2$), each electron interacts with the closest ^{14}N nucleus. Secondly, the effective electronic spin $S_{\text{eff}} = 1$ (2 coupled electrons) interacts with two N nuclei. The half field $\Delta m_s = \pm 2$ forbidden transition is not observed either in the solid state or in solution of polymorph-I of $(\text{Me}_2\text{-cAAC}\cdot)_2\text{SiCl}_2$, which excludes a genuine triplet state of polymorph-I which might be due to weak magnetic interactions. Roques et al. reported^{48b} the exchange in silole-bridged diradicals and most of the compounds showed $\Delta m_s = \pm 2$ forbidden transitions (characteristic of triplet). The half-field signal is not observed for the two diradicals of their report even when large signal amplification and high concentrations are used. The magnetic susceptibility measurements showed that more than 50% of molecules^{48b} of those diradicals are in their singlet ground states. Similar situation is faced for polymorph I of $(\text{Me}_2\text{-cAAC}\cdot)_2\text{SiCl}_2$.⁵⁷ It appears in very low intensity. The ^{29}Si NMR shows a resonance at 4.13 ppm which is shifted to high field, when compared with that of the precursor (^{19}NHC) SiCl_2 (19.06 ppm).⁵⁷

The crystalline powders of polymorph-II are isolated in 98.5% yield with a small content of polymorph-I (~1.5%).⁵⁷ It is concluded from the X-ray single crystal diffractions on several batches of the crystals of polymorph-I of $(\text{Me}_2\text{-cAAC}\cdot)_2\text{SiCl}_2$. Blue powders of $(\text{Me}_2\text{-cAAC}\cdot)_2\text{SiCl}_2$ are stable for more than two years under an inert atmosphere without any decomposition. We have observed that $(\text{Me}_2\text{-cAAC}\cdot)_2\text{SiCl}_2$ retains its color even when dipping the crystalline powder in a base bath or water for several days. The surface of blue blocks of $(\text{Me}_2\text{-cAAC}\cdot)_2\text{SiCl}_2$ slowly turns to colorless after 3-4 days and needs more than a week to completely lose the blue color. Similarly, $(\text{Cy-cAAC}\cdot)_2\text{SiCl}_2$ compound with comparable bonding and stability has been prepared.⁵⁸

Having $(\text{cAAC}\cdot)_2\text{SiCl}_2$ in hand we envisioned that it could be converted to the corresponding dechlorinated analogue, a siladibene $(\text{cAAC})_2\text{Si}$. Previously, theoretical calculations on various $(\text{NHC})_2\text{Si}$ compounds, coined as silylones, suggested that the synthesis of this class of compounds is experimentally feasible. The $(\text{cAAC}\cdot)_2\text{SiCl}_2$ is reduced with two equiv of KC_8 in THF to obtain a dark blue solution of $(\text{cAAC})_2\text{Si}$ (Scheme 13) which separated out from the mixture of KCl and $(\text{cAAC})_2\text{Si}$ by extraction with *n*-hexane in 95% yield.⁵⁹ When $(\text{cAAC}\cdot)_2\text{SiCl}_2$ is treated with two equiv of R-Li (R = Ph, ^tBu) in THF, $(\text{cAAC})_2\text{Si}$ is isolated instead of the functionalized hypothetical product

(cAAC)₂SiPh₂ under the reductive elimination of Ph-Ph. The (cAAC)₂SiPh₂ (Scheme 15)⁵⁹ is believed to be the intermediate species. (Me₂-cAAC)₂Si has singlet spin ground state which has been confirmed by magnetic susceptibility and EPR measurements. The ²⁹Si NMR spectrum of (Me₂-cAAC)₂Si exhibits a singlet at 66.71 ppm which is downfield shifted when compared with that of the precursor (Me₂-cAAC)₂SiCl₂ (4.13 ppm). The physical appearance of (cAAC)₂SiCl₂ (λ_{ab} = 569 nm) and (cAAC)₂Si (λ_{ab} = 570, 611 nm) are similar from the point of view of their color. The latter one is darker blue in color while the former is bright blue.



Scheme 15. Synthesis route of (cAAC)₂Si from (cAAC)₂SiCl₂ [cAAC = Me₂-cAAC and Cy-cAAC] with R-Li.

The molecular structure of (Me₂-cAAC)₂Si consists of a two coordinate silicon atom (Figure 12) at the center.⁵⁹ It is bound to two carbene carbon atoms of the two Me₂-cAAC ligands. The central silicon atom adopts a two coordinate bent geometry. The C_{CAAC}-Si-C_{CAAC} bond angles of the two symmetry independent molecules are more acute by ~5° compared with that of (Me₂-cAAC)₂SiCl₂.⁵⁹

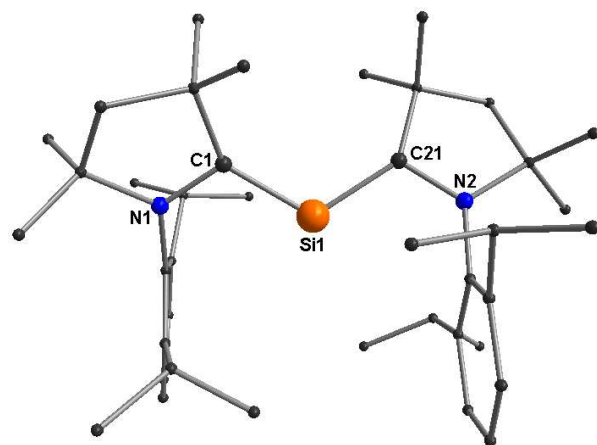


Figure 12. Molecular structure of (Me₂-cAAC)₂Si.

The sum of angles around the C_{CAAC} of (Me₂-cAAC)₂Si⁵⁹ are on average 357.7° (358.1°, (Me₂-cAAC)₂SiCl₂) suggesting slight deviation from the trigonal planar geometry. The C_{CAAC}-Si bond distances of (Me₂-cAAC)₂Si are 1.8411(18) Å and 1.8417(17) Å

which are very close to those of (Me₂-cAAC)₂SiCl₂ (1.8455(16) and 1.8482(17) Å).⁵⁷

The optimized geometry of (Me₂-cAAC)₂Si is in very good agreement with the experimental one rather than that of the triplet state. The triplet state is between 17.2-17.6 kcal mol⁻¹ higher in energy than the singlet state. The HOMO-1 is a σ lone-pair orbital at the Si atom, while the HOMO is a π-type orbital which has the largest extension at the Si but exhibits significant Si-C π bonding (Figure 13). This is the typical feature of a silylone.⁵⁹

The NBO analysis of (Me₂-cAAC)₂Si shows that the central silicon atom possesses two pairs of electrons. One σ lone-pair orbital resides on the silicon atom and the second pair of electrons forms a three-center C-Si-C π-bond. The numerical values for the distribution of the second pair of electrons are 40% at Si and 30% at each of the C_{CAAC}. Theoretically calculated first and second proton affinities are (PAs) 272.2 Kcal mol⁻¹ and 186.7 Kcal mol⁻¹, respectively. The very large value for the second proton affinity clearly supports the assignment that (Me₂-cAAC)₂Si is genuinely a silylone.

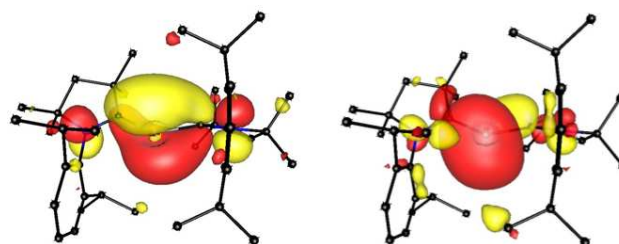


Figure 13. Plots of the HOMO (left) and HOMO-1 (right) of (Me₂-cAAC)₂Si. Reproduced from ref. 59 with permission of John Wiley and Sons. Color version courtesy of Prof. G. Frenking.

Further calculations reveal that it has a 54% of singlet diradical character. The calculation gives coefficients of 0.96 for the closed-shell 2,0 configuration, -0.28 for the 1,1 configuration and 0.0 for the 0,2 configuration. The closed-shell singlet configuration of (Me₂-cAAC)₂Si has a non-negligible contribution from the singly excited state which possesses some diradicaloid character (as shown in Scheme 13) and low electronic excitation energy.⁵⁹

The experimental charge density calculations have confirmed that there are two pairs of electrons on the silicon atom in silylone. NBO calculations show accumulation of positive partial charge at Si which agrees with the electronegativities of silicon and carbon. This indicates that the Si→C_{CAAC} π-back donation is larger than the Si←C_{CAAC} σ-donation. This typical bonding scenario results in the reasonably stronger Si-C_{CAAC} bonds in silylone which is crucial for such a high stability of this compound. The dark blue crystals of (cAAC)₂Si are found to be stable over two years at room temperature in an inert atmosphere without any decomposition.⁶⁰ (cAAC)₂Si is also characterized by EI mass spectrometry. (cAAC)₂Si is thermally stable up to 195 °C and decomposes above 220 °C to a yellow liquid. NMR studies show that (cAAC)₂Si is chemically inert

when it is reacted with molecular hydrogen, ammonia, and carbon dioxide at room temperature. The cyclic voltammetry (CV) studies on $(\text{cAAC})_2\text{Si}$ in 0.1 M $[\text{n-Bu}_4\text{N}]\text{PF}_6$ THF solution suggest that $(\text{cAAC})_2\text{Si}$ is quasi-reversible reduced to its corresponding radical anion $(\text{cAAC})_2\text{Si}^{\cdot-}$ at $E_{1/2} = -1.55$ V (against the reference $\text{Cp}^*\text{Fe}/\text{Cp}^*\text{Fe}^+$) (Figure 14).⁶⁰ The radical anion intermediate $(\text{cAAC})_2\text{Si}^{\cdot-}$ has been further confirmed by the EPR spectroscopy. The reaction mixture of $(\text{Me}_2\text{-CAAC})_2\text{Si}$ is stirred in the presence of potassium metal for 30 min to *in situ* generate the radical anion $(\text{Me}_2\text{-CAAC})_2\text{Si}^{\cdot-}$ in THF at 298 K.⁶⁰ The EPR spectrum (Figure 15) of $(\text{Me}_2\text{-CAAC})_2\text{Si}^{\cdot-}$ produces five hyperfine lines at $g = 2.0058$ due to the coupling of a radical electron with two nitrogen nuclei ($a(^{14}\text{N}) = 5.89$ G; $I = 1$). Two satellites ($a(^{13}\text{C}) = 40$ G; $I = 1/2$) are originated due to coupling with C_{cAAC} atoms suggesting that the radical electron is delocalized in the C-Si-C backbone of $(\text{Me}_2\text{-CAAC})_2\text{Si}^{\cdot-}$. The radical electron resides on the p orbitals of the carbene carbon atoms (see the LUMO (Figure 16) of $(\text{cAAC})_2\text{Si}$ and SOMO ($(\text{cAAC})_2\text{Si}^{\cdot-}$)).⁶⁰ The Mulliken spin density plot of the radical anion shows that the unpaired electron is delocalized (Figure 17) between the two carbene carbon atoms via the vacant d-orbital of the silicon atom.

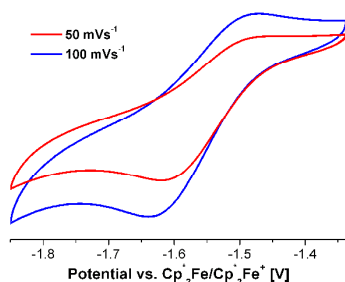


Figure 14. Cyclic voltammogram (CV) of $(\text{Cy-cAAC})_2\text{Si}$ in THF solution (0.1 M $[\text{n-Bu}_4\text{N}]\text{PF}_6$) at indicated scan rates (potential versus $\text{Cp}^*\text{Fe}/\text{Cp}^*\text{Fe}^+$).

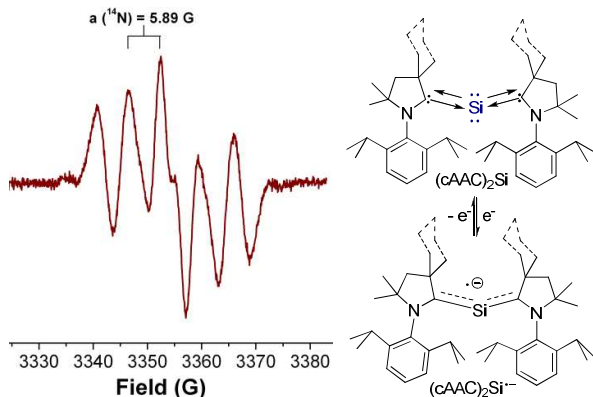
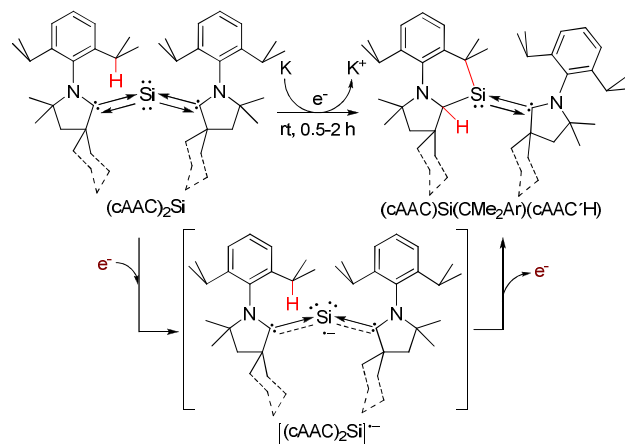


Figure 15. X-band EPR spectrum of *in situ* generated $(\text{Me}_2\text{-cAAC})_2\text{Si}^{\cdot-}$ in THF at 298 K (left). Formation of $(\text{cAAC})_2\text{Si}^{\cdot-}$ from of $(\text{cAAC})_2\text{Si}$ (right). [cAAC = $\text{Me}_2\text{-cAAC}$ and Cy-cAAC]. Reproduced with permission from ref. 60.

Potassium metal is an electro-positive metal and it has a high tendency to donate electron to the low lying antibonding orbitals. Potassium metal is chosen as an electron donor and THF as the preferred solvent due to its high polarity and electron transport ability. Accordingly, we set up a reaction by adding THF to a 1:1 molar mixture of $(\text{cAAC})_2\text{Si}$ and metallic potassium.⁶⁰ The resultant dark blue color of the reaction solution is changed to a greenish yellow color after 35 min of vigorous stirring. Afterwards the solution was filtered to separate out the unreacted potassium metal. The concentrated THF solution is stored at -32 °C in a freezer to form yellow blocks of $(\text{cAAC})\text{Si}(\text{CMe}_2\text{Ar})(\text{cAAC}^*\text{H})$ (Scheme 16) in reasonable $(\text{Me}_2\text{-cAAC})$ to high yields (Cy-cAAC).⁶⁰



Scheme 16. Conversion of $(\text{cAAC})_2\text{Si}$ with two coordinate silicon to $(\text{cAAC})\text{Si}(\text{CMe}_2\text{Ar})(\text{cAAC}^*\text{H})$ with three coordinate silicon [cAAC = $\text{Me}_2\text{-cAAC}$ and Cy-cAAC].

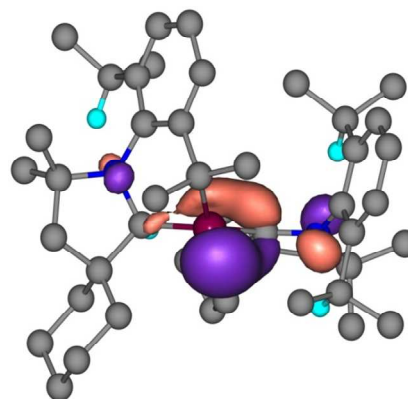


Figure 16. LUMO of $(\text{Cy-cAAC})_2\text{Si}$. Reproduced with permission from ref. 60.

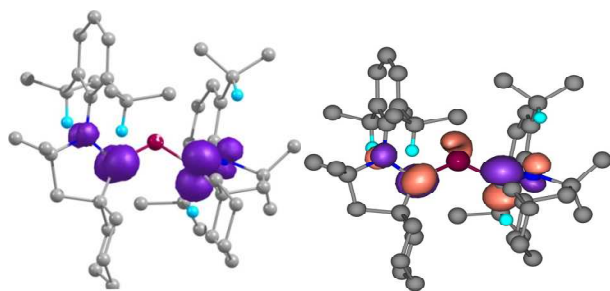


Figure 17. Mulliken spin density plot (left) and SUMO (right) of $(\text{Cy-cAAC})_2\text{Si}^{\bullet-}$. Reproduced with permission from ref. 60.

X-ray single crystal diffraction reveals the formation of a six-membered cyclic silylene $(\text{cAAC})\text{Si}(\text{CMe}_2\text{Ar})(\text{cAAC}'\text{H})$ with a three coordinate silicon atom in the center (Scheme 16, Figure 18).⁶⁰

The recovery of the 67% of unreacted potassium metal reveals that 33% of the metal had been consumed during the reaction course (Scheme 16). This means that only a sub-stoichiometric amount of the metal atom can successfully induce the reaction of the apparently unreactive silylone $(\text{cAAC})_2\text{Si}$ to its structural isomer $(\text{cAAC})\text{Si}(\text{CMe}_2\text{Ar})(\text{cAAC}'\text{H})$ in an atom economical fashion. In this respect it is important to mention that stirring of the reaction solution for longer time leads to the further rearrangement of $(\text{cAAC})\text{Si}(\text{CMe}_2\text{Ar})(\text{cAAC}'\text{H})$ to different products which could not be isolated. The crystals of $(\text{cAAC})\text{Si}(\text{CMe}_2\text{Ar})(\text{cAAC}'\text{H})$ are stable at room temperature for more than one month in an inert atmosphere and they melt above 211 °C. $(\text{cAAC})\text{Si}(\text{CMe}_2\text{Ar})(\text{cAAC}'\text{H})$ is stable enough to be further characterized by EI mass spectrometry.⁶⁰ The ²⁹Si NMR spectrum of $(\text{cAAC})\text{Si}(\text{CMe}_2\text{Ar})(\text{cAAC}'\text{H})$ exhibits resonances at 55.98 (cAAC = Cy-cAAC) and 54.55 ppm (cAAC = Me₂-cAAC), which are upfield-shifted when compared to those of $(\text{cAAC})_2\text{Si}$ (71.15 and 66.71 ppm, respectively). The ¹³C NMR spectrum of $(\text{cAAC})\text{Si}(\text{CMe}_2\text{Ar})(\text{cAAC}'\text{H})$ shows resonances at 69.4(CH)/173.5(C:) and 66.2(CH)/172.1(C:) ppm, respectively, which are upfield-shifted when compared to those of $(\text{cAAC})\text{Si}(\text{CMe}_2\text{Ar})(\text{cAAC}'\text{H})$ (210.8 and 210.9 ppm, respectively). A detailed investigation of the reaction mechanism reveals that the formation of $(\text{cAAC})\text{Si}(\text{CMe}_2\text{Ar})(\text{cAAC}'\text{H})$ from $(\text{cAAC})_2\text{Si}$ could be rationalized as the activation of the C-H bond of one of the two CHMe₂ groups of $(\text{cAAC})_2\text{Si}$ which has selectively reacted (Scheme 1) with one C_{cAAC}-Si bond, producing the H-C_{cAAC}-Si(CMe₂) moiety in $(\text{cAAC})\text{Si}(\text{CMe}_2\text{Ar})(\text{cAAC}'\text{H})$. A plausible reaction mechanism (Scheme 16) is proposed on the basis of the DFT calculations.⁶⁰

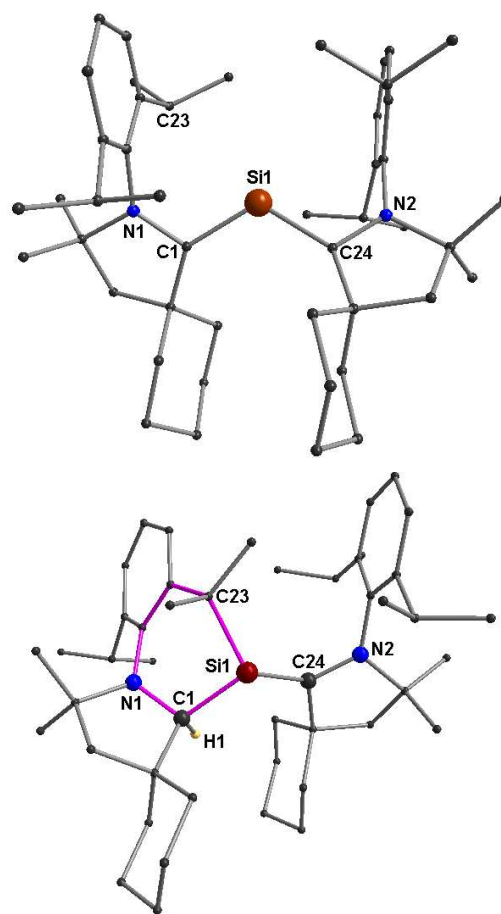


Figure 18. Molecular structure of $(\text{Me}_2\text{-cAAC})_2\text{Si}$ (top) and $(\text{Cy-cAAC})\text{Si}(\text{CMe}_2\text{Ar})(\text{Cy-cAAC}'\text{H})$ (bottom). Reproduced with permission from ref. 60.

The formation of the silylone radical anion intermediate $(\text{cAAC})_2\text{Si}^{\bullet-}$ is assumed to be the key step for the activation of the very strong C-H bond. This could finally help to overcome the challenge behind the so far elusive reactivity of the highly stable silylone $(\text{cAAC})_2\text{Si}$ to produce the corresponding six-membered silylene $(\text{cAAC})\text{Si}(\text{CMe}_2\text{Ar})(\text{cAAC}'\text{H})$.⁶⁰ The closed-shell singlet electronic state of $(\text{Cy-cAAC})\text{Si}(\text{CMe}_2\text{Ar})(\text{Cy-cAAC}'\text{H})$ is lower in energy by 16.8 kcal mol⁻¹ than its triplet form. Geometry optimization with broken symmetry formalism reveals that the diradical singlet state again is higher in energy than the closed-shell singlet state by 14.5 kcal mol⁻¹ (ΔG_L^S).⁶⁰ The optimized geometrical parameters of the singlet state are in much better agreement to the X-ray crystal structure of $(\text{Cy-cAAC})\text{Si}(\text{CMe}_2\text{Ar})(\text{Cy-cAAC}'\text{H})$ than its diradical singlet or triplet states (Figure 19).⁶⁰

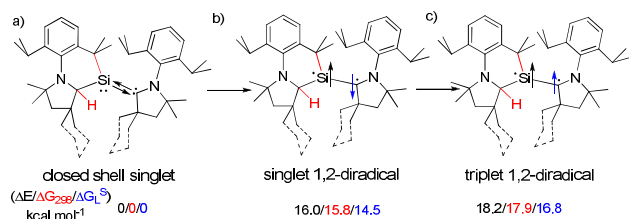
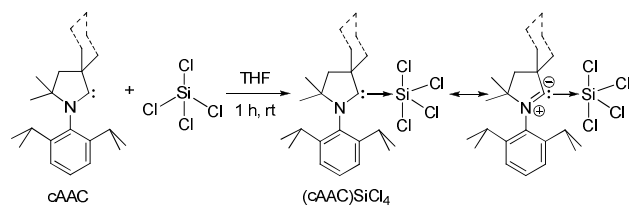


Figure 19. Calculated energy values of the a) singlet (left), b) singlet 1,2-diradical (middle) and c) triplet 1,2-diradical (right) species implying the preference for singlet ground state (left) of (cAAC)Si(CMe₂Ar)(cAAC').

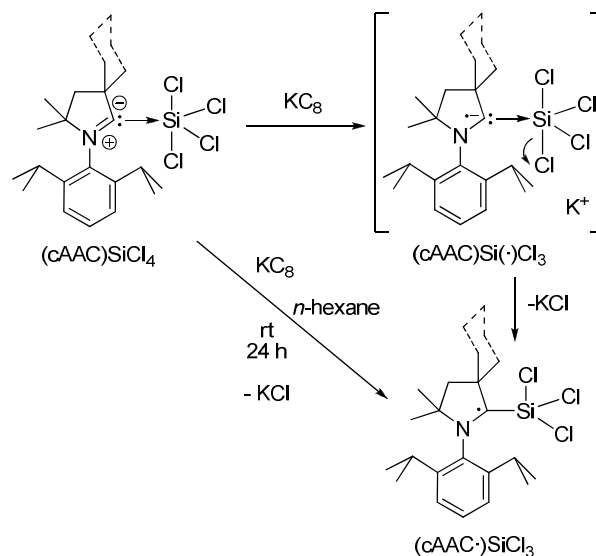
The detail structural investigations (Figure 18) of (Cy-cAAC)Si(CMe₂Ar)(Cy-cAAC'H) show that one carbene carbon atom (C_{CAAC}) contains one proton and the silicon atom is further bound to the CMe₂ group (C23) of one of the former isopropyl groups (CHMe₂; C23-Si1 = 1.961(2) Å).⁶⁰ The C_{CAAC}-Si and C_{CAAC}-N bonds of (Cy-cAAC)Si(CMe₂Ar)(Cy-cAAC'H) are elongated from 1.8404(11) to 1.952(2) and 1.3827(15) to 1.461(3) Å, respectively. The C24(C_{CAAC})-Si1 and C24-N2 bond distances are very close to the values (C_{CAAC}-Si = 1.8535(12) Å, C24-N2 = 1.3724(14) Å) of silylone (Cy-cAAC)₂Si. A newly formed six-membered ring containing two hetero atoms are shown in purple color in Figure 18.⁶⁰

Unlike carbon, silicon has vacant d orbitals and hence silicon can form higher coordinate compounds via the mixing of s and p with d orbitals. As a result, a five coordinate (cAAC)SiCl₄ adduct (Scheme 17) is formed in high yield (97-98%) when cAAC is reacted with SiCl₄ in 1:1 molar ratio in THF.⁶¹ (cAAC)SiCl₄ is very polar in nature and soluble in polar solvent THF. The ²⁹Si chemical shift value of (Me₂-cAAC)SiCl₄ is -103.5 ppm. It is also partially soluble in non-polar solvents like *n*-hexane, benzene and toluene. The colorless crystals of (cAAC)SiCl₄ decompose above 123 °C. They are also prone to decomposition in THF if the solution of (cAAC)SiCl₄ is stored for longer time (several days). This simple looking higher coordinate adduct (cAAC)SiCl₄ has been eventually found to be a very important precursor for the syntheses of several low coordinate cAAC-silicon compounds. The (cAAC)SiCl₄ is believed to have zwitterionic character based on bond parameters. The bond between carbene carbon atom (C_{CAAC}) and silicon atom is a coordinate bond (C_{CAAC}→Si; 1.944(2) Å), while the C_{CAAC}-N has a partial double bond character (1.3040(2) Å) which is close to that of a free carbene (1.315 Å).⁶¹



Scheme 17. Synthesis of (cAAC)SiCl₄. [cAAC = Me₂-cAAC and Cy-cAAC].

The LUMO of the cAAC is lower lying when compared with that of NHC. The LUMO of the carbene is located at π_{C-N^*} of cAAC. It can be argued that both the HOMO and LUMO of cAAC are further lower due to donation of electron pair on the carbene carbon atom to the silicon atom of (cAAC)SiCl₄. Thus, reducing agents, like KC₈ are very much effective to eliminate the chlorine atoms from (cAAC)SiCl₄. We have observed that the reduction of (cAAC)SiCl₄ with KC₈ even starts at very low temperature (< -78 °C) in polar solvents, like THF. Non-polar solvents like *n*-hexane are effective for the selective reduction of (cAAC)SiCl₄ to (cAAC)SiCl₃ at room temperature. The temperature of the reaction must be kept very low (< -78 °C) for the controlled reduction of (cAAC)SiCl₄ to (cAAC)SiCl₃ in THF. The electron transfer from KC₈ to the (cAAC)SiCl₄ is very slow in non-polar solvents. The electron transfer from KC₈ to (cAAC)SiCl₄ possibly occurs via THF solvated electron transport and hence the kinetics of the reduction is very fast.⁶¹



Scheme 18. Reduction of (cAAC)SiCl₄ to (cAAC)SiCl₃ by KC₈. [cAAC = Me₂-cAAC and Cy-cAAC].

We believe that KC₈ donates the electron to the LUMO of (π_{C-N^*} of cAAC) of (cAAC)SiCl₄ to form a radical anion intermediate [(cAAC)SiCl₄]⁻ which then eliminates a chloride anion with the formation of KCl and (cAAC)SiCl₃ (Scheme 18).⁶¹ The bond parameters obtained from the X-ray single crystal diffraction of (cAAC)SiCl₃ lead to the conclusion that the bond between carbene carbon atom (C_{CAAC}) and silicon atom is an electron sharing covalent single bond (C_{CAAC}-Si; 1.8152(12) Å) with an elongated C_{CAAC}-N bond (137.79(14) Å). The synthesis of a carbene centered stable radical via the transformation of a C_{CAAC}→Si coordinate bond to an electron sharing covalent single bond C_{CAAC}-Si is unique.⁶¹

The fluorescent yellow plates/needles of (cAAC)SiCl₃ are isolated either at room temperature from a concentrated solution or a dilute solution at 0 °C from a refrigerator. They

ARTICLE

Journal Name

are highly soluble in both polar and non-polar solvents. They melt at around 115 °C. They can be characterized by electron ionization (EI) mass spectrometry. They are stable for more than a year under an inert atmosphere at room temperature.⁶¹

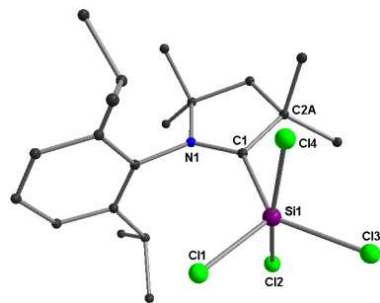


Figure 20. Molecular structures of $(\text{Me}_2\text{-cAAC})_2\text{SiCl}_4$.

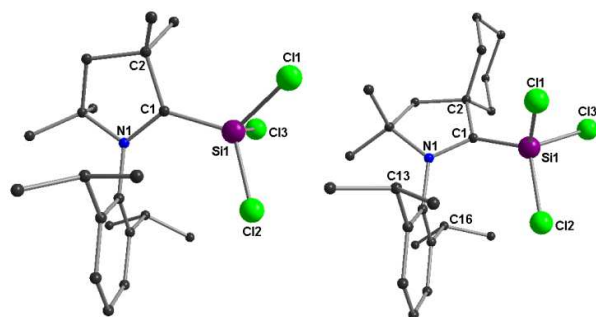


Figure 21. Molecular structure of $(\text{Me}_2\text{-cAAC})\text{SiCl}_3$ (left) and $(\text{Cy-cAAC})\text{SiCl}_3$ (right).

The silicon atom in the $(\text{Me}_2\text{-cAAC})\text{SiCl}_4$ adduct adopts a trigonal bipyramidal coordination geometry. The important structural feature of $(\text{Me}_2\text{-cAAC})\text{SiCl}_4$ is that the axial Si–Cl bond distances (~2.18 Å) are significantly longer than those of equatorial Si–Cl bonds (~2.04 Å) (Figure 20). The $C_{\text{carbene}}\text{-Si}$ and $C_{\text{carbene}}\text{-N}$ bond distances are 1.944(2) Å and 1.3040(2) Å, respectively.⁶¹

The silicon atom of compound $(\text{cAAC})\text{SiCl}_3$ [$\text{cAAC} = \text{Me}_2\text{-cAAC}$ and Cy-cAAC] is bound to three chlorine atoms and one carbene carbon atom. The silicon atom adopts a near-tetrahedral geometry (Figure 21).⁶¹ The $C_{\text{carbene}}\text{-Si}$ bond distances in $(\text{Me}_2\text{-cAAC})\text{SiCl}_3$ and $(\text{Cy-cAAC})\text{SiCl}_3$ are 1.8152(12) and 1.8193(8) Å, respectively. The $C_{\text{carbene}}\text{-Si}$ bond distance in $(\text{cAAC})\text{SiCl}_3$ is slightly shorter than that of the electron sharing Si–C single bond distances of $(\text{cAAC})_2\text{SiCl}_2$ (1.8455(16) and 1.8482(17) Å) but significantly shorter than that of the precursor $(\text{cAAC})\text{SiCl}_4$ (1.944(2) Å). The $C_{\text{carbene}}\text{-N}$ bond lengths are 1.3779(14)–1.3827(10) Å which are close to those (1.3994(19)–1.400(2) Å)⁵⁷ obtained for the diradical $(\text{cAAC})_2\text{SiCl}_2$ but it is shorter by 0.07 Å when compared with that of the precursor $(\text{cAAC})\text{SiCl}_4$ (1.3040(2) Å). All the bond parameters of $(\text{cAAC})\text{SiCl}_3$ suggest that the $C_{\text{carbene}}\text{-Si}$ is an electron sharing Si–C single bond while the same one is a $C_{\text{cAAC}}\text{-Si}$ coordinate σ -bond in $(\text{cAAC})\text{SiCl}_4$ (Scheme 18).⁶¹

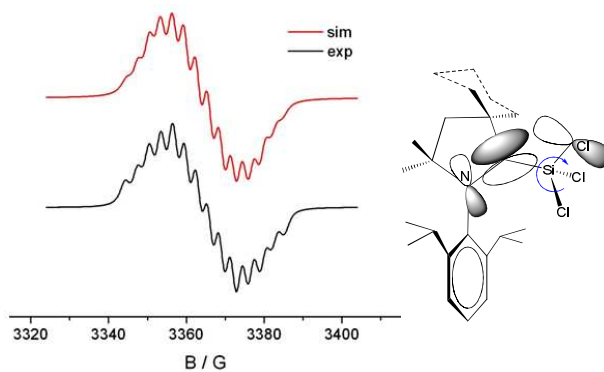


Figure 22. Experimental and simulated X-band EPR spectrum of a C_6D_6 solution of $(\text{Cy-cAAC})\text{SiCl}_3$ at 298 K. Reproduced from ref. 61 with permission of John Wiley and Sons. Color version courtesy of Dr. D. Koley.

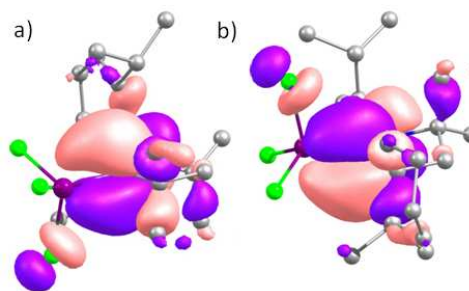
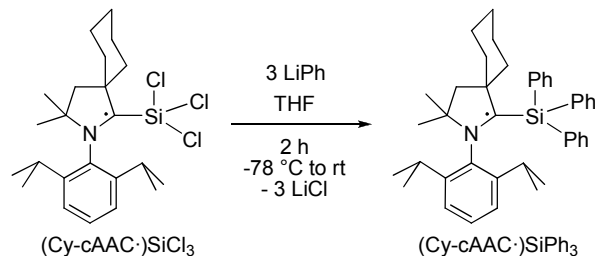


Figure 23. The KS-SOMO (a) $(\text{Me}_2\text{-cAAC})\text{SiCl}_3$ and (b) $(\text{Cy-cAAC})\text{SiCl}_3$ at UM05-2X/TZVP//UM05-2X/SVP level. Reproduced from ref. 61 with permission of John Wiley and Sons. Color version courtesy of Dr. D. Koley.

DFT calculations concerning the bonding and electron density distribution has been carried out on $(\text{cAAC})\text{SiCl}_3$.⁶¹ The calculations show that the unpaired electron (Figure 23) is mainly located on the carbene carbon of cAAC (ca. 52%), with a smaller contribution from the N1 atom (23%) and the remaining 25% of the electron density is scattered over the Dipp/cAAC units and one of the Cl atoms (oriented parallel to the p_z orbital of C_{cAAC} atom). The EPR spectrum of $(\text{cAAC})\text{SiCl}_3$ [$\text{cAAC} = \text{Me}_2\text{-cAAC}$ and Cy-cAAC] is recorded in C_6D_6 which shows multiple hyperfine lines. The EPR spectrum of $(\text{Cy-cAAC})\text{SiCl}_3$ is better resolved than that of $(\text{Me}_2\text{-cAAC})\text{SiCl}_3$. The simulation considering the electronic coupling of one radical electron with one ^{14}N ($I = 1$) and one $^{35/37}\text{Cl}$ ($I = 3/2$) nuclei does not reproduce the experimental pattern suggesting that the free rotation of the SiCl_3 group around the carbon-silicon bond ($C_{\text{cAAC}}\text{-Si}$) might be possible.⁶¹

The simulation of the experimental EPR spectrum (Figure 22) of $(\text{Cy-cAAC})\text{SiCl}_3$ reveals a ^{14}N coupling constant ($I = 1$) of 6.4 G, and smaller couplings of about 3.4 G (1 Cl) and 2.7 G (2 Cl), with three Cl atoms ($I = 3/2$, gyromagnetic ratio = 1.20). The relatively intensified outermost lines suggest the non-equivalence of the chlorine couplings. This also suggests a partially hindered rotation of the SiCl_3 group.⁶¹

It is important to mention that highly reactive trichlorosilane radical $\cdot\text{SiCl}_3$ is frequently generated by flash photolysis. It is an active radical intermediate in many photochemical transformations such as chemical vapour deposition (CVD) and is a product in chlorine plasma etching of silicon. The $(\text{cAAC})\cdot\text{SiCl}_3$ can be considered as cAAC stabilized stable radical of $\cdot\text{SiCl}_3$.⁶¹



Scheme 24. Synthesis of $(\text{Cy-cAAC})\cdot\text{SiPh}_3$ from $(\text{Cy-cAAC})\cdot\text{SiCl}_3$.

When three equivalents of PhLi is added drop by drop to the fluorescent yellow colored solution of $(\text{Cy-cAAC})\cdot\text{SiCl}_3$ in THF at -78°C and the temperature of the reaction solution is slowly raised to rt, a dark red solution of $(\text{Cy-cAAC})\cdot\text{SiPh}_3$ (Scheme 24) is obtained in 90% yield.⁶² The crystals $(\text{Cy-cAAC})\cdot\text{SiPh}_3$ melt in the temperature range of $148\text{--}149^\circ\text{C}$. The compound $(\text{Cy-cAAC})\cdot\text{SiPh}_3$ is further characterized by EI mass spectrometry like its precursor.⁶²

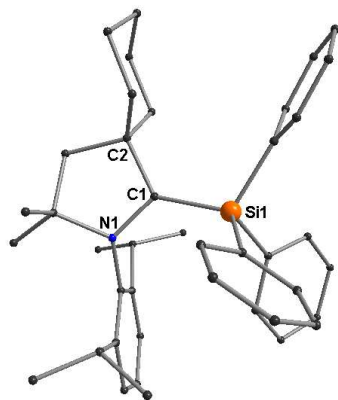


Figure 24. The molecular structure of compound $(\text{Cy-cAAC})\cdot\text{SiPh}_3$.

The molecular structure of $(\text{Cy-cAAC})\cdot\text{SiPh}_3$ is unambiguously established (Figure 24) by the X-ray single crystal structure determination. This reveals that the central silicon atom is bound to three phenyl groups and one carbon atom of the Cy-cAAC ligand with coordination number of four. The silicon atom adopts a slightly distorted geometry due to the asymmetric steric crowding around it.⁶²

The $\text{Si-C}_{\text{cAAC}}$ bond length ($1.8704(17) \text{ \AA}$)⁶² of $(\text{Cy-cAAC})\cdot\text{SiPh}_3$ is slightly longer than that of its precursor $(\text{Cy-cAAC})\cdot\text{SiCl}_3$ ($1.8193(8) \text{ \AA}$).⁶¹ This is possibly due to the substitution of all the three electron-withdrawing chlorine atoms by electron-donating phenyl groups at silicon. Theoretical calculations (Figure 25) on $(\text{Cy-cAAC})\cdot\text{SiPh}_3$ show that 55% of the electron

density (unpaired) is primarily located on C_{cAAC} with 21% contribution from the adjacent nitrogen atom. The remaining 24% of the electron density is delocalized over the Dipp group of cAAC unit and C_{ipso} atom in one of the phenyl groups.⁶²

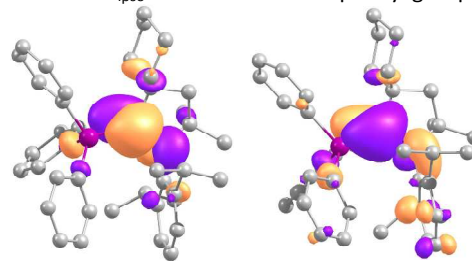


Figure 25. The KS-HOMO (left) and KS-LUMO (right) of $(\text{Cy-cAAC})\cdot\text{SiPh}_3$ at UM05-2X/TZVP//UM05-2X/SVP level. Reproduced with permission from ref. 62.

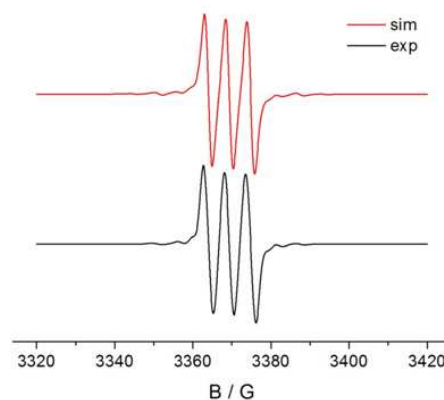


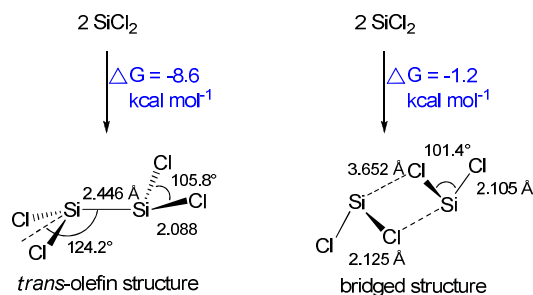
Figure 26. Experimental and simulated X-band EPR spectra of C_6D_6 solution of $(\text{Cy-cAAC})\cdot\text{SiPh}_3$. Reproduced with permission from ref. 62.

The X-band EPR spectrum (Figure 26) of $(\text{Cy-cAAC})\cdot\text{SiPh}_3$ exhibits three hyperfine lines at $g = 2.0019$ due to the coupling (5.4 G) with one ^{14}N ($I = 1$) nucleus. The satellites from ^{29}Si (8.0 G ; ^{29}Si : $I = 1/2$, 4.7% natural abundance), and three carbon atoms (25 G), are tentatively identified through simulation of EPR spectrum and theoretically calculated hyperfine coupling constants. Two γ carbons at the cyclohexyl ring of Cy-cAAC ligand transfer spin via hyperconjugation. One carbon atom from a Si-phenyl group (38.0 G) causes the broadening of hyperfine lines. Thus, $(\text{Cy-cAAC})\cdot\text{SiPh}_3$ is identified as the predominantly spin-bearing carbene carbon centered p radical. The hyperfine coupling constants of ^1H are calculated to be very small and are not observed experimentally.⁶² It has been mentioned before that $(^{\text{IP}}\text{NHC})\text{SiCl}_2$ is exclusively obtained from the reaction of HSiCl_3 with two equiv of NHC under the elimination of $^{\text{IP}}\text{NHC}\cdot\text{HCl}$.^{16a} Alternatively, $(^{\text{IP}}\text{NHC})\text{SiCl}_2$ is also prepared via the reduction of $(^{\text{IP}}\text{NHC})\text{SiCl}_4$ adduct with two equiv of KC_8 under the elimination of KCl (Scheme 12). Both the NHC and cAAC stabilized $(\text{L})\text{ECl}_2$ ($\text{L} =$

ARTICLE

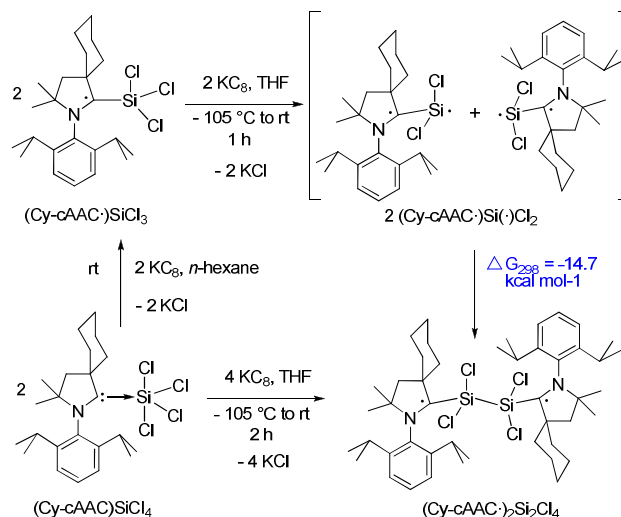
NHC, for E = Si, Ge, Sn; L = cAAC for Ge, Sn) have been reported.^{16a,17}

The dechlorination reaction is regarded to be an important technical process, due to the formation of SiCl₄ as a side product during the reduction of HSiCl₃ to Si with hydrogen gas. It has been observed that dichlorosilylene (SiCl₂) is generated from trichlorosilane (HSiCl₃) in the presence of a base. It can be trapped as (NHC)SiCl₂ by NHC.^{16a,28} In the presence of triethylamine, the dimer Si₂Cl₆ produces SiCl₄ and Si₆Cl₁₄. The exact mechanism has not been established yet. Hexachlorodisilane (Si₂Cl₆) undergoes disproportionation to produce SiCl₄ and SiCl₂, both of which have been trapped by NHC too.^{16a} SiCl₂ could also be generated from Si₃Cl₈ in the presence of tertiary amine. Gaseous SiCl₂ is known for a long time but it condenses to polymeric (SiCl₂)_n.^{16a} The stabilization of the dimer (Si₂Cl₄) of SiCl₂ has not been even suggested previously before our report. In 2003, Boganov et al. suggested that the dimerization of 2SiCl₂ → Si₂Cl₄ is energetically favorable over complexation between SiCl₂ and molecular N₂.^{63a} This has been concluded from the quantum chemical calculations and experiments at low temperature by an argon-nitrogen matrix isolation of pyrolysis product (N₂-SiCl₂) from Si₂Cl₆. The Si₂Cl₄ is predicted to exist in two forms (*trans*-olefin and bridged structure; Scheme 25). The calculated dimerization energy (2SiCl₂ → Si₂Cl₄) is evaluated to be -8.6 Kcal mol⁻¹ for *trans*-olefin structure and -1.2 Kcal mol⁻¹ for the bridged structure.⁶³



Scheme 25. Calculated dimerization energies and bond parameters of Si₂Cl₄.

Having (cAAC)SiCl₃ in hand,⁶¹ the possibility of studying the dimerization of (cAAC)₂SiCl₂ seems to be elusive.⁶⁴ The NHC analogue (NHC)SiCl₃ is still not isolated. Note, that (^{IP}NHC)SiCl₂ is stable in the monomeric form at room temperature for months under an inert atmosphere and does not undergo any sort of dimerization/polymerization.²⁸ The cAAC reacts with (NHC)SiCl₂ to exclusively produce (cAAC)₂SiCl₂.⁵⁷ To attempt the synthesis of Si₂Cl₄, stabilized by carbenes, compound (Cy-cAAC)SiCl₃ has been chosen as the precursor instead of (NHC)SiCl₂, because treatment of the latter with cAAC resulted exclusively in the formation of (cAAC)₂SiCl₂.⁵⁷



Scheme 26. Synthesis route of (Cy-cAAC)₂Si₂Cl₄.

(Cy-cAAC)SiCl₃ is thus treated with one equiv of KC₈ in THF at low temperature to generate the desired species (Cy-cAAC)₂Si₂Cl₄ (Scheme 26).⁶⁴ Green crystals of (Cy-cAAC)₂Si₂Cl₄ are isolated from a concentrated solution stored at -32 °C in a freezer in 85% yield. The same product is obtained when (cAAC)SiCl₄ adduct is reduced with two equiv of KC₈ (Scheme 26). The green crystals of (Cy-cAAC)₂Si₂Cl₄ decompose above 93 °C and are stable at -32 °C for several months but slowly decompose at higher temperature. The ²⁹Si chemical shift value of (Cy-cAAC)₂Si₂Cl₄ is 3.3 ppm.⁶⁴

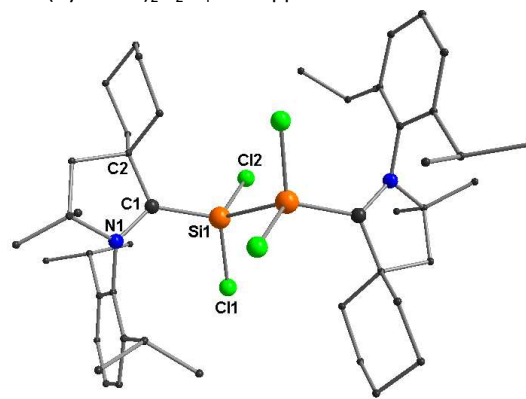


Figure 27. The molecular structure of (Cy-cAAC)₂Si₂Cl₄.

Both the silicon atoms of (Cy-cAAC)₂Si₂Cl₄ adopt a near-tetrahedral geometry and each of them is bound to one carbene carbon atom, two chlorines and one silicon atom (Figure 27). The bond parameters are in good agreement with those of the previously calculated values for a *trans*-olefin structure of the optimized discrete Si₂Cl₄ molecule (Scheme 25).⁶³⁻⁶⁴ The Si₂Cl₄ unit of (Cy-cAAC)₂Si₂Cl₄ adopts a *trans*-olefin like configuration as predicted by Swihart et al. and Boganov et al.⁶³ The Si-Si bond distance in (Cy-cAAC)₂Si₂Cl₄ is 2.454(3) Å which is close to that of the hypothetical Si₂Cl₄ (2.446 Å, Scheme 25). The average Si-Si single bond distances

are close to the value of 2.35 Å. The Si-Si single bond distance of 2.424(8) Å has been reported for the polymeric perchloropolysilane (SiCl₂)_n.⁶⁵ The carbenes of (Cy-cAAC·)₂Si₂Cl₄ are oriented in a *trans*-position with respect to the central Si₂Cl₄ unit with C-Si-Si-C torsion angle of 180°. Hence, (Cy-cAAC·)₂Si₂Cl₄ can be considered as a Si₂Cl₄ bridged carbon centered 1,4-diradical.⁶⁴

Theoretical calculations using the broken symmetry formalism reveals that the diradical singlet state is 2.8 Kcal mol⁻¹ lower in energy than the triplet state. The CASSCF(2,2)/SVP method has been employed for the optimization of the geometry of (Cy-cAAC·)₂Si₂Cl₄ in the singlet state. The coefficient values for the three singlet components are 0.80(2/0), -0.60(0/2), 0.0(1/1) and the diagonal elements of the final one electron symbolic density matrix are 1.3 and 0.7, respectively, suggesting that the singlet form of (Cy-cAAC·)₂Si₂Cl₄ possesses two unpaired electrons with opposite sign.⁶⁴ The unpaired electrons are stabilized by coupling with the neighboring lone-pairs of the nitrogen atoms in cAAC.

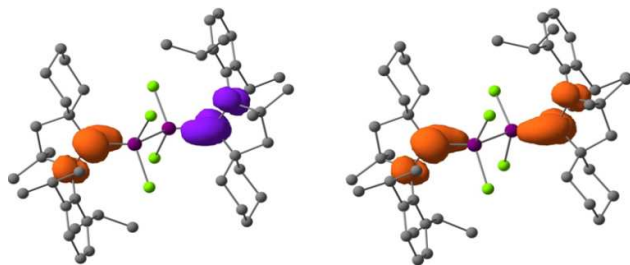


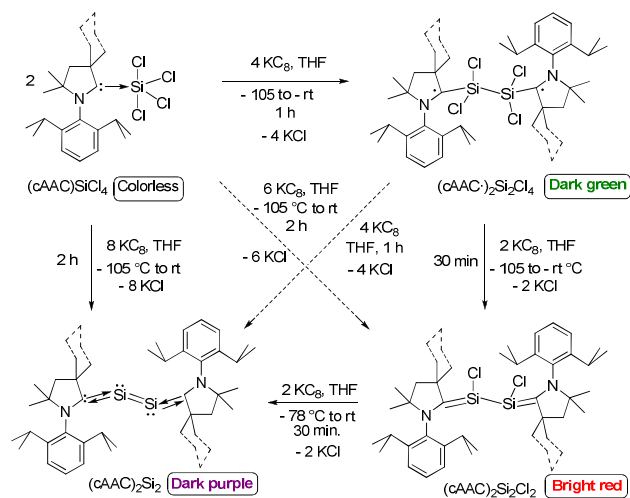
Figure 28. Computed Mulliken spin density plots (isosurface = 0.006 au) of (Cy-cAAC·)₂Si₂Cl₄ in the diradical singlet (left) and triplet state (right). Reproduced with permission from ref. 64.

Mulliken spin density distribution plot of singlet diradical and the triplet (Figure 28) form entails that the two unpaired electrons are localized at the C_{cAAC} of the Cy-cAAC.⁶⁴ It has been concluded from the theoretical investigations that the radical intermediate (Cy-cAAC·)Si(·)Cl₂ formed⁶⁴ from the reaction of (Cy-cAAC·)SiCl₃ and KC₈ depicted in Scheme 26 possesses a singlet ground state (Cy-cAAC·↑)Si(·↓)Cl₂. Dimerization of two such species to form the 1,4-diradical (Cy-cAAC·)₂Si₂Cl₄ is found to be favorable with an exothermicity of -30.9 Kcal mol⁻¹ (ΔG₂₉₈ = -14.7 kcal mol⁻¹, Figure 27, Scheme 26).⁶⁴

The dark green solution of (cAAC·)₂Si₂Cl₄ is reduced with two equiv of KC₈ with the goal of isolation of the hypothetical 1,2,3,4-tetra radical (cAAC·)₂Si(·)₂Cl₂. A dark green solution of composition (cAAC)₂Si₂Cl₂ is obtained. The molecular structure has been confirmed by X-ray single crystal diffraction (Figure 29). The ²⁹Si NMR spectrum of (Me₂-cAAC)₂Si₂Cl₂ exhibits⁶⁶ a singlet at 25.62 ppm which is downfield shifted when compared to that of (Me₂-cAAC)SiCl₄ (-103.5 ppm). The same compound (Me₂-cAAC)₂Si₂Cl₂ can be directly synthesized from

the reduction of (Me₂-cAAC)SiCl₄ adduct with three equiv of KC₈ in THF (Scheme 27).⁶⁶

The C_{cAAC}-Si bond distances of (Me₂-cAAC)₂Si₂Cl₂ (1.823(3)–1.826(3) Å) are slightly shorter when compared with that of (Cy-cAAC·)₂Si₂Cl₄ (1.846(5) Å). The Si-Si bond distances of (Me₂-cAAC)₂Si₂Cl₂⁶⁶ and (Cy-cAAC·)₂Si₂Cl₄⁶⁴ are 2.3058(13) Å and 2.454(3) Å, respectively, suggesting significant shortening of the Si-Si bond length in the former species.



Scheme 27. Synthetic strategy of (cAAC·)₂Si₂Cl₄, (cAAC)₂Si₂Cl₂, and (cAAC)₂Si₂ from (cAAC)SiCl₄ with KC₈ [cAAC = Me₂-cAAC and Cy-cAAC]

However, the theoretical calculation reveals⁶⁶ that four electrons of (Me₂-cAAC)₂Si₂Cl₂ are involved in weak π-bonding and hence it should be termed as a 1,4-diaryl-amino-2,3-disiladichlorobutadiene (C_{cAAC}=Si(Cl)-Si(Cl)=C_{cAAC}) derivative (Scheme 27, Figure 29)⁶⁶ rather than a hypothetical 1,2,3,4-tetra radical (cAAC·)₂Si(·)₂Cl₂. The C_{cAAC}-Si and Si-Si bonds are shorter due to delocalized π-bonding which is extended to the delocalized C-Si-Si-C backbone. It has a singlet ground state which is stable by 27.9 Kcal mol⁻¹, when compared with that of the triplet state.⁶⁶

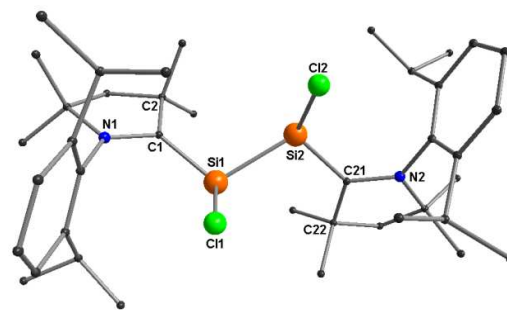
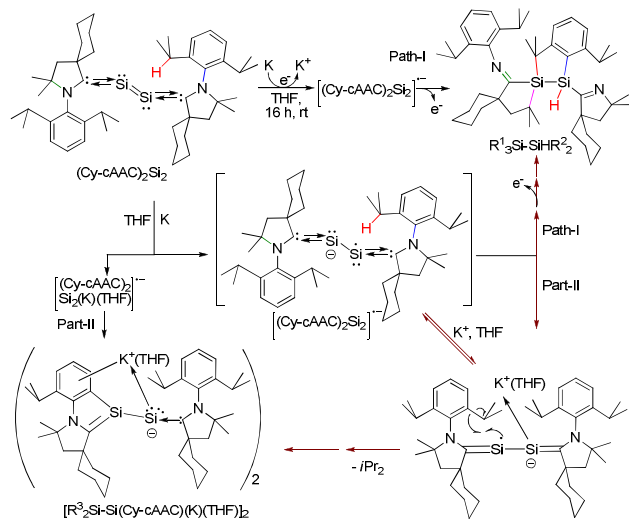


Figure 29. The molecular structure of (Me-cAAC)₂Si₂Cl₂.

The 2,3-disiladichlorobutadiene (cAAC)₂Si₂ is isolated in 47–48% when (cAAC)SiCl₄ is reduced with four equiv of KC₈ in THF (Scheme

27). Compound $(\text{cAAC})_2\text{Si}_2$ ⁶⁷ is isolated as dark purple needles. They are stable for months under an inert atmosphere without any decomposition. $(\text{Cy-cAAC})_2\text{Si}_2$ melts in the range of 188–190 °C and has been further characterized by EI mass spectrometry. The ²⁹Si NMR spectrum of $(\text{Cy-cAAC})_2\text{Si}_2$ shows a singlet resonance at 249.1 ppm in C₆D₆.⁶⁷ X-ray single crystal diffraction exhibits that each silicon atom is bound to one Cy-cAAC ligand and one silicon atom (Figure 30). The C_{cAAC}–Si bond lengths of $(\text{Cy-cAAC})_2\text{Si}_2$ are 1.849(4) to 1.876(4) Å.



Scheme 28. One electron mediated rearrangement of $(\text{Cy-cAAC})_2\text{Si}_2$.

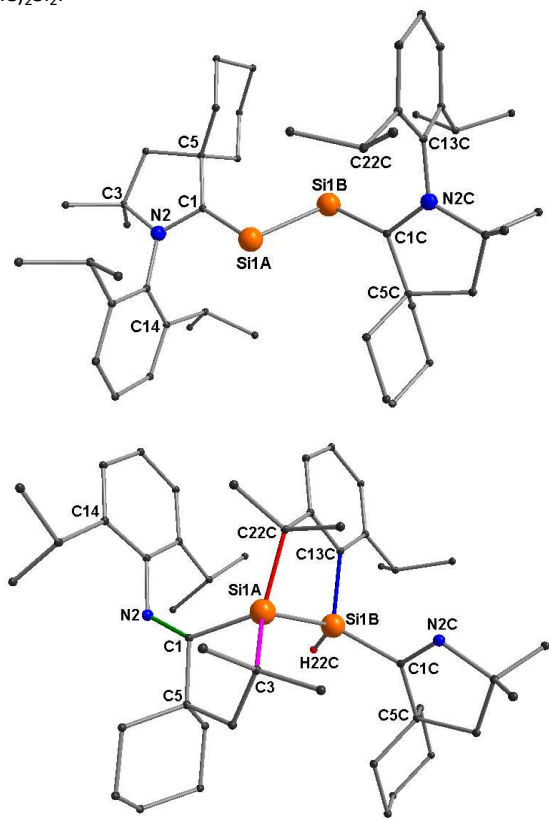


Figure 30. The molecular structures of $(\text{Cy-cAAC})_2\text{Si}_2$ (top) and its rearranged product $\text{R}^1_3\text{Si-SiHR}^2_2$ (bottom).

The cyclic voltammogram of $(\text{Cy-cAAC})_2\text{Si}_2$ has been studied in THF containing 0.1 M *n*-Bu₄NPF₆ as an electrolyte. The CV shows a quasi-reversible reduction at $E_{1/2} = -1.40$ V versus Cp*₂Fe/Cp*₂Fe⁺ indicating the possible formation of a radical anion $(\text{Cy-cAAC})_2\text{Si}_2^{\bullet-}$ (Figure 31).⁶⁷

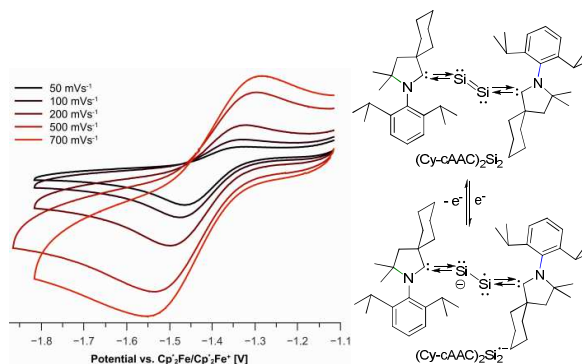


Figure 31. CV of $(\text{Cy-cAAC})_2\text{Si}_2^{\bullet-}$ in THF (left) (potential versus Cp*₂Fe/Cp*₂Fe⁺). Formation of $(\text{Cy-cAAC})_2\text{Si}_2^{\bullet-}$ from $(\text{Cy-cAAC})_2\text{Si}_2$ (right). Reproduced with permission from ref. 67.

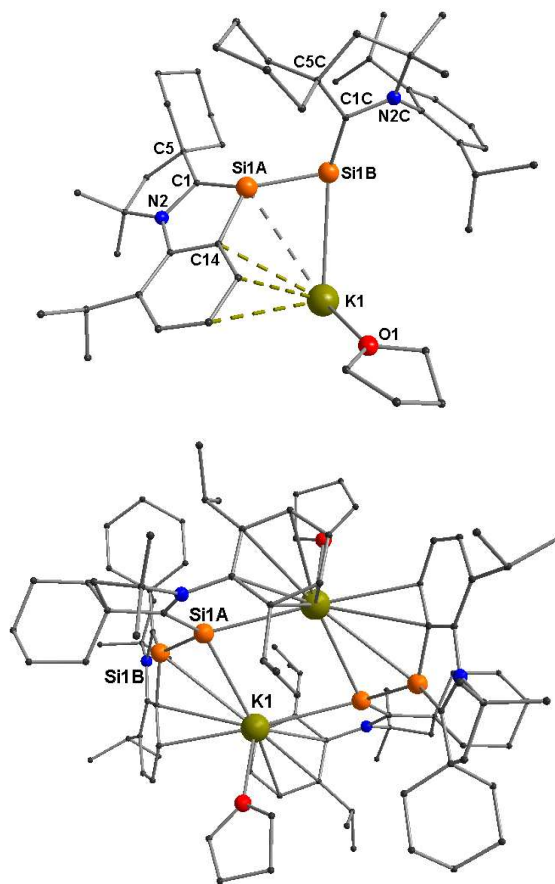
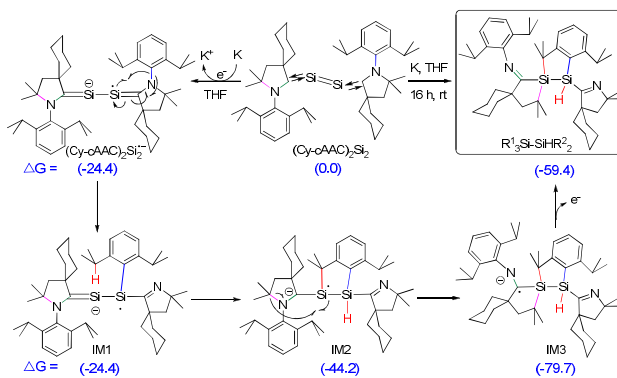


Figure 32. The monomeric (top) and dimeric (bottom) views of $[\text{R}^3\text{Si-Si}(\text{Cy-cAAC})(\text{K})(\text{THF})]_2$.

The purple color of the THF solution gradually changes to red when $(\text{Cy-cAAC})_2\text{Si}_2$ is treated with metallic potassium at room temperature for 16 h.⁶⁷ The formation of a pale yellow colored solution is easily visible around the surface of the piece of potassium. Pale yellow rods are isolated when the concentrated THF solution of the reaction mixture is stored at -32 °C. X-ray single crystal diffraction reveals a rearranged structure of $\text{R}^3\text{Si-SiHR}^2_2$ which is shown in Scheme 28. Compound $\text{R}^3\text{Si-SiHR}^2_2$ (Figure 30) can be considered as an isomer of $(\text{Cy-cAAC})_2\text{Si}_2$. After the separation of $(\text{Cy-cAAC})_2\text{Si}_2$ some red rods of $[\text{R}^3\text{Si-Si}(\text{Cy-cAAC})(\text{K})(\text{THF})]_2$ are isolated (Figure 32).⁶⁷

X-ray single crystal diffraction (Figure 30) reveals that $\text{R}^3\text{Si-SiHR}^2_2$ underwent multiple structural rearrangements when compared with $(\text{Cy-cAAC})_2\text{Si}_2$.⁶⁷ Both the silicon atoms of $\text{R}^3\text{Si-SiHR}^2_2$ (Figure 30) maintain a slightly distorted tetrahedral geometry in the formal oxidation state four. The Si1A center is bound to three carbons (C1, C3, C22C) and one silicon (Si1B) atom. The second silicon atom (Si1B) is bound to two carbons (C1C, C13C), one hydrogen (H22C) and one silicon (Si1A) atom. All the four Si-C/H bonds are electron sharing covalent single bonds. The structural features of $\text{R}^3\text{Si-SiHR}^2_2$ are unique. It possesses one exo-cyclic (C1-N2) and one endo-cyclic (C1C-N2C) double bonds with two five-membered spiro rings (Figure 30).⁶⁷

The CV suggests the formation of the radical anion $(\text{Cy-cAAC})_2\text{Si}_2^{\bullet-}$ (Figure 31)⁶⁷ via a quasi-reversible electron transfer process between $(\text{Cy-cAAC})_2\text{Si}_2$ and metallic potassium. Intermediate $(\text{Cy-cAAC})_2\text{Si}_2^{\bullet-}$ might not be stable enough as indicated by CV, it undergoes numerous bond activations followed by rearrangements. Theoretical calculation shows that $(\text{Cy-cAAC})_2\text{Si}_2^{\bullet-}$ can take two pathways (path-I and path-II) and both of them are energetically favorable (Scheme 29). The path-I is suggested to proceed via the intermediates IM1, IM2, and IM3 finally gives the rearranged product $\text{R}^3\text{Si-SiHR}^2_2$. The path-II involves the coordination of the lone pair of electrons to potassium ion to produce $(\text{Cy-cAAC})_2\text{Si}_2(\text{K})(\text{THF})^{\bullet-}$ which loses isopropyl radical to give a THF coordinated dimeric $[\text{R}^3\text{Si-Si}(\text{Cy-cAAC})(\text{K})(\text{THF})]_2$ salt.⁶⁷ In general, several stable radical anions or radical cations are often generated for the isolation and characterization via electron addition or electron snatching processes from some compounds if those species have long life-time. Scheme 28 shows a classic example that illustrates what might be possibly happen if a radical intermediate is not stable enough.⁶⁷

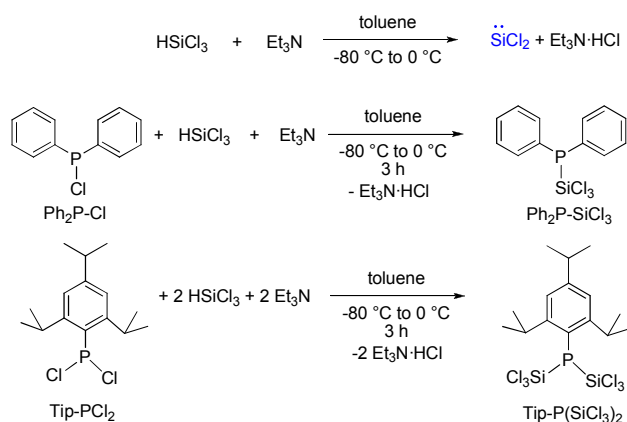


Scheme 29. Proposed reaction pathway (path-I) for the formation of $\text{R}^3\text{Si-SiHR}^2_2$ from $(\text{Cy-cAAC})_2\text{Si}_2$. Relative free energies ΔG at BP86/SVP are given in Kcal mol^{-1} .

CARBENE CENTERED RADICALS AND RADICAL ANIONS BEARING UNIQUE DIPHENYLPHOSPHINO-DICHLOROSILANE GROUP

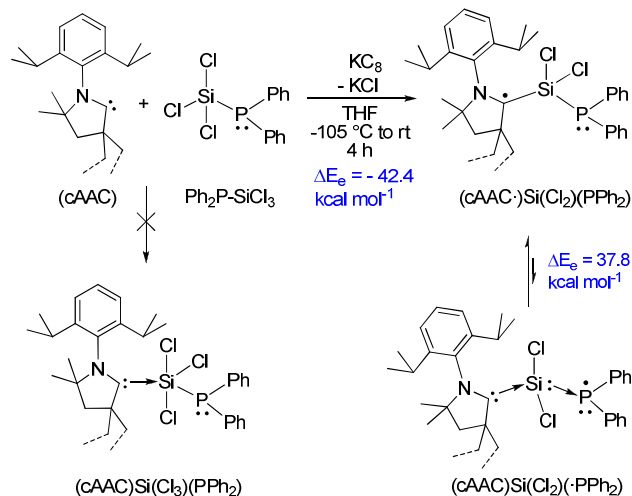
NHCs favor the formation of $\text{NHC} \rightarrow \text{PCl}_3$ adduct with trichlorophosphine (PCl_3).⁶⁸ $\text{NHC} \rightarrow \text{PCl}_3$ has been reduced to bisphosphinedene ($\text{NHC} \rightarrow \text{P}$)₂ by six equiv of KC_8 . The cAAC analogue of $(\text{NHC} \rightarrow \text{P})_2$ is suggested to have a $\text{C}_{\text{cAAC}}=\text{P}$ double bond in $(\text{cAAC}=\text{P})_2$ rather than a coordinate single bond like in $(\text{NHC} \rightarrow \text{P})_2$. So far, the comparative carbene affinity of silicon and phosphorus centers when present in the same compound is only rarely studied. Two decades ago du Mont et al. developed the first synthesis route of phosphine substituted chlorosilanes.⁶⁹ We realized that the chemistry of carbenes/phosphino-chlorosilane follows a significantly diverse path when compared to that of carbene/ SiCl_4 and carbene/ PCl_3 .⁷⁰

An attempt is made to synthesize a hypothetical stable radical species incorporating two different neutral compounds, viz. cAAC and phosphinochlorosilane. Initially, the intermediate species SiCl_2 is *in situ* generated by reacting HSiCl_3 with Et_3N in toluene in 1:1.1 molar ratio below -80 °C and subsequently reacted with Ph_2PCl and Tip-PCl_2 [Tip = 2,4,6-trisopropylphenyl] in 1:1 and 2:1 molar ratio, respectively (Scheme 30).

Scheme 30. Synthesis strategy of $\text{Ph}_2\text{P-SiCl}_3$ and $\text{Tip-P(SiCl}_3)_2$.

A one pot reaction of $\text{Ph}_2\text{P-SiCl}_3$, cAAC and KC_8 in 1:1:1 molar ratio in THF always resulted in the formation of the yellow blocks of $[(\text{cAAC})\text{PPh}_2]^+\text{Cl}^-$ as the major product.

To avoid the formation of $[(\text{cAAC})\text{PPh}_2]^+\text{Cl}^-$, a 1:1 molar mixture of cAAC and KC_8 and one equiv of $\text{Ph}_2\text{P-SiCl}_3$ are placed separately in two different Schlenk flasks. Both the flasks are cooled utilizing liquid nitrogen baths.⁷⁰ Pre-cooled THF ($\sim -100^\circ\text{C}$) is added to the flask containing $\text{Ph}_2\text{P-SiCl}_3$ through a canula. The solution of $\text{Ph}_2\text{P-SiCl}_3$ is then passed into the other flask containing cAAC and KC_8 ($\sim -105^\circ\text{C}$) with continuing stirring for 5 min at the same temperature. The temperature of the reaction solution is slowly raised to produce a greenish-red solution.

Scheme 31. Synthesis strategy of $(\text{cAAC})\text{Si(Cl}_2)(\text{PPh}_2)$ [cAAC = $\text{Me}_2\text{-cAAC}$ and $\text{Et}_2\text{-cAAC}$].

The red needles of compound $(\text{cAAC})\text{Si(Cl}_2)(\text{PPh}_2)$ [cAAC = $\text{Me}_2\text{-cAAC}$, $\text{Et}_2\text{-cAAC}$] (Scheme 31) are isolated in 22–25% yield.⁷⁰ For comparison, when the similar reaction is carried out with equivalent amount of NHC instead of cAAC, $\text{NHC} \rightarrow \text{SiCl}_2$ ²⁸ is isolated instead of $(\text{NHC})\text{Si(Cl}_2)(\text{PPh}_2)$.

The above mentioned protocol is mandatory for the synthesis and isolation of the compound $(\text{cAAC})\text{Si(Cl}_2)(\text{PPh}_2)$ in a pure form.⁷⁰ If the reaction is initiated at -78°C using a frozen solvent bath and the temperature of the reaction slurry is slowly raised, a dark blue solution of the previously reported $(\text{cAAC})_2\text{SiCl}_2$ is obtained as the major product with a much decreased amount of the desired $(\text{cAAC})\text{Si(Cl}_2)(\text{PPh}_2)$.⁷⁰ This suggests that further cleavage of the Si-PPh_2 bond of $(\text{cAAC})\text{Si(Cl}_2)(\text{PPh}_2)$ occurs in the absence of proper temperature controlling followed by the anchoring of another cAAC which leads to the formation of the undesired compound $(\text{cAAC})_2\text{SiCl}_2$. The isolation of $(\text{cAAC})\text{Si(Cl}_2)(\text{PPh}_2)$ from this mixture via partial crystallization is not fruitful since the presence of $(\text{cAAC})_2\text{SiCl}_2$ hinders the crystallization of $(\text{cAAC})\text{Si(Cl}_2)(\text{PPh}_2)$ in its pure form. The previously mentioned protocol minimizes the formation of $(\text{cAAC})_2\text{SiCl}_2$ and increases the yield of $(\text{cAAC})\text{Si(Cl}_2)(\text{PPh}_2)$ to a large extent.⁷⁰

The central silicon atom in $(\text{cAAC})\text{Si(Cl}_2)(\text{PPh}_2)$ adopts a near-tetrahedral coordination geometry and is bound to one phosphorus, one carbene carbon, and two chlorine atoms (Figure 33). The $\text{Si-C}_{\text{cAAC}}$ bond distance in $(\text{cAAC})\text{Si(Cl}_2)(\text{PPh}_2)$ [cAAC = $\text{Me}_2\text{-cAAC}$ and $\text{Et}_2\text{-cAAC}$] is 1.826(3)–1.839(2) Å which is longer (~ 0.12 Å) than the $\text{C}_{\text{cAAC}} \rightarrow \text{Si}$ coordinate bond of $(\text{cAAC})\text{SiCl}_4$ but close to the covalent electron sharing Si-C single bond of $(\text{cAAC})\text{SiCl}_3$. One chlorine atom tries to orient perpendicular to the C2C1N1 plane (angle between C2C1N1 and C1Si1Cl2 is 66.85°).⁷⁰

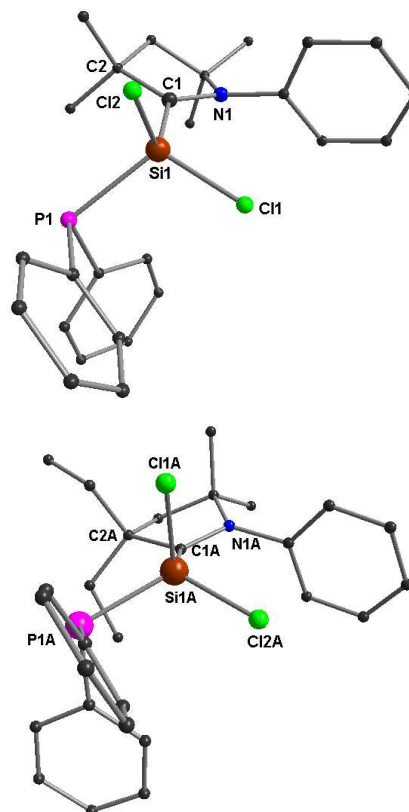
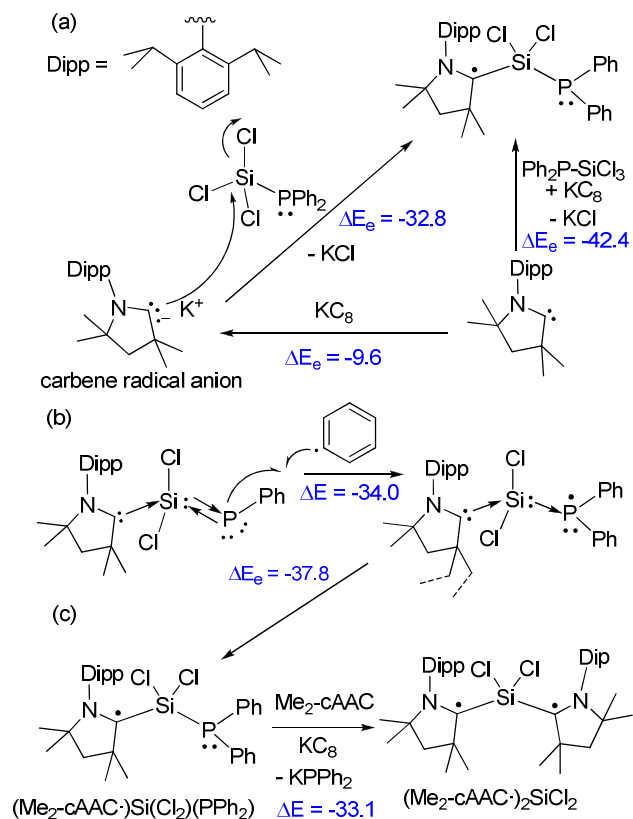


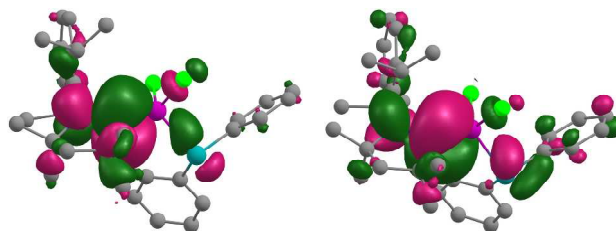
Figure 33. Molecular structures of $(\text{Me}_2\text{-cAAC})\text{Si}(\text{Cl}_2)(\text{PPh}_2)$ (top) and $(\text{Et}_2\text{-cAAC})\text{Si}(\text{Cl}_2)(\text{PPh}_2)$ (bottom). H-atoms and isopropyl groups from Dipp are omitted for clarity.

As mentioned previously that the compound $[(\text{Me}_2\text{-cAAC})\text{PPh}_2]^+\text{Cl}^-$ is obtained as a major product when $\text{Ph}_2\text{P-SiCl}_3$ is directly reacted with $\text{Me}_2\text{-cAAC}$ in 1:1 molar ratio suggesting that $\text{Me}_2\text{-cAAC}$ prefers to bind at the phosphorus center with the elimination of SiCl_2 . The reaction of $\text{Ph}_2\text{P-SiCl}_3$ with KC_8 is very slow in THF at room temperature and thus the unreacted $\text{Ph}_2\text{P-SiCl}_3$ is recovered from the reaction mixture even after two days suggesting that the formation of $\text{Ph}_2\text{P-Si}(\cdot)\text{Cl}_2$ is not facile. Based on the experimental observations a possible mechanism for the formation of $(\text{Me}_2\text{-cAAC})\text{Si}(\text{Cl}_2)(\text{PPh}_2)$ is proposed in Scheme 32 and the energetics are calculated for $(\text{Me}_2\text{-cAAC})\text{Si}(\text{Cl}_2)(\text{PPh}_2)$. The *in situ* formation of a carbene radical anion (cAAC^\cdot) intermediate is favorable since $\text{Me}_2\text{-cAAC}$ has a lower lying LUMO. $\text{cAAC}^\cdot\text{K}^+$ knocks out one chloride from $\text{Ph}_2\text{P-SiCl}_3$ to produce $(\text{Me}_2\text{-cAAC})\text{Si}(\text{Cl}_2)(\text{PPh}_2)$ with the formation of KCl . All the steps of the reaction are energetically favorable. Theoretical calculations further suggest that $(\text{Me}_2\text{-cAAC})\text{Si}(\text{Cl}_2)(\text{PPh}_2)$ (carbene centered radical form) is more stable by an energy of $-37.8 \text{ Kcal mol}^{-1}$ than $(\text{Me}_2\text{-cAAC})\text{Si}(\text{Cl}_2)(\cdot\text{PPh}_2)$ (phosphorus centered radical form). The formation of $(\text{Me}_2\text{-cAAC})_2\text{SiCl}_2$ from the reaction of $(\text{Me}_2\text{-cAAC})\text{Si}(\text{Cl}_2)(\cdot\text{PPh}_2)$ with $\text{Me}_2\text{-cAAC}/\text{KC}_8$ is energetically preferred. This might be the reason why the temperature of the reaction has to be controlled so minutely to minimize the formation of $(\text{cAAC})_2\text{SiCl}_2$ and maximize the yield of $(\text{cAAC})\text{Si}(\text{Cl}_2)(\text{PPh}_2)$. We also have observed that the undesired product $(\text{cAAC})_2\text{SiCl}_2$ is produced in good yield if a mixture of $\text{Ph}_2\text{P-SiCl}_3$, cAAC , and KC_8 is reacted in 1:2:2 molar ratio at -78°C to room temperature in THF for 2-3 h.⁷⁰



Scheme 32. (a) The proposed mechanism for the formation of $(\text{cAAC})\text{Si}(\text{Cl}_2)(\text{PPh}_2)$, (b) Energetics for hypothetical reaction of $(\text{cAAC})\text{Si}(\text{Cl}_2)(\text{P-Ph})$ to $(\text{cAAC})\text{Si}(\text{Cl}_2)(\cdot\text{PPh}_2)$ and $(\text{cAAC})\text{Si}(\text{Cl}_2)(\text{PPh}_2)$ and (c) $(\text{cAAC})\text{Si}(\text{Cl}_2)(\text{PPh}_2)$ to $(\text{cAAC})_2\text{SiCl}_2$. ΔE in Kcal mol^{-1} . [$\text{cAAC} = \text{Me}_2\text{-cAAC}$]

Importantly, C_{cAAC} atom has contributed $\sim 73\%$ electron density to the $\text{C}_{\text{cAAC}}\text{-Si}$ bond indicating polar character.⁷⁰ The calculated Mulliken spin density plots, for $\text{Me}_2\text{-cAAC}$ and $\text{Et}_2\text{-cAAC}$ analogues shown in Figure 34 (top), suggest that the unpaired electron is mostly located on the carbene carbon (75-76%), with a comparatively lower contribution from the N1 atom (18-20%) present in the cAAC fragment. Moreover, the unpaired electron exhibits some finite occupancy over one chlorine atom (1%) and the phosphorus ($\sim 3\%$) atom.



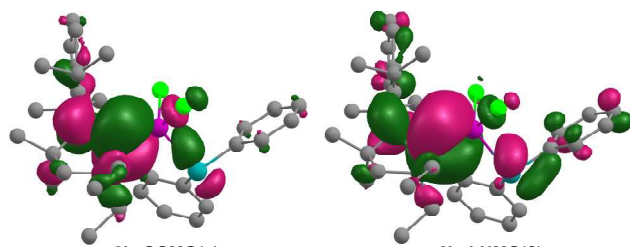


Figure 34. KS-MO (frontier MO; SOMO (left) and LUMO (right)) for (cAAC)Si(Cl₂)(PPh₂) [cAAC = Me₂-cAAC (top) and Et₂-cAAC (bottom)], (isodensity = 0.03 electron/bohr³). Reproduced with permission from ref. 70.

The EPR resonance spectra of (Me₂-cAAC)Si(Cl₂)(PPh₂) and (Et₂-cAAC)Si(Cl₂)(PPh₂) are recorded in toluene (Figures 35–36). Compound (Me₂-cAAC)Si(Cl₂)(PPh₂) exhibits a partially resolved EPR spectrum which could be simulated with data according to the DFT calculated hyperfine coupling: $a(^{31}\text{P})$ 15.6 G (calc. 20.5 G), $a(^{14}\text{N})$ 6.5 G (calc. 4.2 G), $a(^{35}\text{Cl})$ 4.1 G (calc. 3.1 G).

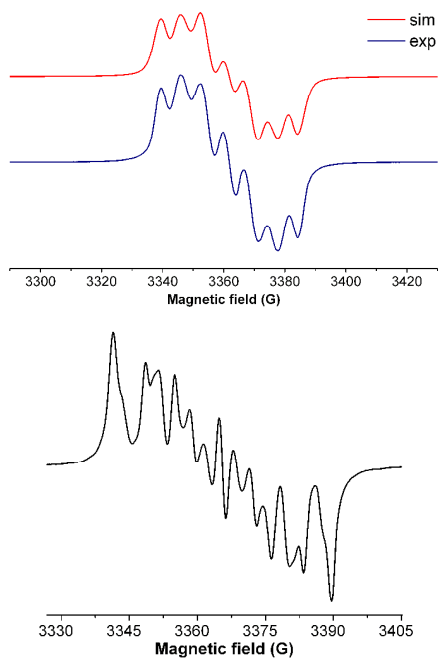


Figure 35. Experimental and simulated EPR spectra of (Me₂-cAAC)Si(Cl₂)(PPh₂) at 298 K (top) and experimental EPR of (Et₂-cAAC)Si(Cl₂)(PPh₂) at 299 K (bottom). Reproduced with permission from ref. 70.

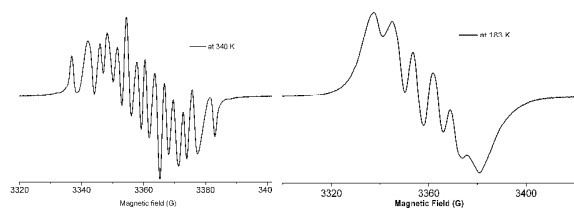


Figure 36. Experimental and simulated EPR spectra of (Et₂-cAAC)Si(Cl₂)(PPh₂) at 340 K (left) and 183 K (right). Reproduced with permission from ref. 70.

The spin density is mostly concentrated at carbene carbon atom (ca. 75%), and adjacent nitrogen atom (19%). Accordingly, the g factors for both (Me₂-cAAC)Si(Cl₂)(PPh₂) (2.0027) and (Et₂-cAAC)Si(Cl₂)(PPh₂) (2.0024) are very close to that of the free electron (2.0023). The heteroatom ³¹P and one of the chlorine atoms in β -position exhibit detectable hyperfine coupling despite rather small spin densities <5%. A ²⁹Si satellite coupling (4.7% nat. abundance, $I = 1/2$) could be observed for (Et₂-cAAC)Si(Cl₂)(PPh₂) at about 10 G (calcd 13.4 G; 3.6% spin density).⁷⁰

The ethyl substituents of Et₂-cAAC at (Et₂-cAAC)Si(Cl₂)(PPh₂) are labile. The Si(Cl₂)(PPh₂) group can rotate around Si-C_{CAAC} bond depending upon the substitutions at the C2 atom which is clearly observed when the molecules in (Me₂-cAAC)Si(Cl₂)(PPh₂) and (Et₂-cAAC)Si(Cl₂)(PPh₂) are viewed along the Si-C_{CAAC} bond (Figure 33). Moreover, the five-membered rings of the carbene part adopt different conformations. One chlorine atom Cl2 of (Me₂-cAAC)Si(Cl₂)(PPh₂) and Cl1A of (Et₂-cAAC)Si(Cl₂)(PPh₂) are differently oriented with respect to the p_z-orbital of carbene carbon atoms which exerts hyperfine interaction of different strengths in (Me₂-cAAC)Si(Cl₂)(PPh₂) and (Et₂-cAAC)Si(Cl₂)(PPh₂). It is noteworthy that there are two molecules present in the asymmetric unit of (Et₂-cAAC)Si(Cl₂)(PPh₂) with slightly different bond parameters. This leads to the superposition of EPR signals from the two conformers (Figures 35–36) leading to a complicated EPR resonance, the signature of which changes dramatically when the temperature is varied (Figure 36). As a consequence, the temperature dependent EPR spectra between 183 and 340 K show variable line widths. Thus simulation could not be achieved within the accessible temperature range for (Et₂-cAAC)Si(Cl₂)(PPh₂).⁷⁰

The redox property is also investigated for (cAAC)Si(Cl₂)(PPh₂) by cyclic voltammetry measurements [Figure 37; (Me₂-cAAC)Si(Cl₂)(PPh₂)] in THF solution. The CV shows one electron quasi-reversible process at $E_{1/2} = -0.86$ V against Cp^{*}₂Fe/Cp^{*}₂Fe⁺, suggesting the formation of the anion (cAAC)Si(Cl₂)(PPh₂)⁻.

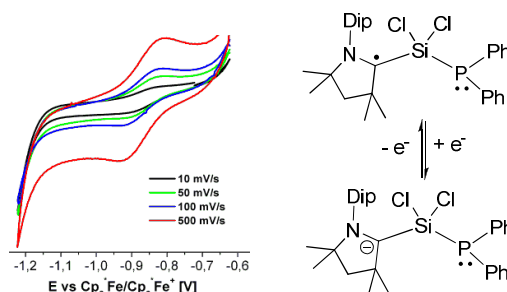
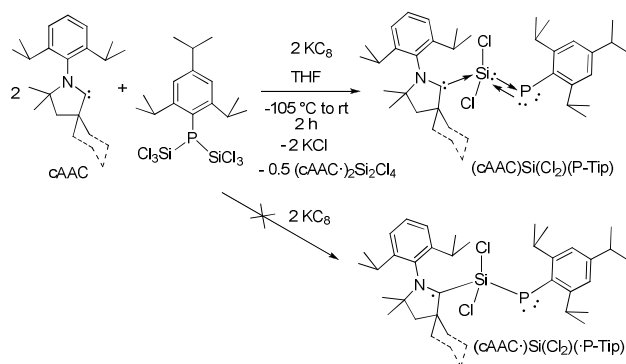


Figure 37. Cyclic voltammogram of a THF solution of (Me₂-cAAC)Si(Cl₂)(PPh₂) at indicated scan rates (potential versus Cp^{*}₂Fe/Cp^{*}₂Fe⁺), containing 0.1M [n-Bu₄N]ClO₄ as an

electrolyte (left) suggesting $(\text{cAAC})\text{Si}(\text{Cl}_2)(\text{P-Ph}_2)$ converts to $(\text{cAAC})\text{Si}(\text{Cl}_2)(\text{PPh}_2)^-$. Reproduced with permission from ref. 70.

In analogy with $(\text{cAAC})_2\text{SiCl}_2$,⁵⁷ we hypothesized the synthesis of a novel carbene (cAAC)/phosphinidene (P-Ar, Ar = 2,4,6-triisopropylphenyl) stabilized dichlorosilylene $(\text{cAAC})\text{SiCl}_2(\text{P-Ar})$ as a stable diradical (Scheme 33). When a precooled THF is added at -78°C to a 2:1:2 molar mixture of cAAC, Tip-P(SiCl_2)₂, and KC_8 , an immediate color change is observed from colorless to green and then to dark blue. The dark blue blocks of $(\text{cAAC})\text{SiCl}_2(\text{P-Tip})$ are obtained in 45% yield (Scheme 33).⁷¹ When ^{IP}NHC [$:\text{C}\{\text{N}(2,6\text{-}i\text{Pr}_2\text{C}_6\text{H}_3)(\text{CH})\}_2$] is employed instead of cAAC, the analogous compound (^{IP}NHC)(SiCl_2)(P-Tip) is obtained as a bright red crystalline solid in 90% yield.



Scheme 33. Synthesis strategy of $(\text{cAAC})\text{Si}(\text{Cl}_2)(\text{P-Tip})$ [cAAC = $\text{Me}_2\text{-cAAC}$, $\text{Et}_2\text{-cAAC}$ and Cy-cAAC].

The ²⁹Si NMR spectra of $(\text{Cy-cAAC})\text{Si}(\text{Cl}_2)(\text{P-Tip})$, (^{IP}NHC)(SiCl_2)(P-Tip) exhibit doublets at -6.56 ($J_{\text{Si-P}} = 198.4$ Hz), and -19.12 ($J_{\text{Si-P}} = 197.7$ Hz) ppm, respectively, which are upfield shifted when compared with that of $(\text{Me}_2\text{-cAAC})_2\text{SiCl}_2$ (+ 4.13 ppm).⁷¹ The ¹³C NMR resonances of $(\text{Cy-cAAC})\text{Si}(\text{Cl}_2)(\text{P-Tip})$, (^{IP}NHC)(SiCl_2)(P-Tip) (for $\text{C}_{\text{carbene}}$) are observed at 208.05, and 211.44 ppm, respectively which are again upfield shifted when compared with that of the free carbene (309.4 ppm for Cy-cAAC) but close to that of $\text{Cy-cAAC}\rightarrow\text{SiCl}_4$ (207.0 ppm), and $(\text{cAAC})_2\text{Si}$ (210 ppm). The UV-vis spectrum of $(\text{Cy-cAAC})\text{Si}(\text{Cl}_2)(\text{P-Tip})$ is recorded in THF which shows a broad (500–900 nm) absorption band at 665 nm, while the corresponding (400–600 nm) value for compound (^{IP}NHC)(SiCl_2)(P-Tip) is observed at 475 nm.⁷¹

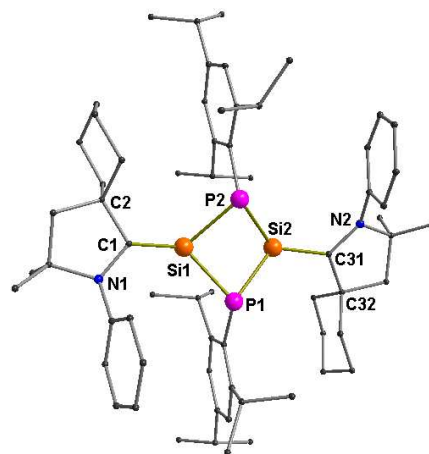
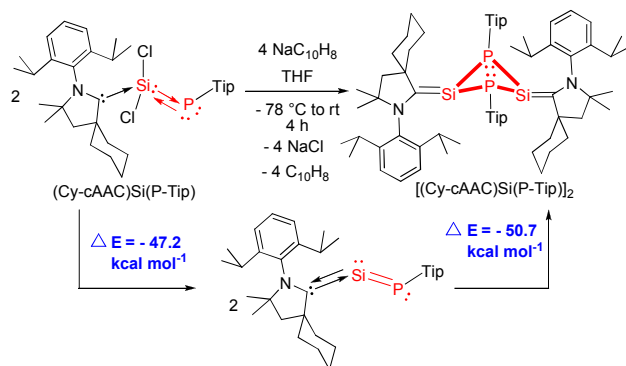


Figure 38. Molecular structure of $(\text{Cy-cAAC})\text{Si}(\text{Cl}_2)(\text{P-Tip})$. All H-atoms and *i*PR groups of Dipp are omitted for clarity.

The compounds (carbene)(SiCl_2)(P-Tip) are characterized by single crystal X-ray structure determinations. The molecular structure of $(\text{Cy-cAAC})\text{Si}(\text{Cl}_2)(\text{P-Tip})$ shows (Figure 38) that the central SiCl_2 unit is bound to one carbene (Cy-cAAC) and one phosphorus atom of the P-Tip group. The silicon atom adopts a distorted tetrahedral geometry while the phosphorus atom attends a bent geometry. The phosphorus atom is bound to one silicon (Si1-P1 2.1225(9) Å) and one carbon atom (P1-C24 1.874(2) Å) of the Tip group. The $\text{C}_{\text{cAAC-Si}}$ and $\text{C}_{\text{cAAC-N}}$ bond distances were found to be 1.945(2) and 1.308(3) Å, respectively, which are close to those values (1.944(2) and 1.303(2) Å), found in $\text{Me}_2\text{-cAAC}\rightarrow\text{SiCl}_4$. The aforementioned bond parameters of $(\text{Cy-cAAC})\text{Si}(\text{Cl}_2)(\text{P-Tip})$ suggest that the bond between the carbene carbon atom and the silicon atom is a coordinate bond (C \rightarrow Si) rather than an electron sharing single bond (which is supposed to be ~ 1.84 Å). To elucidate the exact bonding situations in the compounds $\text{cAAC}\rightarrow\text{SiCl}_2\rightarrow\text{P-Tip}$, and ^{IP}NHC $\rightarrow\text{SiCl}_2\rightarrow\text{P-Tip}$ detailed theoretical calculations have been carried out on the model compounds **2M**, and **3M**, respectively, where the Dipp groups at the cAAC and NHC donors moieties and the *i*Pr groups at P-Tip are replaced by the methyl groups. NBO analysis reveals that the bonding scenario of these molecules could be best represented in terms of the donor-acceptor interactions $\text{D}\rightarrow\text{SiCl}_2\rightarrow\text{P-Tip}$ (D = cAAC, NHC). As a result, we can say that the DSiCl_2 moiety as a whole forms a coordinate bond ($\text{DCl}_2\text{Si}\rightarrow\text{P}$) with the phosphorus atom of the P-Tip group leaving two pairs of electrons on the phosphorus atom with σ and π symmetry where the latter is engaged in some π -backdonation to the Si. Hence, in reality there is no diradical character found in the dark blue colored $\text{cAAC}\rightarrow\text{SiCl}_2\rightarrow\text{P-Tip}$ as hypothesized previously in comparison with $(\text{cAAC})_2\text{SiCl}_2$. The HOMO of $\text{cAAC}\rightarrow\text{SiCl}_2\rightarrow\text{P-Tip}$ is located on the $\pi_{\text{Si-P}}$ bond while the LUMO is located on the carbene moiety (cAAC or NHC). The characteristic dark blue color of $\text{cAAC}\rightarrow\text{SiCl}_2\rightarrow\text{P-Tip}$ is originated from the strong intramolecular charge transfer transition (ICT) from $\pi_{\text{Si-P}}\rightarrow\pi^*_{\text{carbene}}$. The dramatic change in

color from red (${}^{\text{IP}}\text{-NHC}\rightarrow\text{SiCl}_2\rightarrow\text{P-Tip}$) to blue ($\text{cAAC}\rightarrow\text{SiCl}_2\rightarrow\text{P-Tip}$) is attributed to the lower lying LUMO of cAAC.⁷¹

We have seen before that $(\text{Cy-cAAC}\cdot)\text{SiCl}_2$ has a singlet diradical spin ground state $[(\text{Cy-cAAC}\cdot)\text{Si}(\cdot)\text{Cl}_2]$ and as a consequence, dimeric 1,4-diradical $(\text{Cy-cAAC}\cdot)_2\text{Si}_2\text{Cl}_4$ ⁶⁴ is eventually isolated (Scheme 26). Thus, it has been intriguing what might be the electronic structure of the dechlorinated product of $(\text{Cy-cAAC}\rightarrow\text{SiCl}_2\rightarrow\text{P-Tip})$. The employment of KC_8 as the reducing agent for this purpose has not been successful. However, $(\text{Cy-cAAC}\rightarrow\text{SiCl}_2\rightarrow\text{P-Tip})$ is successfully reduced with two equiv of sodium naphthalene ($\text{NaC}_{10}\text{H}_8$) in THF at room temperature to obtain the dark purple colored monomeric compound $(\text{Cy-cAAC})\text{Si}(\text{P-Tip})$ (Scheme 34).⁷² It is stable for several hours at room temperature. The ${}^{29}\text{Si}$ and ${}^{31}\text{P}$ chemical shift values of $(\text{Cy-cAAC})\text{Si}(\text{P-Tip})$ are observed at 288.3 ppm and 309.6 ppm ($J_{\text{Si-P}} = 163$ Hz), respectively. Theoretical calculation concerning the nature of the ground state reveals that $(\text{Cy-cAAC})\text{Si}(\text{P-Tip})$ does not possess a singlet diradical ground state. The cAAC-Si and Si-P are found to be donor acceptor type partial double bond ($\text{C}_{\text{cAAC}}\rightarrow\text{Si}$) and double bond ($\text{Si}=\text{P}$), respectively. The $\text{Si}=\text{P}$ double bond becomes weak due to the donation of one lone pair of electrons on silicon atom to the π^* of $\text{Si}=\text{P}$ double bond. Thus, this monomer undergoes dimerization to produce the thermodynamically more stable (-50.7 Kcal mol⁻¹) and isolable compound $[(\text{Cy-cAAC})\text{Si}(\text{P-Tip})]_2$ (Scheme 34).⁷² It is characterized by X-ray single crystal diffraction. In $[(\text{Cy-cAAC})\text{Si}(\text{P-Tip})]_2$ each phosphorus atom is bound to a Tip group and each silicon atom to a carbene (Cy-cAAC). The P-Tip groups are oriented in *cis* conformation with respect to the Si_2P_2 ring. The aromatic rings of Tip groups are arranged perpendicular to the Si_2P_2 ring, while the five-membered carbene rings of Cy-cAAC are parallel to the average plane of the Si_2P_2 ring.⁷²



Scheme 34. Synthesis strategy of monomeric $(\text{Cy-cAAC})\text{Si}(\text{P-Tip})$ and dimeric $[(\text{Cy-cAAC})\text{Si}(\text{P-Tip})]_2$.

${}^{31}\text{P}$ NMR spectrum of $[(\text{Cy-cAAC})\text{Si}(\text{P-Tip})]_2$ in $\text{THF-}d_8$ solution exhibits a singlet at -113.4 ppm, flanked by a pair of ${}^{29}\text{Si}$ satellites ($J_{\text{Si-P}} = 44$ Hz).⁷² It is downfield shifted when compared with that of the precursor $(\text{Cy-cAAC})\text{Si}(\text{Cl}_2)(\text{P-Tip})$ (-123.0 ppm; $J_{\text{Si-P}} = 198$ Hz). A triplet signal at 37.1 ppm with the same coupling constant ($J_{\text{Si-P}} = 44$ Hz) is observed in the ${}^{29}\text{Si}$ NMR spectrum. Theoretical calculations on an optimized geometry of both the singlet and triplet states of $[(\text{Cy-}$

$\text{cAAC})\text{Si}(\text{P-Tip})]_2$ shows that the former is the electronic ground state with an energy difference ($\Delta E_{\text{S-T}}$) of 14.2 Kcal mol⁻¹.

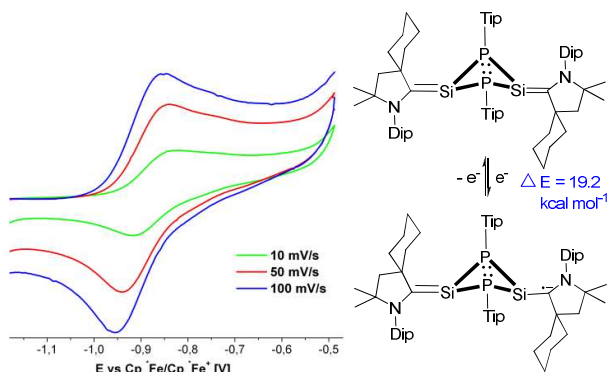


Figure 39. Cyclic voltammogram of THF solution of $[(\text{Cy-cAAC})\text{Si}(\text{P-Tip})]_2$, containing 0.1M $[\text{n-Bu}_4\text{N}]\text{ClO}_4$ as electrolyte (potential versus $\text{Cp}^*_2\text{Fe}/\text{Cp}^*_2\text{Fe}^+$). Reproduced with permission from ref. 72.

The diamagnetic spin ground state of $[(\text{Cy-cAAC})\text{Si}(\text{P-Tip})]_2$ is confirmed by magnetic susceptibility measurements.⁷² The CV shows a one electron quasi-reversible process at $E_{1/2} = -0.87$ V against $\text{Cp}^*_2\text{Fe}/\text{Cp}^*_2\text{Fe}^+$, suggesting the formation of the radical anion $[(\text{Cy-cAAC})\text{Si}(\text{P-Tip})]_2^{\bullet-}$ (Figure 39).⁷² $[(\text{Cy-cAAC})\text{Si}(\text{P-Tip})]_2^{\bullet-}$ could not be isolated. However, it is characterized by EPR spectroscopy and its bonding and electron density distribution are studied by theoretical calculations. The X-band EPR spectrum of the *in situ* generated radical anion (a typical $S = 1/2$ species) in toluene solution at 285 K consists of twelve well-resolved lines of equal intensity (Figure 40).⁷² The splitting pattern is reproduced by simulation (Figure 40, top), which shows a doublet of doublets, where each component splits further into three equidistant lines. The latter splitting is assigned to the coupling of electron spin with one ${}^{14}\text{N}$ nucleus ($I = 1$) at 5.9 G. This value is in the range of values reported for cAAC centered radicals. The two larger doublet hyperfine splittings at 44.1 and 20.6 G are attributed to two inequivalent ${}^{31}\text{P}$ nuclei ($I = 1/2$).⁷² EPR coupling constants of ${}^{31}\text{P}$ are frequently large due to the high nuclear magnetic moment, not necessarily reflecting very large spin densities. The inequivalence of the two ${}^{31}\text{P}$ nuclei in the EPR experiment is in good agreement with the calculated difference in orientation of the P-involving bonds with respect to the mainly spin-bearing $p(z)$ orbital at the carbene carbon center. Accordingly, a ${}^{29}\text{Si}$ satellite isotope coupling ($I = 1/2$, 4.7% nat. abundance) with a typical value of about 11 G is also observed.

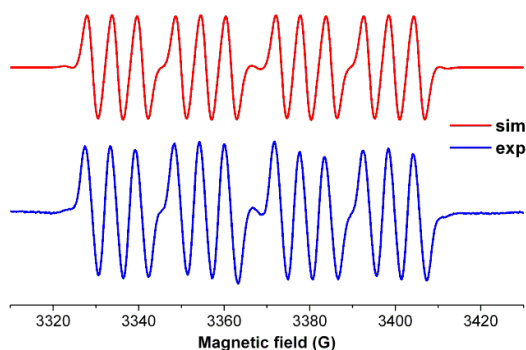


Figure 40. Simulated and experimental EPR spectra of radical $[(\text{Cy-cAAC})\text{Si}(\text{P-Tip})]_2^{\bullet-}$ in toluene at 285 K. Reproduced with permission from ref. 72.

One electron reduction of $[(\text{Cy-cAAC})\text{Si}(\text{P-Tip})]_2$ results in an increase of the electron density in its LUMO. Consequently, the C–N bond distances are elongated in $[(\text{Cy-cAAC})\text{Si}(\text{P-Tip})]_2^{\bullet-}$ (1.365/1.364 in $[(\text{Cy-cAAC})\text{Si}(\text{P-Tip})]_2$ vs. 1.405/1.413 in $[(\text{Cy-cAAC})\text{Si}(\text{P-Tip})]_2^{\bullet-}$).⁷² The $\text{C}_{\text{cAAC}}\text{--Si}$ bond lengths become unsymmetrical (1.778/1.896) in $[(\text{Cy-cAAC})\text{Si}(\text{P-Tip})]_2^{\bullet-}$, as the radical resides on the C_{cAAC} atom in $\alpha\text{-HOMO}$ (Figure 41). The calculated spin density points unambiguously the position of the unpaired electron at the carbene carbon (C_{cAAC}), with a minor contribution from neighboring N and Si atoms of the other side.⁷²

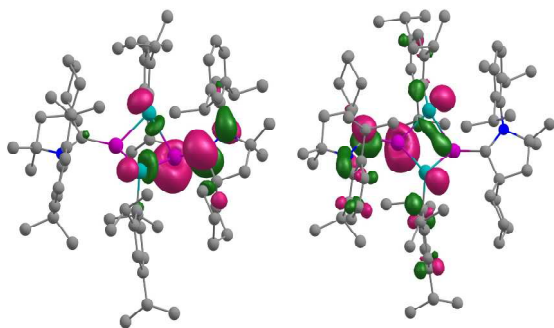


Figure 41. a) KS-MOs [$\alpha(\text{HOMO})$ left; and $\alpha(\text{LUMO})$; middle] of $[(\text{Cy-cAAC})\text{Si}(\text{P-Tip})]_2^{\bullet-}$. Reproduced with permission from ref. 72.

However, one electron oxidation is observed for monomeric compound $(^{\text{IP}}\text{NHC})\text{Si}(\text{P-Mes}^*)$ ⁷³ at -0.053 V suggesting formation of the corresponding radical cation which has neither been isolated nor characterized by EPR measurement. Till now, we have mostly discussed on the radicals and diradicals of cAAC-silicon chemistry. However, group of G. Bertrand and others also have developed novel synthetic routes to the carbene (both cAAC and NHC) stabilized radicals and radical ions of main group elements.⁷⁴⁻⁸⁹ The number of reports on cAAC stabilized radicals are higher than those of NHC due to the fact that cAAC is a better π -acceptor. Thus cAACs are comparatively more suitable for anchoring the radical species. It is important to mention that cAACs not only stabilize the radicals and radical-ions of main group elements,

they also stabilize transition metals with two coordinate geometry, having radical electrons spanning over two carbene carbon atoms of $(\text{cAAC})_2\text{M}$ [$\text{M} = \text{Au}, \text{Cu}, \text{Mn}, \text{Zn}$].⁹⁰⁻⁹³

Conclusions

In conclusion we have summarized the synthesis and characterization of stable silyl radical and silyl radical ions via the reduction or oxidation of suitable precursors under highly controlled synthesis conditions. Some of the synthesis routes are found to be unique. In few cases the steric bulk of the adjacent ligands has played significant role for the preparation of some of these species in unusual directions. The radical species are isolated and characterized by X-ray single crystal diffraction and studied by EPR. Similarly, disilene radical anion and cation are stabilized by bulky ligands. The structural and bonding aspects are illustrated by X-ray single crystal structure determination and theoretical calculations. The fine electronic interactions of these radicals with adjacent nuclei are investigated by EPR measurements. The silylene radical anion is characterized only in solution at low temperature while carbene coordinated silylene radical cation is isolated in a stable form. The disilyne radical anion is also synthesized, isolated and characterized by X-ray single crystal diffraction and EPR measurements. The singlet 1,3-diradicaloid with cyclic four-membered ring is synthesized by reaction of Ar-N=N-Ar compound with silyne or bis-silylene. All these radicals, radical ions, diradical, and diradicaloid are stabilized mostly by steric effect of the ligands. The radical centers are well protected and prevented from undergoing dimerization or polymerization. However, it is found that the radical intermediates can also be stabilized by strong σ -donation of carbene. The NHC carbene is a poor π -acceptor and hence stabilizes the radical intermediate by σ -donation. The cAAC ligand is significantly better π -acceptor and strong σ -donor. cAAC can switch its nature of bonding with the bound silicon atom depending upon the accumulation of electron density around it. The mono radicals of $\cdot\text{SiCl}_3$ and $\cdot\text{SiPh}_3$ are stabilized by cAAC with the formation of $\text{C}_{\text{cAAC}}\text{--Si}$ single bond having the radical electron on the carbene carbon atom. The diradical of SiCl_2 is stabilized by two cAACs $[(\text{cAAC})_2\text{SiCl}_2]$ while singlet SiCl_2 species is stabilized by one NHC in a non-radical monomeric form $(\text{NHC})\text{SiCl}_2$. The cAAC analogue of the latter one undergoes dimerization to produce 1,4-diradical $(\text{cAAC})_2\text{Si}_2\text{Cl}_4$ with a Si_2Cl_4 unit in the middle. Further two electrons reduction of $(\text{cAAC})_2\text{Si}_2\text{Cl}_4$ does not produce a hypothetical tetra radical $(\text{cAAC})_2\text{Si}(\cdot)_2\text{Cl}_2$ rather it can be termed as 1,4-diamino-2,3-disilabutadiene derivative $(\text{cAAC})_2\text{Si}_2\text{Cl}_2$ with the $\text{C}_{\text{cAAC}}=\text{Si}(\text{Cl})\text{--Si}(\text{Cl})=\text{C}_{\text{cAAC}}$ unit in the center of the molecule. A disiladibene $(\text{cAAC})_2\text{Si}_2$ is obtained from the reduction of $(\text{cAAC})\text{SiCl}_4$, $(\text{cAAC})_2\text{Si}_2\text{Cl}_4$, and $(\text{cAAC})_2\text{Si}_2\text{Cl}_2$ with the required equiv amounts of KC_8 . Furthermore, diradical $(\text{cAAC})_2\text{SiCl}_2$ is reduced to silylene $(\text{cAAC})_2\text{Si}$ which possesses significant singlet diradicaloid character due to small HOMO-LUMO energy gap. Moreover, the CV of $(\text{cAAC})_2\text{Si}$ and $(\text{cAAC})_2\text{Si}_2$ show that both of them can form radical anion

intermediates in a quasi-reversible process. These radical anions are very reactive and hence undergo one electron induced multiple bond activations leading to unforeseen intra molecular rearrangements.

The synthesis route for the stable carbene centered radical with silicon-phosphine functionalities are little different. The sequence of addition of reactants should be properly adjusted along with the temperature of reduction. Monoradical (CAAC)SiCl₂(PPh₂) is isolated and characterized by X-ray single crystal diffraction. The experimental and simulated EPR spectra show that the hyperfine coupling of radical electron with chlorine and phosphorus nuclei depends upon their relative orientations with respect to the p_z orbital of carbene carbon atom. The rotation of the SiCl₂(PPh₂) group around the C_{CAAC}-Si bond of (CAAC)SiCl₂(PPh₂) is comparatively more restricted than that of SiCl₃ in (CAAC)SiCl₃. The analysis of bonding and optical property of blue colored compound (CAAC)(SiCl₂)(P-TiP) show that it is not like an open shell blue colored diradical species (CAAC)₂SiCl₂. (CAAC)(SiCl₂)(P-TiP) has a singlet ground state with (CAAC:) \rightarrow (Cl₂Si:) \rightarrow (P-TiP) type donation of electron pairs. The blue color originates from the intra molecular charge transfer from silicon-phosphorus π -type orbital to LUMO of the carbene. (CAAC)(SiCl₂)(P-TiP) is further converted to the diamagnetic monomeric (CAAC)Si(P-TiP) and dimeric [(CAAC)Si(P-TiP)]₂ species having low HOMO-LUMO energy gap. The later species is quasi-reversibly converted to its radical anion [(CAAC)Si(P-TiP)]₂^{•-} which has been characterized by EPR measurements. All of these compounds are further studied by theoretical calculations which show that CAAC can display a wide range bonding interactions such as C_{CAAC} \rightarrow Si coordinate σ -bond, electron sharing covalent single bond C_{CAAC}-Si, donor acceptor partial double bond. The nature of these bonds has measureable effect on the C_{CAAC}-N bond lengths.

Acknowledgements

H. W. R. thanks the Deutsche Forschungsgemeinschaft (DFG RO 224/64-I) for financial support.

BIOGRAPHIES

Kartik Chandra Mondal received his Ph.D in 2011 from Karlsruhe Institute of Technology (KIT) under the supervision of Professor Annie K. Powell. He worked on mixed 3d-4f ion based single molecule magnets. After a short stay as a postdoctoral researcher in the same group he moved to University of Göttingen in October, 2011. Since then he has been working with Professor Herbert W. Roesky as a postdoctoral fellow. His research interest mainly focuses on the stabilization of low valent low coordinate group 14 elements and transition metal complexes. Dr. Mondal has coauthored more than 45 peer-reviewed publications in leading scientific journals.



Sudipta Roy received her Ph.D in 2012 from the University of Regensburg under the supervision of Professor Oliver Reiser. Afterwards she worked as a postdoctoral fellow at the Institute of Organic and Biomolecular Chemistry, University of Göttingen on transition metal catalyzed C-H bond activation. Since 2014 she has been working as a postdoctoral fellow with Professor Herbert W. Roesky. Her research interests include the synthesis of cyclic alkyl(amino) carbene stabilized highly sensitive Si-P compounds, and transition metal complexes with their application in catalysis.



Herbert W. Roesky obtained his doctorate from University of Göttingen. After working at Du Pont in the United States, he returned to Göttingen and finished his habilitation. Then he became a professor at the Johann-Wolfgang-Goethe-Universität, Frankfurt am Main in 1971. He moved to University of Göttingen in 1980 and was the director of the Institute for Inorganic Chemistry until 2004. He is primarily known for his pioneering work on fluorides of both transition and main group elements. His current research interest is focused on the synthesis and reactivity of compounds with heavier group 13 and 14 elements in low oxidation states. More than 1250 peer-reviewed papers, articles, patents, and books record his research activity in the areas of Inorganic Chemistry and Material sciences.



References

- (a) M. Gomberg, *J. Am. Chem. Soc.*, 1900, **22**, 757–771; (b) *Stable Radicals: Fundamental and Applied Aspects of Odd-Electron Compounds*; R. G. Hicks, Ed.; Wiley: Chichester, 2010; (c) Ph.D thesis of J. B. Gilroy, *The design, synthesis, and chemistry of stable verdazyl radicals and their precursors*, 2003; (d) A. Rajca, *Chem. Rev.* 1994, **94**, 871–893; (e) R. G. Hicks, *Org. Biomol. Chem.*, 2007, **5**, 1321–1338; (f) P. P. Power, *Chem. Rev.*, 2003, **103**, 789–809; (g) C. D. Martin, M. Soleilhavoup and G. Bertrand, *Chem. Sci.*, 2013, **4**, 3020–3030; (h) M. Abe, *Chem. Rev.* 2013, **113**, 7011–7088; (i) D. Astruc, *Electron Transfer and Radical Processes in Transition Metal Chemistry*. Wiley, New York, 1995.
- (a) J. Fossey, D. Lefort and J. Serba, *Free Radicals in Organic Chemistry*, John Wiley and Sons, 1995; (b) P. Renaud and M. P. Sibi, *Radicals in Organic Synthesis*, Wiley-VCH, 2008; (c) C. Chatgililoglu and A. Studer, *Encyclopedia of Radicals in Chemistry, Biology and Materials*, Wiley-VCH, 2012.
- (a) J. A. Murphy, T. A. Khan, S. Z. Zhou, D. W. Thomson and M. Mahesh, *Angew. Chem. Int. Ed.*, 2005, **44**, 1356–1360; *Angew. Chem.*, 2005, **117**, 1380–1384; (b) J. A. Murphy, S.-Z. Zhou, D. W. Thomson, F. Schoenebeck, M. Mohan, S. R. Park, T. Tuttle and L. E. A. Berlouis, *Angew. Chem. Int. Ed.*, 2007, **46**, 5178–5183; *Angew. Chem.*, 2007, **119**, 5270–5275; (c) S. O'Sullivan, E. Doni, T. Tuttle and J. A. Murphy, *Angew. Chem., Int. Ed.*, 2014, **53**, 474–478; *Angew. Chem.*, 2014, **126**, 484–488; (d) S. F. Nelsen, *Acc. Chem. Res.* 1987, **20**, 269–276.
- B. Halliwell and J. M. C. Gutteridge, *Free Radicals Biology and Medicine*, Oxford University Press, 2007.
- (a) D. Griller and K. U. Ingold, *Acc. Chem. Res.*, 1976, **9**, 13–19; (b) A. Sekiguchi, T. Tanaka, M. Ichinohe, K. Akiyama, S. Tero-Kubota, *J. Am. Chem. Soc.*, 2003, **125**, 4962–4963.
- (a) O. Armet, J. Veciana, C. Rovira, J. Riera, J. Castaner, E. Molins, J. Rius, C. Miravittles, S. Olivella and J. Brichfeus, *J. Phys. Chem.*, 1987, **91**, 5608–5616; (b) J. Carilla, L. Fajari, L. Julia, J. Riera and L. Viadel, *Tetrahedron Lett.*, 1994, **35**, 6529–6532.
- C. J. Hawker, A. W. Bosman and E. Harth, *Chem. Rev.*, 2001, **101**, 3661–3688.
- R. A. Sheldon, I. Arends, G. J. Ten Brink and A. Dijkstra, *Acc. Chem. Res.*, 2002, **35**, 774–781.
- K. Matyjaszewski, H.-j. Paik, D. A. Shipp, Y. Isobe and Y. Okamoto, *Macromolecules*, 2001, **34**, 3127–3129.
- E. M. Fatila, M. Rouzières, M. C. Jennings, A. J. Lough, R. Clérac and K. E. Preuss, *J. Am. Chem. Soc.*, 2013, **135**, 9596–9599.
- A. Caneschi, D. Gatteschi, N. Laloti, C. Sangregorio, R. Sessoli, G. Venturi, A. Vindigni, A. Rettori, M. G. Pini and M. A. Novak, *Angew. Chem. Int. Ed.*, 2001, **40**, 1760–1763.
- D. Gatteschi and R. Sessoli, *Angew. Chem. Int. Ed.*, 2003, **42**, 268–297.
- (a) J. S. Wright, D. J. Carpenter, D. J. McKay and K. U. Ingold, *J. Am. Chem. Soc.*, 1997, **119**, 4245–4252; (b) J. S. Wright, E. R. Johnson and G. A. DiLabio, *J. Am. Chem. Soc.*, 2001, **123**, 1173–1183.
- (a) *IUPAC Compendium of Chemical Terminology*, release 2.3.2; International Union of Pure and Applied Chemistry (IUPAC): Research Triangle Park, NC, 2012; p 168; (b) *IUPAC Compendium of Chemical Terminology*, release 2.3.2; International Union of Pure and Applied Chemistry (IUPAC): Research Triangle Park, NC, 2012; p 427; (c) S. S. Eaton, K. M. More, B. M. Sawant and G. R. Eaton, *J. Am. Chem. Soc.*, 1983, **105**, 6550; (d) H. Sato, V. Kathirvelu, G. Spagnol, S. Rajca, A. Rajca, S. S. Eaton and G. R. Eaton, *J. Phys. Chem. B*, 2008, **112**, 2818–2828; (e) P. Bertrand, C. More, B. Guigliarelli, A. Fournel, B. Bennett and B. Howes, *J. Am. Chem. Soc.*, 1994, **116**, 3078–3086; (f) C. Riplinger, J. P. Y. Kao, G. M. Rosen, V. Kathirvelu, G. R. Eaton, S. S. Eaton, A. Kutateladze and F. Neese, *J. Am. Chem. Soc.*, 2009, **131**, 10092–10106; (g) T. Sawai, K. Sato, T. Ise, D. Shiomi, K. Toyota, Y. Morita and T. Takui, *Angew. Chem., Int. Ed.*, 2008, **47**, 3988–3990; *Angew. Chem.*, 2008, **120**, 4052–4054; (h) M. S. Robinson, M. L. Polak, V. M. Bierbaum, C. H. DePu and W. C. Lineberger, *J. Am. Chem. Soc.*, 1995, **117**, 6766–6778; (i) M. J. S. Dewar, and L. E. Wade, *J. Am. Chem. Soc.*, 1977, **99**, 4417–4424; (j) A. Hinz, A. Schulz, and A. Villinger, *Angew. Chem., Int. Ed.*, 2015, **54**, 668–672; *Angew. Chem.*, 2015, **127**, 678–682.
- (a) L. Loodleman, *J. Chem. Phys.*; 1981, **74**, 5737. (b) L. Noodleman and E. J. Baerends, *J. Am. Chem. Soc.*, 1984, **106**, 2316–2327; (c) K. Yamaguchi, F. Jensen, A. Dorigo and K. N. Houk, *Chem. Phys. Lett.*, 1988, **149**, 537–542; (d) K. Kitagawa, T. Saito, M. Itoh, M. Shoji, K. Koizumi, S. Yamanaka, T. Kawakami, M. Okumura, and K. Yamaguchi, *Chem. Phys. Lett.*, 2007, **442**, 445–450; (e) T. Saito, S. Nishihara, Y. Kataoka, Y. Nakanishi, T. Matsui, Y. Kitagawa, T. Kawakami, M. Okumura and K. Yamaguchi, *Chem. Phys. Lett.*, 2009, **483**, 168–171; (f) D. H. Ess, E. R. Johnson, Z. Hu and W. Yang, *J. Phys. Chem. A*, 2011, **115**, 76–83.
- (a) R. S. Ghadwal, S. Azhakar and H. W. Roesky, *Acc. Chem. Res.*, 2013, **46**, 444–456; (b) S. K. Mandal and H. W. Roesky, *Chem. Commun.*, 2010, **46**, 6016–6041; (c) S. S. Sen, S. Khan, S. Nagendran and H. W. Roesky, *Acc. Chem. Res.*, 2012, **45**, 578–587; (d) B. Bolm and M. Driess, *In Functional Molecular Silicon Compounds II*; Scheschkewitz, D., Ed.; *Structure and Bonding* 156; Springer: Berlin, 2014; pp 85–123; (e) P. P. Power, *Chem. Rev.*, 1999, **99**, 3463–3503.
- (a) Y. Wang and G. H. Robinson, *Dalton Trans.*, 2012, **41**, 337–345; (b) Y. Wang and G. H. Robinson, *Inorg. Chem.*, 2014, **53**, 11815–11832.
- Y. Wang, M. Chen, Y. Xie, P. Wei, H. F. Schaefer III, P. V. R. Schleyer and G. H. Robinson, *Nat. Chem.*, 2015, **7**, 509–513.
- C. Caltagirone, A. Bettoschi, A. Garau and R. Montis, *Chem. Soc. Rev.*, 2015, **44**, 4645–4671.
- A. F. Holleman, E. Wiberg, N. Wiberg, *Lehrbuch der Anorganischen Chemie*; Walter de Gruyter & Co.: Berlin, 1995.
- W. Simmler, "Silicon Compounds, Inorganic", *Ullmann's Encyclopedia of Industrial Chemistry*; Wiley-VCH: Weinheim, 2005, DOI:10.1002/14356007.a24_001.
- R. West, M. J. Fink, J. Michl, *Science*, 1981, **214**, 1343–1344.
- M. Denk, R. Lennon, R. Hayashi, R. West, A. V. Belyakov, H. P. Verne, A. Haaland, M. Wagner and N. Metzler, *J. Am. Chem. Soc.*, 1994, **116**, 2691–2692.
- M. Kira, *Chem. Commun.*, 2010, **46**, 2893–2903.
- V. Ya. Lee and A. Sekiguchi, *Organometallic Compounds of Low-Coordinate Si, Ge, Sn and Pb: From Phantom Species to Stable Compounds*; Wiley: New York, 2010.
- A. J. Arduengo, III, R. L. Harlow and M. Kline, *J. Am. Chem. Soc.*, 1991, **113**, 361–363.

- 27 Y. Wang, Y. Xie, P. Wei, R. B. King, H. F. Schaefer III, P. V. R. Schleyer and G. H. Robinson, *Science*, 2008, **321**, 1069–1071.
- 28 R. S. Ghadwal, H. W. Roesky, S. Merkel, J. Henn and D. Stalke, *Angew. Chem., Int. Ed.* 2009, **48**, 5683–5686; *Angew. Chem.*, 2009, **121**, 5793–5796.
- 29 M. N. Hopkinson, C. Richter, M. Schedler, F. Glorius, *Nature*, 2014, **510**, 485–496.
- 30 (a) S. Ishida, T. Iwamoto, C. Kabuto and M. Kira, *Nature*, 2003, **421**, 725–727; (b) A. Sekiguchi, R. Kinjo and M. Ichinohe, *Science*, 2004, **305**, 1755–1757.
- 31 (a) H. Sakurai, *Free Radicals*; J. K. Kochi, Ed.; John Wiley & Sons Ltd.: New York, 1973; Vol. II; (b) C. Chatgililoglu, *Chem. Rev.*, 1995, **95**, 1229–1251.
- 32 (a) A. Hudson, R. A. Jackson, C. J. Rhodes and A. L. D. Vecchio, *J. Organomet. Chem.*, 1985, **280**, 173–176; (b) M. J. S. Gynane, M. F. Lappert, P. I. Riley, P. Riviere, M. Riviere-Baudet, *J. Organomet. Chem.*, 1980, **202**, 5–12; (c) H. Sakurai, H. Umino and H. Sugiyama, *J. Am. Chem. Soc.*, 1980, **102**, 6837–6840; (d) A. J. Mckinley, T. Karatsu, G. M. Wallraff, D. P. Thompson, R. D. Miller and J. Michl, *J. Am. Chem. Soc.*, 1991, **113**, 2003–2010. (e) S. Kyushin, H. Sakurai, T. Betsuyaku and H. Matsumoto, *Organometallics*, 1997, **16**, 5386–5388.
- 33 A. Sekiguchi, T. Matsuno and M. Ichinohe, *J. Am. Chem. Soc.*, 2001, **123**, 12436–12437.
- 34 A. Sekiguchi, T. Matsuno and M. Ichinohe, *J. Am. Chem. Soc.*, 2000, **122**, 11250–11251.
- 35 (a) M. Kira, T. Iwamoto, C. Kabuto, *J. Am. Chem. Soc.*, 1996, **118**, 10303–10304; (b) N. Wiberg, H. Auer, H. Noth, J. Knizek and Polborn, *Angew. Chem., Int. Ed.*, 1998, **37**, 2869–2872.
- 36 A. Sekiguchi, T. Fukawa, M. Nakamoto, V. Ya. Lee and M. Ichinohe, *J. Am. Chem. Soc.*, 2002, **124**, 9865–9869.
- 37 (a) J. Thiele and H. Balhorn, *Chem. Ber.* 1904, **37**, 1463–1470; (b) L. K. Montgomery, J. C. Huffman, E. A. Jurczak and M. Grendze, *M. P. J. Am. Chem. Soc.*, 1986, **108**, 6004–6011.
- 38 (a) W. Schlenk and M. Brauns, *Chem. Ber.* 1915, **48**, 661–669; (b) J. J. Gajewski, M.-J. Chang, P.-J. Stang and T. E. Fisk, *J. Am. Chem. Soc.* 1980, **102**, 2096–2097; (c) B. B. Wright and M. S. Platz, *J. Am. Chem. Soc.* 1983, **105**, 628–630; (d) A. Rajca, and S. Utamapanya, *J. Am. Chem. Soc.*, 1993, **115**, 2396–2401.
- 39 T. Nozawa, M. Nagata, M. Ichinohe and A. Sekiguchi, *J. Am. Chem. Soc.*, 2011, **133**, 5773–5775.
- 40 (a) A. Sekiguchi, S. Inoue, M. Ichinohe and Y. Arai, *J. Am. Chem. Soc.*, 2004, **126**, 9626–9629. (b) S. Inoue, M. Ichinohe and A. Sekiguchi, *Chem. Lett.* 2005, **34**, 1564–1565; (c) S. Inoue, M. Ichinohe and A. Sekiguchi, *J. Am. Chem. Soc.*, 2008, **130**, 6078–6079; (d) R. Kinjo, M. Ichinohe and Sekiguchi, *J. Am. Chem. Soc.*, 2007, **129**, 26–27.
- 41 D. Bethell and V. D. Parker, *Acc. Chem. Res.*, 1988, **21**, 400–407.
- 42 L. R. Sita and I. Kinoshita, *J. Am. Chem. Soc.*, 1992, **114**, 7024–7029.
- 43 S. Ishida, T. Iwamoto and M. Kira, *J. Am. Chem. Soc.*, 2003, **125**, 3212–3213.
- 44 S. Inoue, M. Ichinohe and A. Sekiguchi, *J. Am. Chem. Soc.*, 2007, **129**, 6096–6097.
- 45 T. Bally, S. Matzinger, L. Truttman, M. S. Platz, A. Admasu, F. Gerson, A. Arnold and R. Schmidlin, *J. Am. Chem. Soc.*, 1993, **115**, 7007–7008.
- 46 L. B. Knight, M. Winiski, P. Kudelko, C. A. Arrington, *J. Chem. Phys.*, 1989, **91**, 3368–3377.
- 47 H. Tanaka, M. Ichinohe and A. Sekiguchi, *J. Am. Chem. Soc.*, 2012, **134**, 5540–5543.
- 48 (a) E. Niecke, A. Fuchs, F. Baumeister, M. Nieger and W. W. Schoeller, *Angew. Chem., Int. Ed.*, 1995, **34**, 555–557; (b) N. Roques, P. Gerbier, U. Schatzschneider, J.-P. Sutter, P. Guionneau, J. Vidal-Gancedo, J. Veciana, E. Rentschler and C. Guérin, *Chem. Eur. J.*, 2006, **12**, 5547–5562; (c) W.G. Bentrude, S.-G. Lee, K. Akutagawa, W.-Z. Ye and Y. Charbonnel, *J. Am. Chem. Soc.*, 1987, **109**, 1577–1579.
- 49 H. Cox, P. B. Hitchcock, M. F. Lappert and L. J.-M. Pierssens, *Angew. Chem., Int. Ed.*, 2004, **43**, 4500–4504; *Angew. Chem.*, 2004, **116**, 4600–4604.
- 50 C. Cui, M. Brynda, M. M. Olmstead and P. P. Power, *J. Am. Chem. Soc.*, 2004, **126**, 6510–6511.
- 51 K. Takeuchi, M. Ichinohe, and A. Sekiguchi, *J. Am. Chem. Soc.*, 2011, **133**, 12478–12481.
- 52 S.-H. Zhang, H.-W. Xi, K.-H. Lim, Q. Meng, M.-B. Huang, C.-W. So, *Chem. Eur. J.* 2012, **18**, 4258–4263.
- 53 V. Lavallo, Y. Canac, C. Präsang, B. Donnadiou and G. Bertrand, *Angew. Chem. Int. Ed.* 2005, **44**, 5705–5709; *Angew. Chem.* 2005, **117**, 5851–5855.
- 54 (a) D. Martin, M. Melaimi, M. Soleilhavoup and G. Bertrand, *Organometallics*, 2011, **30**, 5304–5313; (b) D. Martin, Y. Canac, V. Lavallo and G. Bertrand, *J. Am. Chem. Soc.*, 2014, **136**, 5023–5030.
- 55 O. Back, M. Henry-Ellinger, C. D. Martin, D. Martin and G. Bertrand, *Angew. Chem. Int. Ed.* 2013, **52**, 2939–2943; *Angew. Chem.* 2013, **125**, 3011–3015.
- 56 Martin, D.; Soleilhavoup, M.; Bertrand and G. *Chem. Sci.* 2011, **2**, 389–399.
- 57 K. C. Mondal, H. W. Roesky, M. C. Schwarzer, G. Frenking, I. Tkach, H. Wolf, D. Kratzert, R. Herbst-Irmer, B. Niepötter and D. Stalke, *Angew. Chem. Int. Ed.* 2013, **52**, 1801–1805; *Angew. Chem.* 2013, **125**, 1845–1850.
- 58 K. C. Mondal, P. P. Samuel, M. Tretiakov, A. P. Singh, H. W. Roesky, A. C. Stückl, B. Niepötter, E. Carl, H. Wolf, R. Herbst-Irmer and D. Stalke, *Inorg. Chem.*, 2013, **52**, 4736–4743.
- 59 K. C. Mondal, H. W. Roesky, M. C. Schwarzer, G. Frenking, B. Niepötter, H. Wolf, R. Herbst-Irmer and D. Stalke, *Angew. Chem. Int. Ed.*, 2013, **52**, 2963–2967; *Angew. Chem.*, 2013, **125**, 3036–3040.
- 60 S. Roy, K. C. Mondal, L. Krause, P. Stollberg, R. Herbst-Irmer, D. Stalke, J. Meyer, A. C. Stückl, B. Maity, D. Koley, S. K. Vasa, S. Q. Xiang, R. Linser and H. W. Roesky, *J. Am. Chem. Soc.*, 2014, **136**, 16776–16779.
- 61 K. C. Mondal, H. W. Roesky, A. C. Stückl, F. Ihret, W. Kaim, B. Dittrich, B. Maity and D. Koley, *Angew. Chem. Int. Ed.*, 2013, **52**, 11804–11807; *Angew. Chem.*, 2013, **125**, 12020–12023.
- 62 K. C. Mondal, P. P. Samuel, H. W. Roesky, B. Niepötter, R. Herbst-Irmer, D. Stalke, F. Ehret, W. Kaim, B. Maity and D. Koley, *Chem. Eur. J.*, 2014, **20**, 9240–9245.
- 63 (a) A. V. Lalov, S. E. Boganov, V. I. Faustov, M. P. Egorov and O. M. Nefedov, *Russ. Chem. Bull.*, 2003, **52**, 526–538; (b) M. T. Swihart and R. W. Carr, *J. Phys. Chem. A*, 1998, **102**, 785–792.
- 64 K. C. Mondal, B. Dittrich, B. Maity, D. Koley and H. W. Roesky, *J. Am. Chem. Soc.*, 2014, **136**, 9568–9571.
- 65 J. R. Koe, D. R. Powell, J. J. Buffy, S. Hayase and R. West, *Angew. Chem., Int. Ed.*, 1998, **37**, 1441–1442.
- 66 K. C. Mondal, H. W. Roesky, B. Dittrich, N. Holzmann, M. Hermann, G. Frenking and A. Meents, *J. Am. Chem. Soc.*, 2013, **135**, 15990–15993.
- 67 K. C. Mondal, P. P. Samuel, H. W. Roesky, R. R. Aysin, L. A. Leites, S. Neudeck, J. Lübben, B. Dittrich, M. Hermann and G. Frenking, *J. Am. Chem. Soc.*, 2014, **136**, 8919–8922.
- 68 Y. Wang, Y. Xie, P. Wie, R. B. King, H. F. Schaefer III, P. v. R. Schleyer, and G. H. Robinson, *J. Am. Chem. Soc.*, 2008, **130**, 14970–14971.
- 69 (a) R. Martens and W.-W. duMont, *Chem. Ber.*, 1992, **125**, 657–658; (b) R. Martens and W.-W. duMont, *Chem. Ber.*, 1993, **126**, 1115–1117.
- 70 S. Roy, A. C. Stückl, S. Demeshko, B. Dittrich, J. Meyer, B. Maity, D. Koley, B. Schwederski, W. Kaim and H. W. Roesky, *J. Am. Chem. Soc.*, 2015, **137**, 4670–4673.

- 71 S. Roy, P. Stollberg, R. Herbst-Irmer, D. Stalke, D. M. Andrada, G. Frenking and H. W. Roesky, *J. Am. Chem. Soc.*, 2015, **137**, 150–153.
- 72 S. Roy, B. Dittrich, T. Mondal, D. Koley, A. Claudia Stückl, B. Schwederski, W. Kaim, M. John, S. K. Vasa, R. Linser and H. W. Roesky, *J. Am. Chem. Soc.*, 2015, **137**, 6180–6183.
- 73 D. Geiß, M. I. Arz, M. Straßmann, G. Schnakenburg and A. C. Filippou, *Angew. Chem., Int. Ed.*, 2015, **54**, 2739–2744; *Angew. Chem.*, 2015, **127**, 2777–2782.
- 74 V. Lavallo, Y. Canac, B. Donnadiou, W. W. Schoeller and G. Bertrand, *Angew. Chem., Int. Ed.*, 2006, **45**, 3488–3491.
- 75 D. Martin, C. E. Moore, A. L. Rheingold and G. Bertrand, *Angew. Chem., Int. Ed.*, 2013, **52**, 7014–7017; *Angew. Chem.*, 2013, **125**, 7152–7155.
- 76 (a) J. K. Mahoney, D. Martin, C. E. Moore, A. L. Rheingold and G. Bertrand, *J. Am. Chem. Soc.*, 2013, **135**, 18766–18769. (b) J. K. Mahoney, D. Martin, F. Thomas, C. E. Moore, A. L. Rheingold and G. Bertrand, *J. Am. Chem. Soc.*, 2015, **137**, 7519–7125.
- 77 (a) J. Stubbe and W. A. vander Donk, *Chem. Rev.*, 1998, **98**, 705–762; (b) W. Buckel, B. T. Golding, *Annu. Rev. Microbiol.*, 2006, **60**, 27–49.
- 78 S. Styra, M. Melaimi, C. E. Moore, A. L. Rheingold, T. Augenstein, F. Breher, and G. Bertrand, *Chem. Eur. J.*, 2015, **21**, 8441–8446.
- 79 R. Kinjo, B. Donnadiou, M. A. Celik, G. Frenking and G. Bertrand, *Science*, 2011, **333**, 610–613.
- 80 P. Bissinger, H. Braunschweig, A. Damme, I. Krummenacher, A. K. Phukan, K. Radacki and S. Sugawara, *Angew. Chem., Int. Ed.*, 2014, **53**, 7360–7363; *Angew. Chem.*, 2014, **126**, 7488–7491.
- 81 O. Back, M. A. Celik, G. Frenking, M. Melaimi, B. Donnadiou and G. Bertrand, *J. Am. Chem. Soc.*, 2010, **132**, 10262–10263.
- 82 (a) W. W. Dullea and D. A. A. Williams, *Interstellar Chemistry*, Academic Press, New York, 1984; (b) Y. L. Yung and W. B. DeMore, *Photochemistry of Planetary Atmospheres*, Oxford University Press, Oxford, 1998.
- 83 R. Kinjo, B. Donnadiou and G. Bertrand, *Angew. Chem., Int. Ed.*, 2010, **49**, 5930–5933; *Angew. Chem.*, 2010, **122**, 6066–6069.
- 84 O. Back, B. Donnadiou, M. v. Hopffgarten, S. Klein, R. Tonner, G. Frenking and G. Bertrand, *Chem. Sci.*, 2011, **2**, 858–861.
- 85 P. Agarwal, N. A. Piro, K. Meyer, P. Muller and C. C. Cummins, *Angew. Chem., Int. Ed.*, 2007, **46**, 3111–3114; *Angew. Chem.*, 2007, **119**, 3171–3174.
- 86 O. Back, B. Donnadiou, P. Parameswaran, G. Frenking and G. Bertrand, *Nat. Chem.*, 2010, **2**, 369–373.
- 87 M. Y. Abraham, Y. Wang, Y. Xie, R. J. Gilliard, Jr., P. Wei, B. J. Vaccaro, M. K. Johnson, H. F. Schaefer, III, P. v. R. Schleyer and G. H. Robinson, *J. Am. Chem. Soc.*, 2013, **135**, 2486–2488.
- 88 (a) Y. Li, K. C. Mondal, P. P. Samuel, H. Zhu, C. M. Orben, S. Panneerselvam, B. Dittrich, B. Schwederski, W. Kaim, T. Mondal, D. Koley and H. W. Roesky, *Angew. Chem., Int. Ed.*, 2014, **53**, 4168–4172; *Angew. Chem.*, 2014, **126**, 4252–4256; (b) L. Jin, M. Melaimi, L. Liu and G. Bertrand, *Org. Chem. Front.*, 2014, **1**, 351–354.
- 89 J. Park, H. Song, Y. Kim, B. Eun, Y. Kim, D. Y. Bae, S. Park, Y. M. Rhee, W. J. Kim, K. Kim and E. Lee, *J. Am. Chem. Soc.*, 2015, **137**, 4642–4645.
- 90 D. Weinberger, M. Melaimi, C. E. Moore, A. L. Rheingold, G. Frenking, P. Jerabek, G. Bertrand, *Angew. Chem.*, 2013, **125**, 9134–9137; *Angew. Chem., Int. Ed.*, 2013, **52**, 8964–8967.
- 91 D. S. Weinberger, N. A. SK, K. C. Mondal, M. Melaimi, G. Bertrand, A. C. Stückl, H. W. Roesky, B. Dittrich, S. Demeshko, B. Schwederski, W. Kaim, P. Jerabek and G. Frenking, *J. Am. Chem. Soc.*, 2014, **136**, 6235–6238.
- 92 P. P. Samuel, K. C. Mondal, H. W. Roesky, M. Hermann, G. Frenking, S. Demeshko, F. Meyer, A. C. Stückl, J. H. Christian, N. S. Dalal, L. Ungur, L. F. Chibotaru, K. Pröpper, A. Meents and B. Dittrich, *Angew. Chem., Int. Ed.*, 2013, **52**, 11817–11821; *Angew. Chem.*, 2013, **125**, 12033–12037.
- 93 A. P. Singh, P. P. Samuel, H. W. Roesky, M. C. Schwarzer, G. Frenking, N. S. Sidhu and B. Dittrich, *J. Am. Chem. Soc.*, 2013, **135**, 7324–7329.